

NASA Reference Publication 1376
Volume I

Clouds and the Earth's Radiant Energy System (CERES) Algorithm Theoretical Basis Document

Volume I—Overviews (Subsystem 0)

CERES Science Team

December 1995

Clouds and the Earth's Radiant Energy System (CERES) Algorithm Theoretical Basis Document

Volume I—Overviews (Subsystem 0)

*CERES Science Team
Langley Research Center • Hampton, Virginia*

Available electronically at the following URL address: <http://techreports.larc.nasa.gov/ltrs/ltrs.html>

Printed copies available from the following:

NASA Center for AeroSpace Information
800 Elkridge Landing Road
Linthicum Heights, MD 21090-2934
(301) 621-0390

National Technical Information Service (NTIS)
5285 Port Royal Road
Springfield, VA 22161-2171
(703) 487-4650

Contents

Preface	v
Nomenclature	ix
CERES Top Level Data Flow Diagram	xvii
CERES Algorithm Overview	1
CERES Data Processing System Objectives and Architecture (Subsystem 0)	23

Preface

The Release-1 CERES Algorithm Theoretical Basis Document (ATBD) is a compilation of the techniques and processes that constitute the prototype data analysis scheme for the Clouds and the Earth's Radiant Energy System (CERES), a key component of NASA's Mission to Planet Earth. The scientific bases for this project and the methodologies used in the data analysis system are also explained in the ATBD. The CERES ATBD comprises 11 subsystems of various sizes and complexities. The ATBD for each subsystem has been reviewed by three or four independently selected university, NASA, and NOAA scientists. In addition to the written reviews, each subsystem ATBD was reviewed during oral presentations given to a six-member scientific peer review panel at Goddard Space Flight Center during May 1994. Both sets of reviews, oral and written, determined that the CERES ATBD was sufficiently mature for use in providing archived Earth Observing System (EOS) data products. The CERES Science Team completed revisions of the ATBD to satisfy all reviewer comments. Because the Release-1 CERES ATBD will serve as the reference for all of the initial CERES data analysis algorithms and product generation, it is published here as a NASA Reference Publication.

Due to its extreme length, this NASA Reference Publication comprises four volumes that divide the CERES ATBD at natural break points between particular subsystems. These four volumes are

I: Overviews

CERES Algorithm Overview

Subsystem 0. CERES Data Processing System Objectives and Architecture

II: Geolocation, Calibration, and ERBE-Like Analyses

Subsystem 1.0. Instrument Geolocate and Calibrate Earth Radiances

Subsystem 2.0. ERBE-Like Inversion to Instantaneous TOA and Surface Fluxes

Subsystem 3.0. ERBE-Like Averaging to Monthly TOA

III: Cloud Analyses and Determination of Improved Top of Atmosphere Fluxes

Subsystem 4.0. Overview of Cloud Retrieval and Radiative Flux Inversion

Subsystem 4.1. Imager Clear-Sky Determination and Cloud Detection

Subsystem 4.2. Imager Cloud Height Determination

Subsystem 4.3. Cloud Optical Property Retrieval

Subsystem 4.4. Convolution of Imager Cloud Properties With CERES Footprint Point Spread Function

Subsystem 4.5. CERES Inversion to Instantaneous TOA Fluxes

Subsystem 4.6. Empirical Estimates of Shortwave and Longwave Surface Radiation Budget Involving CERES Measurements

IV: Determination of Surface and Atmosphere Fluxes and Temporally and Spatially Averaged Products

Subsystem 5.0. Compute Surface and Atmospheric Fluxes

Subsystem 6.0. Grid Single Satellite Fluxes and Clouds and Compute Spatial Averages

Subsystem 7.0. Time Interpolation and Synoptic Flux Computation for Single and Multiple Satellites

Subsystem 8.0. Monthly Regional, Zonal, and Global Radiation Fluxes and Cloud Properties

Subsystem 9.0. Grid TOA and Surface Fluxes for Instantaneous Surface Product

Subsystem 10.0. Monthly Regional TOA and Surface Radiation Budget

Subsystem 11.0. Update Clear Reflectance, Temperature History (CHR)

Subsystem 12.0. Regrid Humidity and Temperature Fields

The CERES Science Team serves as the editor for the entire document. A complete list of Science Team members is given below. Different groups of individuals prepared the various subsections that constitute the CERES ATBD. Thus, references to a particular subsection of the ATBD should specify

the subsection number, authors, and page numbers. Questions regarding the content of a given subsection should be directed to the appropriate first or second author. No attempt was made to make the overall document stylistically consistent.

The CERES Science Team is an international group led by 2 principal investigators and 19 coinvestigators. The team members and their institutions are listed below.

CERES Science Team

Bruce A. Wielicki, Interdisciplinary Principal Investigator
Bruce R. Barkstrom, Instrument Principal Investigator

Atmospheric Sciences Division
NASA Langley Research Center
Hampton, Virginia 23681-0001

Coinvestigators

Bryan A. Baum
Atmospheric Sciences Division
NASA Langley Research Center
Hampton, Virginia 23681-0001

Maurice Blackmon
Climate Research Division
NOAA Research Laboratory
Boulder, Colorado 80303

Robert D. Cess
Institute for Terrestrial & Planetary Atmospheres
Marine Sciences Research Center
State University of New York
Stony Brook, New York 11794-5000

Thomas P. Charlock
Atmospheric Sciences Division
NASA Langley Research Division
Hampton, Virginia 23681-0001

James A. Coakley
Oregon State University
Department of Atmospheric Sciences
Corvallis, Oregon 97331-2209

Dominique A. Crommelynck
Institute Royal Meteorologique
B-1180 Bruxelles
Belgium

Richard N. Green
Atmospheric Sciences Division
NASA Langley Research Center
Hampton, Virginia 23681-0001

Robert Kandel
Laboratoire de Meteorologie Dynamique
Ecole Polytechnique
91128 Palaiseau
France

Michael D. King
Goddard Space Flight Center
Greenbelt, Maryland 20771

Robert B. Lee III
Atmospheric Sciences Division
NASA Langley Research Center
Hampton, Virginia 23681-0001

A. James Miller
NOAA/NWS
5200 Auth Road
Camp Springs, Maryland 20233

Patrick Minnis
Atmospheric Sciences Division
NASA Langley Research Center
Hampton, Virginia 23681-0001

Veerabhadran Ramanathan
Scripps Institution of Oceanography
University of California-San Diego
La Jolla, California 92093-0239

David R. Randall
Colorado State University
Department of Atmospheric Science
Foothills Campus, Laporte Avenue
Fort Collins, Colorado 80523

G. Louis Smith
Atmospheric Sciences Division
NASA Langley Research Center
Hampton, Virginia 23681-0001

Larry L. Stowe
NOAA/NWS
5200 Auth Road
Camp Springs, Maryland 20233

Ronald M. Welch
South Dakota School of Mines and Technology
Institute of Atmospheric Sciences
Rapid City, South Dakota 57701-3995

Nomenclature

Acronyms

ADEOS	Advanced Earth Observing System
ADM	Angular Distribution Model
AIRS	Atmospheric Infrared Sounder (EOS-AM)
AMSU	Advanced Microwave Sounding Unit (EOS-PM)
APD	Aerosol Profile Data
APID	Application Identifier
ARESE	ARM Enhanced Shortwave Experiment
ARM	Atmospheric Radiation Measurement
ASOS	Automated Surface Observing Sites
ASTER	Advanced Spaceborne Thermal Emission and Reflection Radiometer
ASTEX	Atlantic Stratocumulus Transition Experiment
ASTR	Atmospheric Structures
ATBD	Algorithm Theoretical Basis Document
AVG	Monthly Regional, Average Radiative Fluxes and Clouds (CERES Archival Data Product)
AVHRR	Advanced Very High Resolution Radiometer
BDS	Bidirectional Scan (CERES Archival Data Product)
BRIE	Best Regional Integral Estimate
BSRN	Baseline Surface Radiation Network
BTD	Brightness Temperature Difference(s)
CCD	Charge Coupled Device
CCSDS	Consultative Committee for Space Data Systems
CEPEX	Central Equatorial Pacific Experiment
CERES	Clouds and the Earth's Radiant Energy System
CID	Cloud Imager Data
CLAVR	Clouds from AVHRR
CLS	Constrained Least Squares
COPRS	Cloud Optical Property Retrieval System
CPR	Cloud Profiling Radar
CRH	Clear Reflectance, Temperature History (CERES Archival Data Product)
CRS	Single Satellite CERES Footprint, Radiative Fluxes and Clouds (CERES Archival Data Product)
DAAC	Distributed Active Archive Center
DAC	Digital-Analog Converter
DB	Database
DFD	Data Flow Diagram
DLF	Downward Longwave Flux

DMSP	Defense Meteorological Satellite Program
EADM	ERBE-Like Albedo Directional Model (CERES Input Data Product)
ECA	Earth Central Angle
ECLIPS	Experimental Cloud Lidar Pilot Study
ECMWF	European Centre for Medium-Range Weather Forecasts
EDDB	ERBE-Like Daily Data Base (CERES Archival Data Product)
EID9	ERBE-Like Internal Data Product 9 (CERES Internal Data Product)
EOS	Earth Observing System
EOSDIS	Earth Observing System Data Information System
EOS-AM	EOS Morning Crossing Mission
EOS-PM	EOS Afternoon Crossing Mission
ENSO	El Niño/Southern Oscillation
ENVISAT	Environmental Satellite
EPHANC	Ephemeris and Ancillary (CERES Input Data Product)
ERB	Earth Radiation Budget
ERBE	Earth Radiation Budget Experiment
ERBS	Earth Radiation Budget Satellite
ESA	European Space Agency
ES4	ERBE-Like S4 Data Product (CERES Archival Data Product)
ES4G	ERBE-Like S4G Data Product (CERES Archival Data Product)
ES8	ERBE-Like S8 Data Product (CERES Archival Data Product)
ES9	ERBE-Like S9 Data Product (CERES Archival Data Product)
FLOP	Floating Point Operation
FIRE	First ISCCP Regional Experiment
FIRE II IFO	First ISCCP Regional Experiment II Intensive Field Observations
FOV	Field of View
FSW	Hourly Gridded Single Satellite Fluxes and Clouds (CERES Archival Data Product)
FTM	Functional Test Model
GAC	Global Area Coverage (AVHRR data mode)
GAP	Gridded Atmospheric Product (CERES Input Data Product)
GCIP	GEWEX Continental-Phase International Project
GCM	General Circulation Model
GEBA	Global Energy Balance Archive
GEO	ISCCP Radiances (CERES Input Data Product)
GEWEX	Global Energy and Water Cycle Experiment
GLAS	Geoscience Laser Altimetry System
GMS	Geostationary Meteorological Satellite
GOES	Geostationary Operational Environmental Satellite
HBTM	Hybrid Bispectral Threshold Method

HIRS	High-Resolution Infrared Radiation Sounder
HIS	High-Resolution Interferometer Sounder
ICM	Internal Calibration Module
ICRCCM	Intercomparison of Radiation Codes in Climate Models
ID	Identification
IEEE	Institute of Electrical and Electronics Engineers
IES	Instrument Earth Scans (CERES Internal Data Product)
IFO	Intensive Field Observation
INSAT	Indian Satellite
IOP	Intensive Observing Period
IR	Infrared
IRIS	Infrared Interferometer Spectrometer
ISCCP	International Satellite Cloud Climatology Project
ISS	Integrated Sounding System
IWP	Ice Water Path
LAC	Local Area Coverage (AVHRR data mode)
LaRC	Langley Research Center
LBC	Laser Beam Ceilometer
LBTM	Layer Bispectral Threshold Method
Lidar	Light Detection and Ranging
LITE	Lidar In-Space Technology Experiment
Lowtran 7	Low-Resolution Transmittance (Radiative Transfer Code)
LW	Longwave
LWP	Liquid Water Path
LWRE	Longwave Radiant Excitance
MAM	Mirror Attenuator Mosaic
MC	Mostly Cloudy
MCR	Microwave Cloud Radiometer
METEOSAT	Meteorological Operational Satellite (European)
METSAT	Meteorological Satellite
MFLOP	Million FLOP
MIMR	Multifrequency Imaging Microwave Radiometer
MISR	Multiangle Imaging Spectroradiometer
MLE	Maximum Likelihood Estimate
MOA	Meteorology Ozone and Aerosol
MODIS	Moderate-Resolution Imaging Spectroradiometer
MSMR	Multispectral, multiresolution
MTSA	Monthly Time and Space Averaging
MWH	Microwave Humidity

MWP	Microwave Water Path
NASA	National Aeronautics and Space Administration
NCAR	National Center for Atmospheric Research
NESDIS	National Environmental Satellite, Data, and Information Service
NIR	Near Infrared
NMC	National Meteorological Center
NOAA	National Oceanic and Atmospheric Administration
NWP	Numerical Weather Prediction
OLR	Outgoing Longwave Radiation
OPD	Ozone Profile Data (CERES Input Data Product)
OV	Overcast
PC	Partly Cloudy
POLDER	Polarization of Directionality of Earth's Reflectances
PRT	Platinum Resistance Thermometer
PSF	Point Spread Function
PW	Precipitable Water
RAPS	Rotating Azimuth Plane Scan
RPM	Radiance Pairs Method
RTM	Radiometer Test Model
SAB	Sorting by Angular Bins
SAGE	Stratospheric Aerosol and Gas Experiment
SARB	Surface and Atmospheric Radiation Budget Working Group
SDCD	Solar Distance Correction and Declination
SFC	Hourly Gridded Single Satellite TOA and Surface Fluxes (CERES Archival Data Product)
SHEBA	Surface Heat Budget in the Arctic
SPECTRE	Spectral Radiance Experiment
SRB	Surface Radiation Budget
SRBAVG	Surface Radiation Budget Average (CERES Archival Data Product)
SSF	Single Satellite CERES Footprint TOA and Surface Fluxes, Clouds
SSMI	Special Sensor Microwave Imager
SST	Sea Surface Temperature
SURFMAP	Surface Properties and Maps (CERES Input Product)
SW	Shortwave
SWICS	Shortwave Internal Calibration Source
SWRE	Shortwave Radiant Excitance
SYN	Synoptic Radiative Fluxes and Clouds (CERES Archival Data Product)
SZA	Solar Zenith Angle
THIR	Temperature/Humidity Infrared Radiometer (Nimbus)

TIROS	Television Infrared Observation Satellite
TISA	Time Interpolation and Spatial Averaging Working Group
TMI	TRMM Microwave Imager
TOA	Top of the Atmosphere
TOGA	Tropical Ocean Global Atmosphere
TOMS	Total Ozone Mapping Spectrometer
TOVS	TIROS Operational Vertical Sounder
TRMM	Tropical Rainfall Measuring Mission
TSA	Time-Space Averaging
UAV	Unmanned Aerospace Vehicle
UT	Universal Time
UTC	Universal Time Code
VAS	VISSR Atmospheric Sounder (GOES)
VIRS	Visible Infrared Scanner
VISSR	Visible and Infrared Spin Scan Radiometer
WCRP	World Climate Research Program
WG	Working Group
Win	Window
WN	Window
WMO	World Meteorological Organization
ZAVG	Monthly Zonal and Global Average Radiative Fluxes and Clouds (CERES Archival Data Product)

Symbols

A	atmospheric absorptance
$B_{\lambda}(T)$	Planck function
C	cloud fractional area coverage
CF_2Cl_2	dichlorofluorocarbon
$CFCl_3$	trichlorofluorocarbon
CH_4	methane
CO_2	carbon dioxide
D	total number of days in the month
D_e	cloud particle equivalent diameter (for ice clouds)
E_o	solar constant or solar irradiance
F	flux
f	fraction
G_a	atmospheric greenhouse effect
g	cloud asymmetry parameter
H_2O	water vapor

I	radiance
i	scene type
m_i	imaginary refractive index
\hat{N}	angular momentum vector
N_2O	nitrous oxide
O_3	ozone
P	point spread function
p	pressure
Q_a	absorption efficiency
Q_e	extinction efficiency
Q_s	scattering efficiency
R	anisotropic reflectance factor
r_E	radius of the Earth
r_e	effective cloud droplet radius (for water clouds)
r_h	column-averaged relative humidity
S_o	summed solar incident SW flux
S'_o	integrated solar incident SW flux
T	temperature
T_B	blackbody temperature
t	time or transmittance
W_{liq}	liquid water path
w	precipitable water
\hat{x}_o	satellite position at t_o
x, y, z	satellite position vector components
$\dot{x}, \dot{y}, \dot{z}$	satellite velocity vector components
z	altitude
z_{top}	altitude at top of atmosphere
α	albedo or cone angle
β	cross-scan angle
γ	Earth central angle
γ_{at}	along-track angle
γ_{ct}	cross-track angle
δ	along-scan angle
ϵ	emittance
Θ	colatitude of satellite
θ	viewing zenith angle
θ_o	solar zenith angle
λ	wavelength
μ	viewing zenith angle cosine

μ_o	solar zenith angle cosine
ν	wave number
ρ	bidirectional reflectance
τ	optical depth
$\tau_{aer}(p)$	spectral optical depth profiles of aerosols
$\tau_{H_2O\lambda}(p)$	spectral optical depth profiles of water vapor
$\tau_{O_3}(p)$	spectral optical depth profiles of ozone
Φ	longitude of satellite
ϕ	azimuth angle
$\tilde{\omega}_o$	single-scattering albedo

Subscripts:

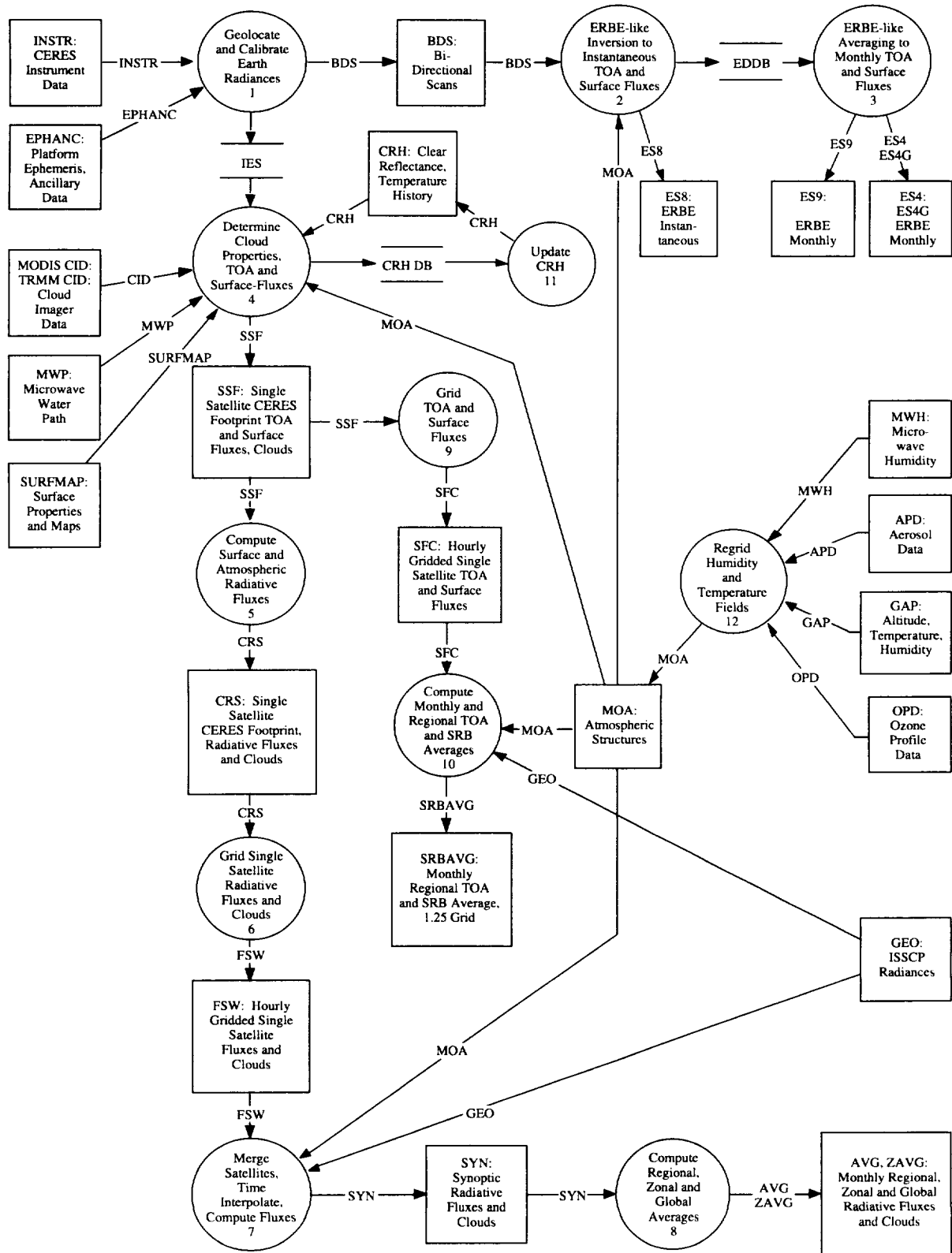
c	cloud
cb	cloud base
ce	cloud effective
cld	cloud
cs	clear sky
ct	cloud top
ice	ice water
lc	lower cloud
liq	liquid water
s	surface
uc	upper cloud
λ	spectral wavelength

Units

AU	astronomical unit
cm	centimeter
cm-sec ⁻¹	centimeter per second
count	count
day	day, Julian date
deg	degree
deg-sec ⁻¹	degree per second
DU	Dobson unit
erg-sec ⁻¹	erg per second
fraction	fraction (range of 0–1)
g	gram
g-cm ⁻²	gram per square centimeter
g-g ⁻¹	gram per gram
g-m ⁻²	gram per square meter

h	hour
hPa	hectopascal
K	Kelvin
kg	kilogram
kg-m ⁻²	kilogram per square meter
km	kilometer
km-sec ⁻¹	kilometer per second
m	meter
mm	millimeter
μm	micrometer, micron
N/A	not applicable, none, unitless, dimensionless
ohm-cm ⁻¹	ohm per centimeter
percent	percent (range of 0–100)
rad	radian
rad-sec ⁻¹	radian per second
sec	second
sr ⁻¹	per steradian
W	watt
W-m ⁻²	watt per square meter
W-m ⁻² sr ⁻¹	watt per square meter per steradian
W-m ⁻² sr ⁻¹ μm ⁻¹	watt per square meter per steradian per micrometer

CERES Top Level Data Flow Diagram



Clouds and the Earth's Radiant Energy System (CERES)

Algorithm Theoretical Basis Document

CERES Algorithm Overview

Bruce A. Wielicki, Interdisciplinary Principal Investigator¹

Bruce R. Barkstrom, Instrument Principal Investigator¹

¹Atmospheric Sciences Division, NASA Langley Research Center, Hampton, Virginia 23681-0001

Abstract

CERES (Clouds and the Earth's Radiant Energy System) is a key part of NASA's Earth Observing System (EOS). CERES objectives are

- 1. For climate change analysis, provide a continuation of the ERBE (Earth Radiation Budget Experiment) record of radiative fluxes at the top of the atmosphere (TOA) analyzed using the same techniques as the existing ERBE data.*
- 2. Double the accuracy of estimates of radiative fluxes at TOA and the Earth's surface.*
- 3. Provide the first long-term global estimates of the radiative fluxes within the Earth's atmosphere.*
- 4. Provide cloud property estimates which are consistent with the radiative fluxes from surface to TOA.*

These CERES data are critical for advancing the understanding of cloud-radiation interactions, in particular cloud feedback effects on the Earth's radiation balance. CERES data are fundamental to our ability to understand and detect global climate change. CERES results are also very important for studying regional climate changes associated with deforestation, desertification, anthropogenic aerosols, and El Niño events.

This overview summarizes the Release 1 version of the planned CERES data products and data analysis algorithms. These algorithms are a prototype for the system which will produce the scientific data required for studying the role of clouds and radiation in the Earth's climate system. This release will produce a data processing system capable of test analysis of global NOAA-9 and NOAA-10 data for two months: October 1986; and December 15, 1986–January 15, 1987, as well as analysis of one month of hourly GOES-Next data. Based on these and other tests, the algorithms will be modified to produce Release 2 algorithms which will be ready to analyze the first CERES data planned for launch on TRMM in August 1997, followed by the EOS-AM platform in June 1998.

CERES Algorithm Theoretical Basis Document (ATBD)

Introduction

The purpose of this overview is to provide a brief summary of the CERES (Clouds and the Earth's Radiant Energy System) science objectives, historical perspective, algorithm design, and relationship to other EOS (Earth Observing System) instruments as well as important field experiments required for validation of the CERES results. The overview is designed for readers familiar with the ERBE (Earth Radiation Budget Experiment) and ISCCP (International Satellite Cloud Climatology Project) data. For other readers, additional information on these projects can be found in the CERES Algorithm Theoretical Basis Document (ATBD) subsystem 0, or in many references (Barkstrom 1984; Barkstrom and Smith 1986; Rossow et al. 1991; Rossow and Garder 1993). Given this background, many of the comments in this overview will introduce CERES concepts by comparison to the existing ERBE and ISCCP state-of-the-art global measurements of radiation budget and cloud properties. The overview will not be complete or exhaustive, but rather selective and illustrative. More complete descriptions are found in

the ATBD's, and they are referenced where appropriate. The overview, as well as the entire set of ATBD's that constitute the CERES design are the product of the entire CERES Science Team and the CERES Data Management Team. We have simply summarized that work in this document.

Scientific Objectives

The scientific justification for the CERES measurements can be summarized by three assertions:

- Changes in the radiative energy balance of the Earth-atmosphere system can cause long-term climate changes (including a carbon dioxide induced “global warming”)
- Besides the systematic diurnal and seasonal cycles of solar insolation, changes in cloud properties (amount, height, optical thickness) cause the largest changes of the Earth's radiative energy balance
- Cloud physics is one of the weakest components of current climate models used to predict potential global climate change

The most recent international assessment of the confidence in predictions using global climate models (IPCC 1992) concluded that “the radiative effects of clouds and related processes continue to be the major source of uncertainty.” The U.S. Global Change Research Program classifies the role of clouds and radiation as its highest scientific priority (CEES, 1994). There are many excellent summaries of the scientific issues (IPCC 1992; Hansen et al. 1993; Ramanathan et al. 1989; Randall et al. 1989) concerning the role of clouds and radiation in the climate system. These issues naturally lead to a requirement for improved global observations of both radiative fluxes and cloud physical properties. The CERES Science Team, in conjunction with the EOS Investigators Working Group representing a wide range of scientific disciplines from oceans, to land processes, to atmosphere, has examined these issues and proposed an observational system with the following objectives:

- For climate change analysis, provide a continuation of the ERBE record of radiative fluxes at the TOA, analyzed using the same algorithms that produced the existing ERBE data
- Double the accuracy of estimates of radiative fluxes at the TOA and Earth's surface
- Provide the first long-term global estimates of the radiative fluxes within the Earth's atmosphere
- Provide cloud property estimates which are consistent with the radiative fluxes from surface to TOA

The CERES Algorithm Theoretical Basis Documents (ATBD's) provide a technical plan for accomplishing these scientific objectives. The ATBD's include detailed specification of data products, as well as the algorithms used to produce those products.

Historical Perspective

We will briefly outline the CERES planned capabilities and improvements by comparison to the existing ERBE, ISCCP, and SRB (Surface Radiation Budget) projects. Figure 1 shows a schematic of radiative fluxes and cloud properties as produced by ERBE, SRB, and ISCCP, as well as those planned for CERES. Key changes are listed below:

Scene Identification

- ERBE measured only TOA fluxes and used only ERBE radiance data, even for the difficult task of identifying each ERBE field of view (FOV) as cloudy or clear.
- CERES will identify clouds using collocated high spectral and spatial resolution cloud imager radiance data from the same spacecraft as the CERES broadband radiance data, (ATBD subsystem 4).
- ERBE only estimated cloud properties as one of four cloud amount classes.
- CERES will identify clouds by cloud amount, height, optical depth, and cloud particle size and phase.

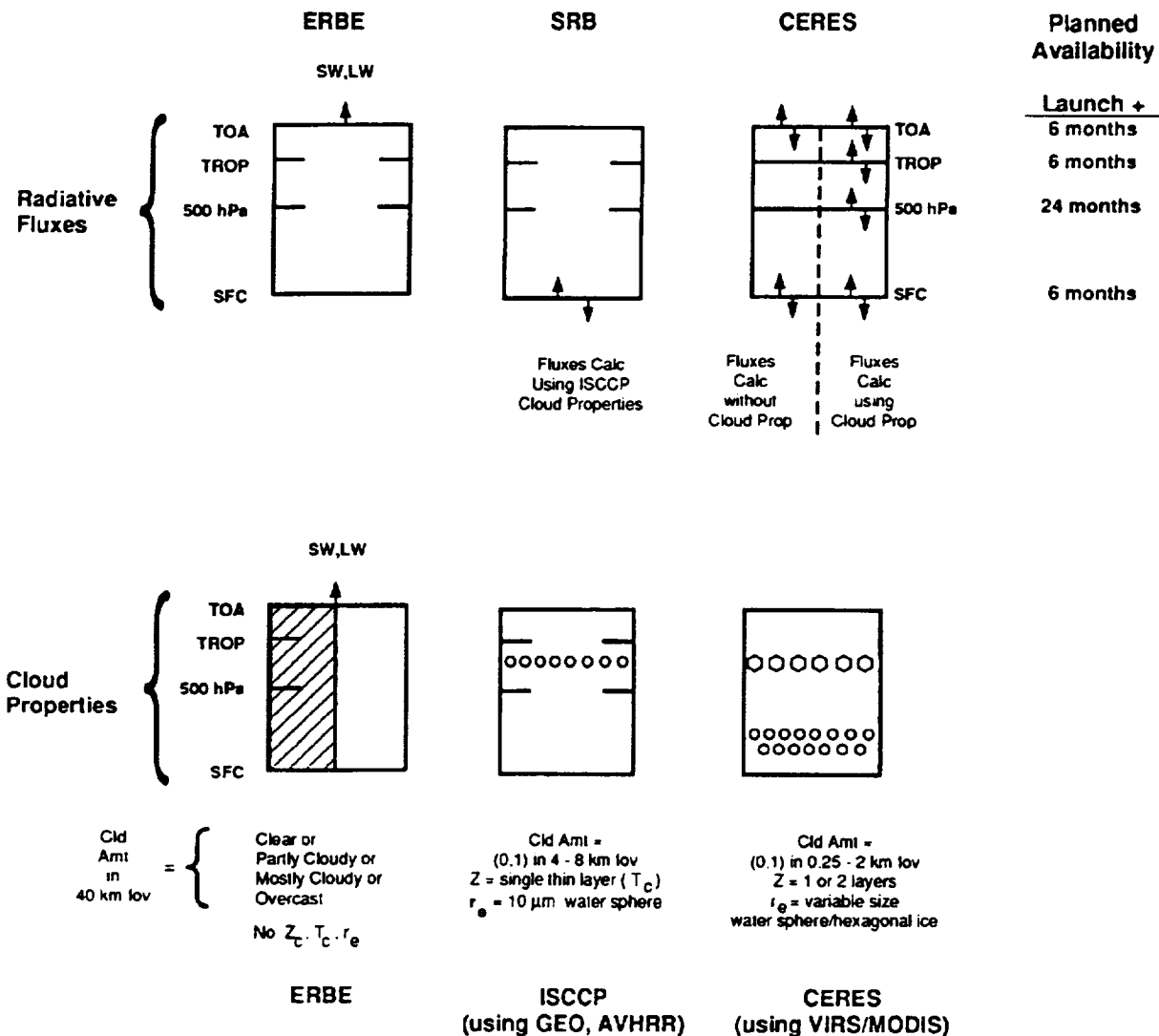


Figure 1. The top of the figure compares radiative fluxes derived by ERBE, SRB, and CERES. The bottom compares cloud amount and layering assumptions used by ERBE, ISCCP, and CERES.

Angular Sampling

- ERBE used empirical anisotropic models which were only a function of cloud amount and four surface types (Wielicki and Green 1989). This caused significant rms and bias errors in TOA fluxes (ATBD subsystem 0, Suttles et al. 1992).
- CERES will fly a new rotating azimuth plane (RAP) scanner to sample radiation across the entire hemisphere of scattered and emitted broadband radiation. The CERES RAP scanner data will be merged with coincident cloud imager derived cloud physical and radiative properties to develop a more complete set of models of the radiative anisotropy of shortwave (SW) and long-wave (LW) radiation. Greatly improved TOA fluxes will be obtained.

Time Sampling

- ERBE used a time averaging strategy which relied only on the broadband ERBE data and used other data sources only for validation and regional case studies.

- CERES will use the 3-hourly geostationary satellite data of ISCCP to aid in time interpolation of TOA fluxes between CERES observation times. Calibration problems with the narrowband ISCCP data will be eliminated by adjusting the data to agree at the CERES observation times. In this sense, the narrowband data are used to provide a diurnal cycle perturbation to the mean radiation fields.

Surface and In-Atmosphere Radiative Fluxes

- SRB uses ISCCP-determined cloud properties and calibration to estimate surface fluxes.
- CERES will provide two types of surface fluxes: *first*, a set which attempts to directly relate CERES TOA fluxes to surface fluxes; *second*, a set which uses the best information on cloud, surface, and atmosphere properties to calculate surface, in-atmosphere, and TOA radiative fluxes, and then constrains the radiative model solution to agree with CERES TOA flux observations.
- Radiative fluxes within the atmosphere will initially be provided at the tropopause and at selected levels in the stratosphere (launch plus 6 months). Additional radiative flux estimates at 500 hPa (launch + 24 months) and at 4-12 additional levels in the troposphere (launch + 36 months) are planned, with the number of tropospheric levels dependent on the results of post-launch validation studies.

CERES Algorithm Summary

Data Flow Diagram

The simplest way to understand the structure of the CERES data analysis algorithms is to examine the CERES data flow diagram shown in figure 2. Circles in the diagram represent algorithm processes which are formally called subsystems. Subsystems are a logical collection of algorithms which together convert input data products into output data products. Boxes represent archival data products. Boxes with arrows entering a circle are input data sources for the subsystem, while boxes with arrows exiting the circles are output data products. Data output from the subsystems falls into three major types of archival products:

1. **ERBE-like Products** which are as identical as possible to those produced by ERBE. These products are used for climate monitoring and climate change studies when comparing directly to ERBE data sources (process circles and ATBD subsystems 1, 2, and 3).
2. **SURFACE Products** which use cloud imager data for scene classification and new CERES-derived angular models to provide TOA fluxes with improved accuracy over those provided by the ERBE-like products. Second, direct relationships between surface fluxes and TOA fluxes are used where possible to construct SRB estimates which are as independent as possible of radiative transfer model assumptions, and which can be tuned directly to surface radiation measurements. These products are used for studies of land and ocean surface energy budget, as well as climate studies which require higher accuracy fluxes than provided by the ERBE-like products (process circles and ATBD subsystems 1, 4, 9, and 10).
3. **ATMOSPHERE Products** which use cloud-imager-derived cloud physical properties, NMC (National Meteorological Center) temperature and moisture fields, ozone and aerosol data, CERES observed surface properties, and a broadband radiative transfer model to compute estimates of SW and LW radiative fluxes (up and down) at the surface, at levels within the atmosphere, and at the TOA. By adjusting the most uncertain surface and cloud properties, the calculations are constrained to agree with the CERES TOA-measured fluxes, thereby producing an internally consistent data set of radiative fluxes and cloud properties. These products are designed for studies of energy balance within the atmosphere, as well as climate studies which require consistent cloud, TOA, and surface radiation data sets. Data volume is larger than ERBE-like or Surface products (process circles and ATBD subsystems 1, 4, 5, 6, 7, and 8).

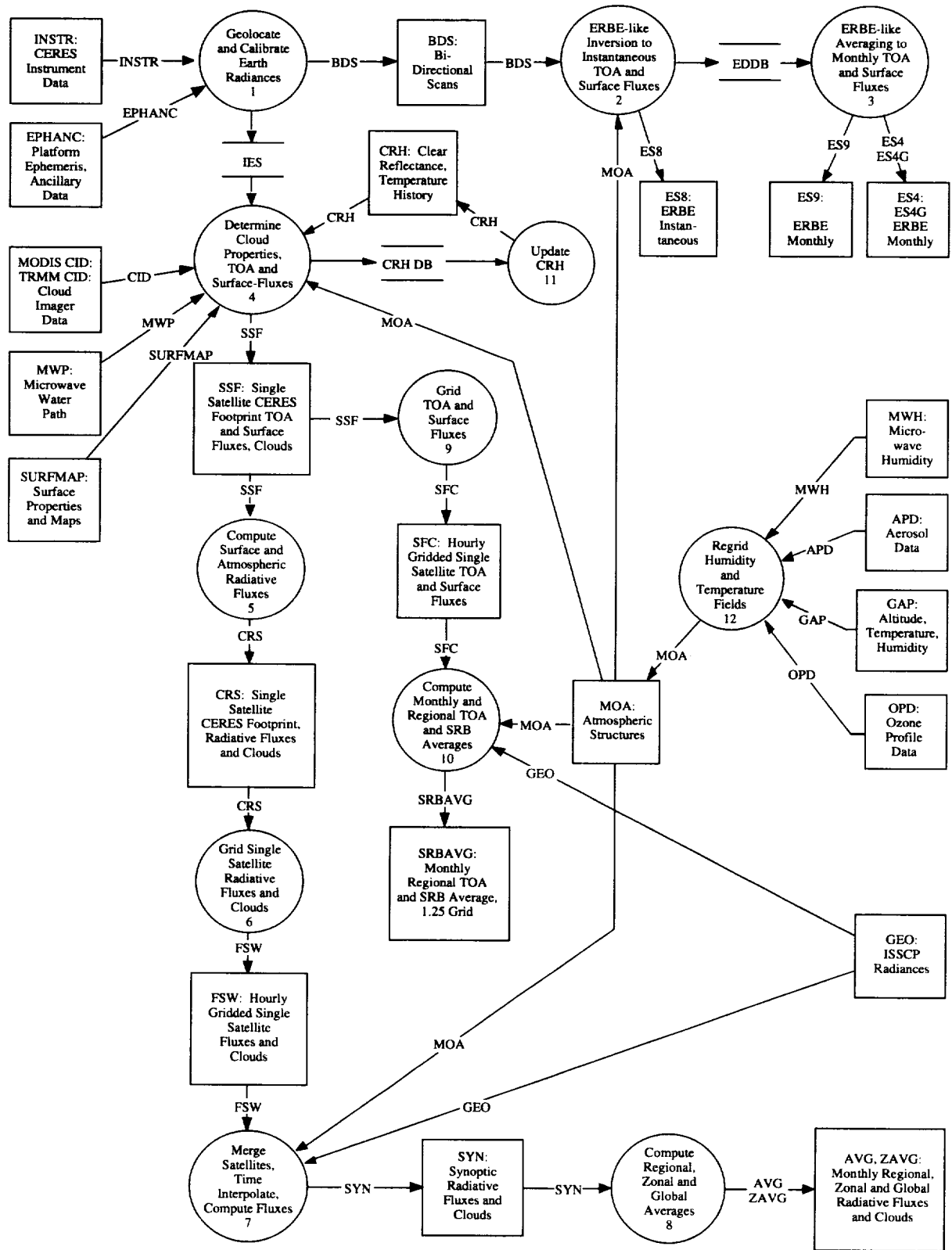


Figure 2. The CERES data flow diagram. Boxes represent input or output archived data products. The circles represent algorithm processes.

The data flow diagram and the associated ATBD's are a work in progress. They represent the current understanding of the CERES Science Team and the CERES Data Management Team. The ATBD's are meant to change with time. To manage this evolution, the data products and algorithms will be developed in four releases or versions.

Version 0 consisted of experimental testing of available analysis algorithms meant to mimic some of the planned CERES capabilities. These studies provided many of the sensitivity analyses found in the ATBD's.

Release 1 is the initial prototype system and is the subject of this overview and the current ATBD's. Release 1 will be sufficiently complete to allow testing on 2 months of existing global satellite data from ERBE, AVHRR (Advanced Very High Resolution Radiometer), and HIRS (High-Resolution Infrared Sounder) instruments for October 1986 on NOAA-9, and for December 15, 1986–January 15, 1987 on NOAA-9 and NOAA-10.

Release 2 is the first operational system. It will be designed using the experience from Release 1, and will be ready to process the first CERES data following the planned launch of the Tropical Rainfall Measuring Mission (TRMM) in August 1997, as well as the first CERES data from the EOS-AM platform planned for launch in June 1998.

Release 3 is planned for 3 to 4 years after the launch of the EOS-AM platform. Release 3 improvements will include new models of the anisotropy of SW and LW radiation (subsystem 4.5) using the CERES RAP scanner (subsystem 1.0) and additional vertical levels of radiative fluxes within the atmosphere (subsystem 5.0). Note that Release 3 will require a reprocessing of the earlier Release 2 data to provide a time-consistent climate data set for the CERES observations.

The following sections will give a brief summary of the algorithms used in each of the subsystems shown in figure 2. For more complete descriptions, the ATBD's are numbered by the same subsystem numbers used below.

Subsystem 1: Instrument Geolocate and Calibrate Earth Radiances

The instrument subsystem converts the raw, level 0 CERES digital count data into geolocated and calibrated filtered radiances for three spectral channels: a total channel (0.3–200 μm), a shortwave channel (0.3–5 μm), and a longwave window channel (8–12 μm) (Lee et al. 1993). Details of the conversion, including ground and on-board calibration can be found in ATBD subsystem 1. The CERES scanners are based on the successful ERBE design, with the following modifications to improve the data:

- Improved ground and onboard calibration by a factor of 2. The accuracy goal is 1% for SW and 0.5% for LW.
- Angular FOV reduced by a factor of 2 to about 20 km at nadir for EOS-AM orbit altitude of 700 km. This change is made to increase the frequency of clear-sky and single-layer cloud observations, as well as to allow better angular resolution in the CERES derived angular distribution models (ADM's), especially for large viewing zenith angles.
- Improved electronics to reduce the magnitude of the ERBE offsets.
- Improved spectral flatness in the broadband SW channel.
- Replacement of the ERBE LW channel (nonflat spectral response) with an 8–12- μm spectral response window.

The CERES instruments are designed so that they can easily operate in pairs as shown in figure 3. In this operation, one of the instruments operates in a fixed azimuth crosstrack scan (CTS) which optimizes spatial sampling over the globe. The second instrument (RAP scanner) rotates its azimuth plane scan as it scans in elevation angle, thereby providing angular sampling of the entire hemisphere of radiation. The RAP scanner, when combined with cloud imager classification of cloud and surface types,

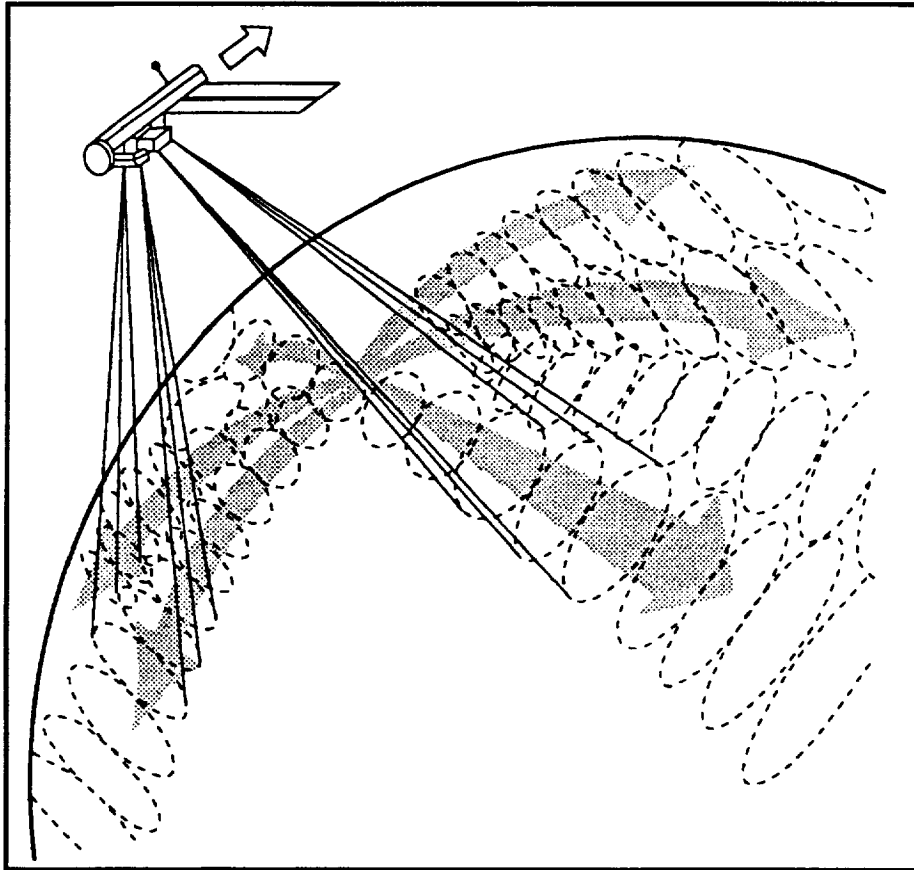


Figure 3. The scan pattern of two CERES scanners on EOS-AM and EOS-PM spacecraft. One scanner is crosstrack, the other scanner rotates in azimuth angle as it scans in elevation, thereby sampling the entire hemisphere of radiation.

will be used to provide improvements over the ERBE ADM's (ATBD subsystem 4.5). Each CERES instrument is identical, so either instrument can operate in either the CTS or RAP scan mode. An initial set of 6 CERES instruments is being built, including deployment on:

- TRMM (1 scanner), 35-degree inclined processing orbit, launch August 1997
- EOS-AM (2 scanners), 10:30 a.m. sun-synchronous orbit, launch June 1998
- EOS-PM (2 scanners), 1:00 p.m. sun-synchronous orbit, launch January 2000

Subsystem 2: ERBE-Like Inversion to Instantaneous TOA and Surface Fluxes

The ERBE-like inversion subsystem converts filtered CERES radiance measurements to instantaneous radiative flux estimates at the TOA and the Earth's surface for each CERES field of view. The basis for this subsystem is the ERBE Data Management System which produced TOA fluxes from the ERBE scanning radiometers onboard the ERBS (Earth Radiation Budget Satellite), NOAA-9 and NOAA-10 satellites over a 5-year period from November 1984 to February 1990 (Barkstrom 1984; Barkstrom and Smith 1986). The ERBE Inversion Subsystem (Smith et al. 1986) is a mature set of algorithms that has been well documented and tested. The strategy for the CERES ERBE-like products is to process the data through the same algorithms as those used by ERBE, with only minimal changes, such as those necessary to adapt to the CERES instrument characteristics.

Since the ERBE analysis, there have been new methods developed to directly relate ERBE TOA broadband fluxes to fluxes at the surface. An example is the relationship of net SW flux at TOA to net

SW flux at the surface (Li and Leighton 1993; Li et al. 1993). ATBD subsystem 4.6 gives another example of an algorithm to derive surface LW downward flux in clear skies using clear-sky TOA LW flux and column precipitable water vapor. Where appropriate, the ERBE-like inversion of CERES data will add these new estimates of surface LW and SW fluxes to the ERBE-like product.

Subsystem 3: ERBE-Like Averaging to Monthly TOA

This subsystem temporally interpolates the instantaneous CERES flux estimates to compute ERBE-like averages of TOA radiative parameters. CERES observations of SW and LW flux are time averaged using a data interpolation method similar to that employed by the ERBE Data Management System. The averaging process accounts for the solar zenith angle dependence of albedo during daylight hours, as well as the systematic diurnal cycles of LW radiation over land surfaces (Brooks et al. 1986).

The averaging algorithms produce daily, monthly-hourly, and monthly means of TOA and surface SW and LW flux on regional, zonal, and global spatial scales. Separate calculations are performed for clear-sky and total-sky fluxes.

The only significant modification to the ERBE processing algorithm for CERES is that estimates of surface flux are made at all temporal and spatial scales using the TOA-to-surface flux parameterization schemes for SW and LW fluxes discussed in subsystem 2.

Subsystem 4: Overview of Cloud Retrieval and Radiative Flux Inversion

One of the major advances of the CERES radiation budget analysis over ERBE is the ability to use high spectral and spatial resolution cloud imager data to determine cloud and surface properties within the relatively large CERES field of view (20-km diameter for EOS-AM and EOS-PM, 10-km diameter for TRMM). For the first launch of the CERES broadband radiometer on TRMM in 1997, CERES will use the VIRS (Visible Infrared Scanner) cloud imager as input. For the next launches on EOS-AM (1998) and EOS-PM (2000), CERES will use the MODIS (Moderate-Resolution Imaging Spectroradiometer) cloud imager data as input. This subsystem matches imager-derived cloud properties with each CERES FOV and then uses either ERBE ADM's (Releases 1 and 2) or improved CERES ADM's (Release 3) to derive TOA flux estimates for each CERES FOV. Until new CERES ADM's are available several years after launch, the primary advance over the ERBE TOA flux method will be to greatly increase the accuracy of the clear-sky fluxes. The limitations of ERBE clear-sky determination cause the largest uncertainty in estimates of cloud radiative forcing. In Release 3 using new ADM's, both rms and bias TOA flux errors for all scenes are expected to be a factor of 3-4 smaller than those for the ERBE-like analysis.

In addition to improved TOA fluxes, this subsystem also provides the CERES FOV matched cloud properties used by subsystem 5 to calculate radiative fluxes at the surface, within the atmosphere, and at the TOA for each CERES FOV. Finally, this subsystem also provides estimates of surface fluxes using direct TOA-to-surface parameterizations. Because of its complexity, this subsystem has been further decomposed into six additional subsystems.

4.1. Imager clear-sky determination and cloud detection. This subsystem is an extension of the ISCCP time-history approach with several key improvements, including the use of

- Spatial coherence information for clear-sky determination (Coakley and Bretherton 1982)
- Multispectral clear/cloud tests (Stowe et al. 1991)
- Texture measures (Welch et al. 1992)
- Artificial intelligence classification for complex backgrounds (snow, mountains)
- Improved navigation (approximately 1 km or better) and calibration of VIRS and MODIS

4.2. Imager cloud height determination. For ISCCP, this step is part of the cloud property determination. CERES separates this step and uses three techniques to search for well-defined cloud layers:

- Spatial coherence (Coakley and Bretherton 1982)
- Infrared sounder radiance ratioing (15- μm band channels) (Menzel et al. 1992; Baum et al. 1994)
- Comparisons of multispectral histogram analyses to theoretical calculations (Minnis et al. 1993)

The algorithm also searches for evidence of imager pixels with multilayer clouds and assigns the nearest well-defined cloud layer heights to these cases. While the analysis of multilevel clouds is at an early development stage, it is considered a critical area and will be examined even in Release 1 of the CERES algorithms. The need for identification of multilayer clouds arises from the sensitivity of surface downward LW flux to low-level clouds and cloud overlap assumptions (ATBD subsystem 5.0).

4.3. Cloud optical property retrieval. For ISCCP, this step involved the determination of a cloud optical depth using visible channel reflectance; an infrared emittance derived using this visible optical depth and an assumption of cloud microphysics (10- μm water spheres); and a cloud radiating temperature corrected for emittance less than 1.0 (daytime only). Future ISCCP analyses will allow for ice particles, depending on cloud temperature.

The CERES analysis extends these properties to include cloud particle size and phase estimation using additional spectral channels at 1.6 and 2.1 μm during the day (King et al. 1992) and 3.7 and 8.5 μm at night. In addition, the use of infrared sounder channels in subsystem 4.2 allows correction of non-black cirrus cloud heights for day and nighttime conditions.

Figure 4 summarizes the CERES cloud property analysis with a schematic drawing showing the cloud imager pixel data overlaid with a geographic mask (surface type and elevation), the cloud mask from subsystem 4.1, the cloud height and overlap conditions specified in subsystem 4.2, and the column of cloud properties for each imager pixel in the analysis region.

4.4. Convolution of imager cloud properties with CERES footprint point spread function. For each CERES FOV, the CERES point spread function (fig. 5) is used to weight the individual cloud imager footprint data to provide cloud properties matched in space and time to the CERES flux measurements. Because cloud radiative properties are non-linearly related to cloud optical depth, a frequency distribution of cloud optical depth is kept for each cloud height category in the CERES FOV. Additional information on cloud property data structures can be found in ATBD subsystem 0 and 4.0.

4.5. CERES inversion to instantaneous TOA fluxes. The cloud properties determined for each CERES FOV are used to select an ADM class to convert measured broadband radiance into an estimate of TOA radiative flux. In Releases 1 and 2, the ERBE ADM classes will be used. After several years of CERES RAP scanner data have been obtained, new ADM's will be developed as a function of cloud amount, cloud height, cloud optical depth, and cloud particle phase.

4.6. Empirical estimates of shortwave and longwave surface radiation budget involving CERES measurements. This subsystem uses parameterizations to directly relate the CERES TOA fluxes to surface fluxes. There are three primary advantages to using parameterizations:

- Can be directly verified against surface measurements
- Maximizes the use of the CERES calibrated TOA fluxes
- Computationally simple and efficient

There are two primary disadvantages to this approach:

- Difficult to obtain sufficient surface data to verify direct parameterizations under all cloud, surface, and atmosphere conditions
- May not be able to estimate all individual surface components with sufficient accuracy

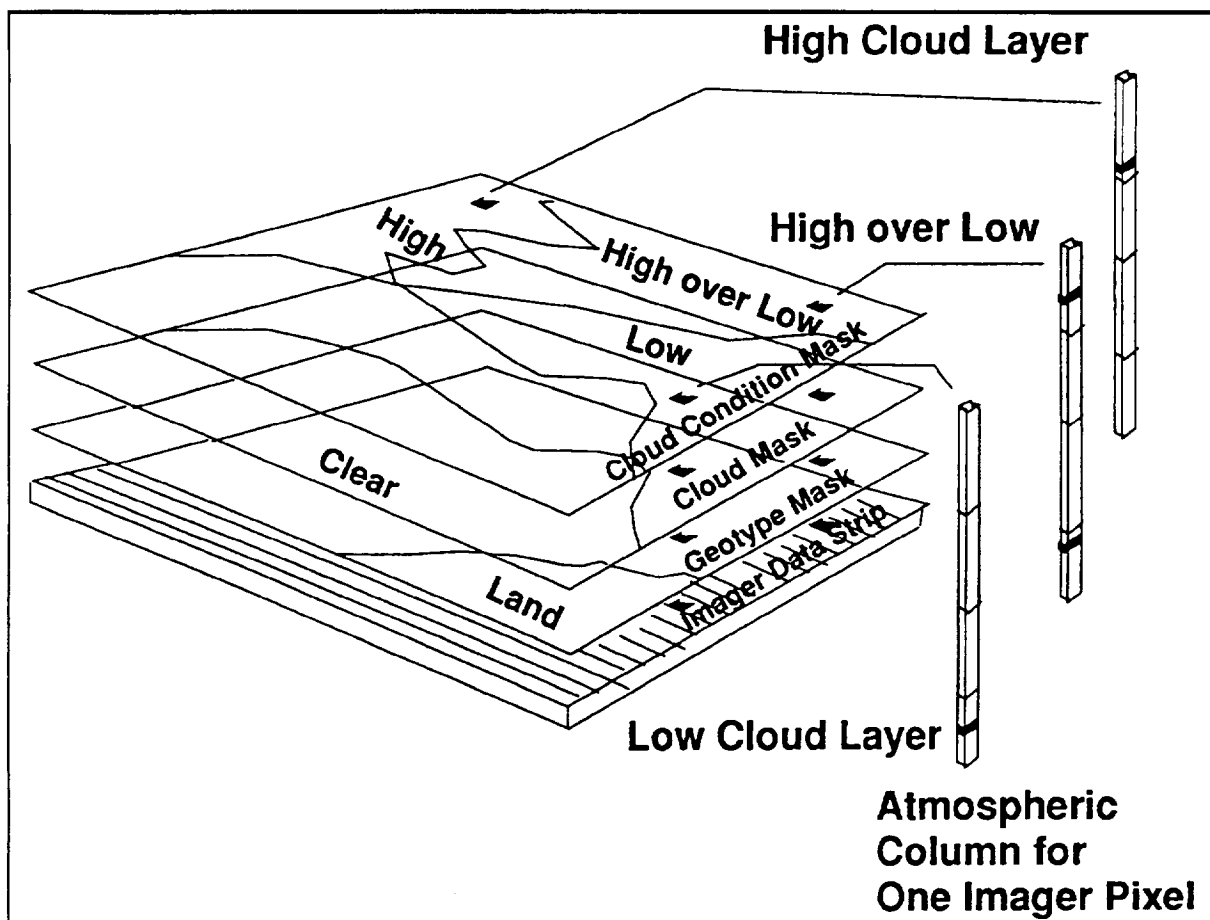


Figure 4. Illustration of the CERES cloud algorithm using cloud imager data from VIRS and MODIS. Imager data are overlaid by a geographic scene map, cloud mask, and cloud overlap condition mask. For each imager field of view, cloud properties are determined for one or two cloud layers.

For Release 1, we have identified parameterizations to derive surface net SW radiation (Cess et al. 1991; Li et al. 1993), clear-sky downward LW flux (ATBD subsystem 4.6.2), and total-sky downward LW flux (Gupta 1989; Gupta et al. 1992). Recent studies (Ramanathan et al. 1995; Cess et al. 1995) have questioned the applicability of the Li et al. 1993 surface SW flux algorithm, but this algorithm will be used in Release 1, pending the results of further validation.

The combined importance and difficulty of deriving surface fluxes has led CERES to a two fold approach. The results using the parameterizations given in subsystem 4.6 are saved in the CERES Surface Product. A separate approach using the imager cloud properties, radiative models, and TOA fluxes is summarized in subsystem 5.0 and these surface fluxes are saved in the CERES Atmosphere Products. Both approaches (subsystem 5.0 and 4.6) use radiative modeling to varying degrees. The difference is that the radiative models in the Surface Product are used to derive the form of a simplified parameterization between satellite observations and surface radiative fluxes. The satellite observations are primarily CERES TOA fluxes but include selected auxiliary observations such as column water vapor amount. These simplified surface flux parameterizations are then tested against surface radiative flux observations. If necessary, the coefficients of the parameterization are adjusted to obtain the optimal consistency with the surface observations.

Ultimately, the goal is to improve the radiative modeling and physical understanding to the point where they are more accurate than the simple parameterizations used in the Surface Product. In

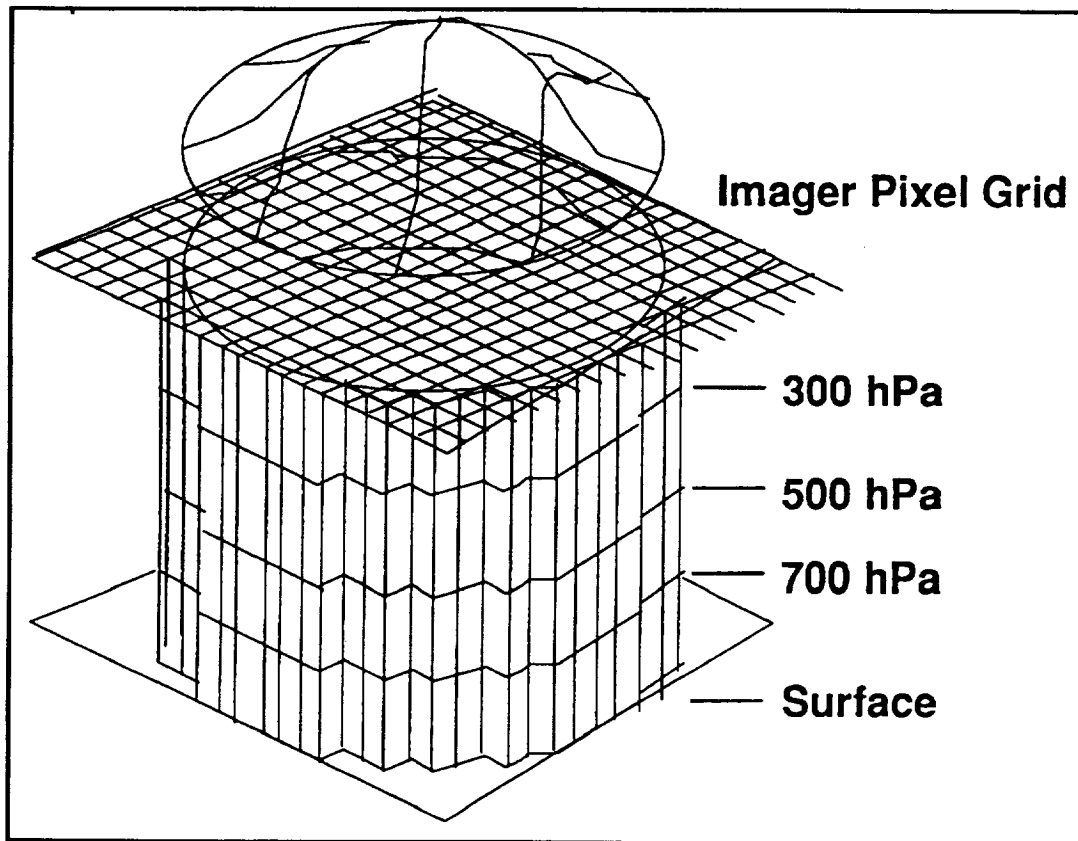


Figure 5. Illustration of the Gaussian-like point spread function for a single CERES field of view, overlaid over a grid of cloud imager pixel data. The four vertical layers represent the CERES cloud height categories which are separated at 700 hPa, 500 hPa, and 300 hPa. Cloud properties are weighted by the point spread function to match cloud and radiative flux data.

the near-term, validation against surface observations of both methods (subsystem 4.6 and 5.0) will be used to determine the most accurate approach. If the simplified surface flux parameterizations prove more accurate, then the surface fluxes derived in subsystem 4.6 will also be used as a constraint on the calculations of in-atmosphere fluxes derived in subsystem 5.0. This would probably be a weaker constraint than TOA fluxes, given the larger expected errors for surface flux estimates.

Subsystem 5: Compute Surface and Atmospheric Fluxes (ATMOSPHERE Data Product)

This subsystem is commonly known as SARB (Surface and Atmospheric Radiation Budget) and uses an alternate approach to obtain surface radiative fluxes, as well as obtaining estimates of radiative fluxes at predefined levels within the atmosphere. All SARB fluxes include SW and LW fluxes for both up and down components at all defined output levels from the surface to the TOA. For Release 1 (shown in fig. 1), output levels are the surface, 500 hPa, tropopause, and TOA. The major steps in the SARB algorithm for each CERES FOV are

1. Input surface data (albedo, emissivity)
2. Input meteorological data (T, q, O₃, aerosol)
3. Input imager cloud properties matched to CERES FOV's
4. Use radiative model to calculate radiative fluxes from observed properties
5. Adjust surface and atmospheric parameters (cloud, precipitable water) to get consistency with CERES observed TOA SW and LW fluxes; constrain parameters to achieve consistency with

subsystem 4.6 surface flux estimates if validation studies show these surface fluxes to be more accurate than radiative model computations of surface fluxes

6. Save final flux calculations, initial TOA discrepancies, and surface/atmosphere property adjustments along with original surface and cloud properties

While global TOA fluxes have been estimated from satellites for more than 20 years, credible, global estimates for surface and in-atmosphere fluxes have only been produced globally in the last few years (Darnell et al. 1992; Pinker and Laszlo 1992; Wu and Chang 1992; Charlock et al. 1993; Stuhlmann et al. 1993; Li et al. 1993; Gupta et al. 1992). Key outstanding issues for SARB calculations include

- Effect of cloud inhomogeneity (Cahalan et al. 1994).
- 3-D cloud effects (Schmetz 1984; Hiedinger and Cox 1994).
- Potential enhanced cloud absorption (Stephens and Tsay 1990; Cess et al. 1995; Ramanathan et al. 1995).
- Cloud layer overlap (see ATBD subsystem 5.0).
- Land surface bidirectional reflection functions, emissivity, and surface skin temperature (see ATBD subsystem 5.0).

For Release 1, SARB will use plane-parallel radiative model calculations and will treat cloud inhomogeneity using the independent pixel approximation (Cahalan et al. 1994) with the cloud imager derived frequency distribution of optical depth provided for each CERES FOV. Because cloud properties are non-linearly related to cloud optical depth, this frequency distribution is carried through the entire set of Atmosphere Products, including monthly average products.

For Release 1, adjustment of the calculated fluxes to consistency with the CERES instantaneous TOA fluxes can then be thought of as providing an “equivalent plane-parallel” cloud. For example, consider a fair weather cumulus field over Brazil viewed from the EOS CERES and MODIS instruments. Because the CERES ADM’s are developed as empirical models which are a function of cloud amount, cloud height, and cloud optical depth, the CERES radiative flux estimates can implicitly include 3-D cloud effects and in principle can produce unbiased TOA flux estimates. Note that this would not be true if CERES had inverted radiance to flux using plane-parallel theoretical models. The cloud optical depth derived from MODIS data, however, has been derived using a plane-parallel retrieval. If this imager optical depth is in error because of 3-D cloud effects, then the calculated SARB TOA SW flux will be in error and the cloud optical depth will be adjusted to compensate, thereby achieving a plane-parallel cloud optical depth which gives the same reflected flux as the 3-D cloud. In the LW, the cloud height might be adjusted to remove 3-D artifacts.

Tests against measured surface fluxes will be required to verify if these adjustments can consistently adjust surface fluxes as well; more limited data on atmospheric fluxes will be obtained from field campaigns such as the FIRE (First ISCCP Regional Experiment) and ARM (Atmospheric Radiation Measurement) programs. The data products from the SARB calculations will include both the magnitude of the required surface and cloud property adjustments, as well as the initial and final differences between calculated and TOA measured fluxes.

Figure 6 shows an example calculation of surface and atmospheric radiative fluxes both before and after adjustment to match TOA observations using ERBE. For Release 1, we will test this approach using AVHRR and HIRS data to derive cloud properties, and ERBE TOA flux data to constrain the calculations at the TOA.

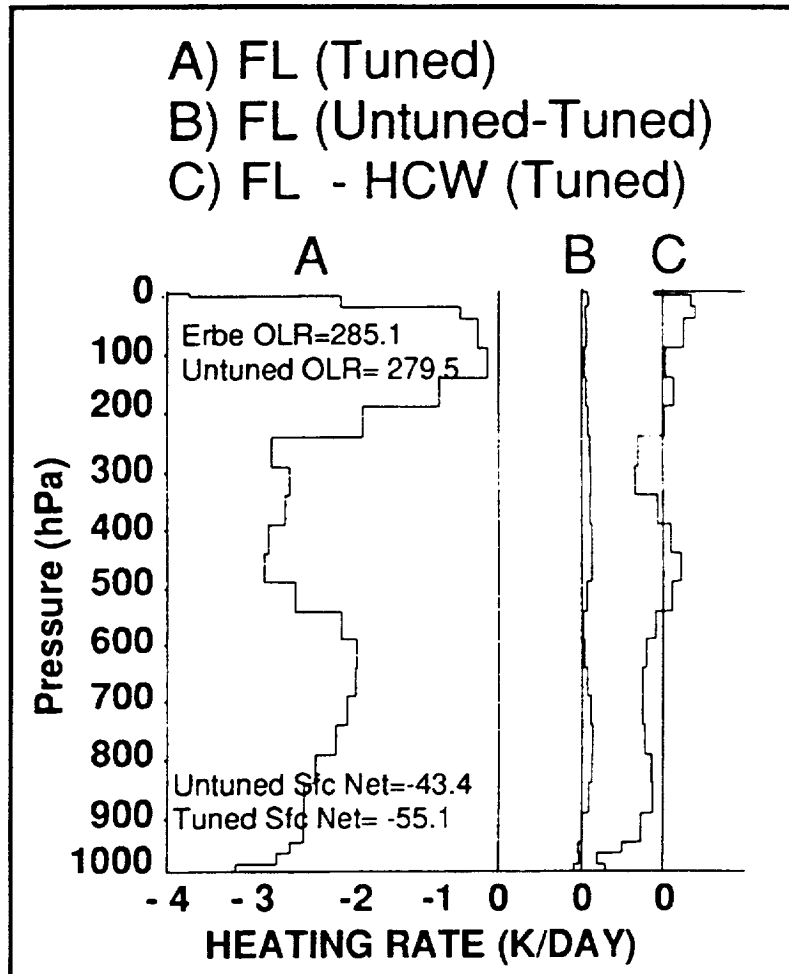


Figure 6. Test analysis of a clear-sky ERBE field of view over ocean using NMC temperature and water vapor. Initial calculation of TOA LW flux is in error by 5.6 Wm^{-2} , and the water vapor amount is tuned to match the TOA value. Curve A shows the tuned LW heating rate profile (degrees/day). Curve B shows the difference between tuned and untuned heating rates. Curve C shows the difference between the calculations of two different radiative transfer models. (See ATBD subsystem 5.0 for details.)

***Subsystem 6: Grid Single Satellite Fluxes and Clouds and Compute Spatial Averages
(ATMOSPHERE Data Product)***

The next step in the processing of the CERES Atmosphere Data Products is to grid the output data from subsystem 5.0 into 1.25 degree equal-area (140-km square) grid boxes. The grid square chosen is exactly half the ISCCP grid, and is well suited to analysis of satellite data which has spatial scales independent of latitude. Cloud properties and TOA fluxes from subsystem 4 and the additional surface and atmospheric radiative fluxes added in subsystem 5 are weighted by their respective area coverage in the grid box.

While spatial averaging of radiative fluxes (surface, in-atmosphere, and TOA) is relatively straightforward, spatial averaging of cloud properties is not so straightforward. The issue is most obvious when we consider the following thought experiment. We compare monthly average LW TOA fluxes in the tropical Pacific Ocean for June of 2 years, one of which was during an ENSO (El Niño/Southern Oscillation) event. We find a large change in TOA LW flux and want to know what change in cloud properties caused the change: cloud amount, cloud height, or cloud optical depth? Because cloud properties are nonlinearly related to radiative fluxes and we have simply averaged over all of those nonlinear

relationships, we cannot guarantee that the question has an unambiguous answer. For example, consider that for TOA LW flux, changes in high cloud amount or optical depth have a large effect on LW flux. For low clouds, they have almost no effect. On the other hand, cloud height changes of either low or high clouds will have a roughly similar effect. Note that if we had selected a change in surface LW flux, the low clouds would dominate and the high clouds would have little effect. These are exactly the type of changes we need to examine and understand in order to address issues of cloud/climate feedback.

If we carry this analogy further, we can see that it is important to consider cloud changes at least as a function of five basic parameters:

- LW TOA flux
- LW surface flux
- SW TOA or surface flux (these are probably similar)
- Liquid water volume
- Ice water volume

The first three of these parameters are critical to cloud radiative forcing issues and the last two are critical to cloud dynamical modeling. We could also add in-atmosphere LW and SW net fluxes, but the five above are a good start. While the CERES team has not yet resolved the optimal way to address this issue, it has included in the data structures the capability to experiment in Release 1 with various formulations. We also plan to lead a workshop to get input from the broader science community, including GCM (General Circulation Model) and satellite remote sensing experts.

Subsystem 7: Time Interpolation and Synoptic Flux Computation for Single and Multiple Satellites (ATMOSPHERE Data Product)

Starting in August 1997, CERES will have one processing satellite (TRMM) sampling twice per day from 45°S to 45°N. In June 1998, the EOS-AM platform (10:30 a.m.; sun-synchronous) will increase diurnal sampling to 4 times per day. In 2000, the EOS-PM satellite (1:30 p.m.; sun-synchronous) will be launched. If TRMM is still functioning, or if the TRMM follow-on is launched, CERES will then have 6 samples per day. Simulation studies using hourly GOES data indicate that the ERBE time-space averaging algorithm gives regional monthly mean time sampling errors (1σ) which are about:

- 9 $\text{W}\cdot\text{m}^{-2}$ for TRMM alone
- 4 $\text{W}\cdot\text{m}^{-2}$ for TRMM plus EOS AM
- 2 $\text{W}\cdot\text{m}^{-2}$ for TRMM plus EOS AM plus EOS PM

Since satellites can fail prematurely, it is very useful to provide a strategy to reduce time sampling errors, especially for the single satellite case.

The CERES strategy is to incorporate 3-hourly geostationary radiance data to provide a correction for diurnal cycles which are insufficiently sampled by CERES. The key to this strategy is to use the geostationary data to supplement the shape of the diurnal cycle, but then use the CERES observations as the absolute reference to anchor the more poorly-calibrated geostationary data. One advantage of this method is that it produces 3-hourly synoptic radiation fields for use in global model testing, and for improved examination of diurnal cycles of clouds and radiation. The output of subsystem 7 is an estimate of cloud properties and surface, atmosphere, and TOA fluxes at each 3-hourly synoptic time. These estimates are also used later in subsystem 8 to aid in the production of monthly average cloud and radiation data.

The process for synoptic processing involves the following steps:

1. Regionally and temporally sort and merge the gridded cloud and radiation data produced by subsystem 6
2. Regionally and temporally sort and merge the near-synoptic geostationary data

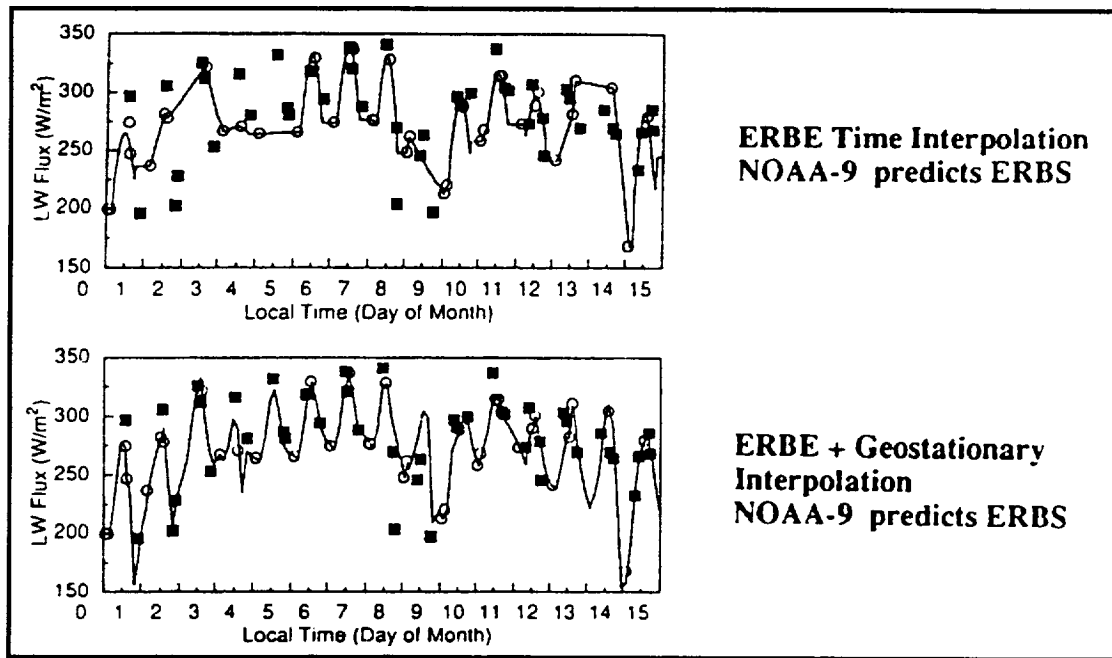


Figure 7. Time Series of ERBE ERBS (solid squares) and NOAA-9 (open circles) LW flux observations and interpolated values from July 1985 over New Mexico. The top curve shows the ERBE time interpolated values; bottom curve the geostationary-data-enhanced interpolation.

3. Interpolate cloud properties from the CERES times of observation to the synoptic times
4. Interpolate cloud information and angular model class, convert the narrowband GOES radiance to broadband (using regional correlations to CERES observations), and then convert the broadband radiance to broadband TOA flux (using the CERES broadband ADM's)
5. Use the time-interpolated cloud properties to calculate radiative flux profiles as in subsystem 5, using the synoptic TOA flux estimates as a constraint
6. Use the diurnal shape of the radiation fields derived from geostationary data, but adjust this shape to match the CERES times of observations (assumed gain error in geostationary data)

Figure 7 gives an example of the enhanced time interpolation using geostationary data.

The system described above could also use the ISCCP geostationary cloud properties. The disadvantage of this approach is that it incorporates cloud properties which are systematically different and less accurate than those from the cloud imagers flying with CERES. The ISCCP cloud properties are limited by geostationary spatial resolution, spectral channels, and calibration accuracy. In this sense, it would be necessary to "calibrate" the ISCCP cloud properties against the TRMM and EOS cloud properties. We are currently performing sensitivity studies on the utility of the ISCCP cloud properties for this purpose.

***Subsystem 8: Monthly Regional, Zonal, and Global Radiation Fluxes and Cloud Properties
(ATMOSPHERE Data Product)***

This subsystem uses the CERES instantaneous synoptic radiative flux and cloud data (subsystem 7) and time averages to produce monthly averages at regional, zonal, and global spatial scales. Initial simulations using both 1-hourly and 3-hourly data have shown that simple averaging of the 3-hourly results is adequate for calculating monthly average LW fluxes. SW flux averaging, however, is more problematic. The magnitude of the solar flux diurnal cycle is 10 to 100 times larger than that for LW flux.

Two methods for SW time averaging are currently planned for testing in Release 1. The first method uses the same techniques as subsystem 7, but to produce 1-hourly instead of 3-hourly synoptic maps. Time averaging then proceeds from the 1-hourly synoptic fields. The second method starts from the 3-hourly synoptic data, and then time interpolates using methods similar to ERBE (Brooks et al. 1986) for other hours of the day with significant solar illumination. While the use of models of the solar zenith angle dependence of albedo are adequate for TOA and surface fluxes, we will examine extensions of these techniques to include interpolation of solar absorption within the atmospheric column. A key issue is to avoid biases caused by the systematic increase of albedo with solar zenith angle for times of observation between sunset and sunrise and the first daytime observation hour.

Subsystem 9: Grid TOA and Surface Fluxes for Instantaneous Surface Product (SURFACE Data Product)

This subsystem is essentially the same process as in subsystem 6. The major difference is that instead of gridding data to be used in the Atmosphere Data Products (subsystems 5, 6, 7, and 8), this subsystem spatially grids the data to be used in the Surface Data Products (subsystems 9 and 10). The spatial grid is the same: 1.25 degree equal area, half the grid size of the ISCCP data. See the data flow diagram (figure 2) and the associated discussion for a summary of the difference between the Atmosphere and Surface Data Products.

Subsystem 10: Monthly Regional TOA and Surface Radiation Budget (SURFACE Data Product)

The time averaging for the Surface Data Product is produced by two methods. The first method is the same as the ERBE method (ERBE-like product in subsystem 3) with the following exceptions:

- Improved CERES models of solar zenith angle dependence of albedo
- Improved cloud imager scene identification (subsystem 4) and improved CERES ADM's to provide more accurate instantaneous fluxes
- Simulation studies indicate that the monthly averaged fluxes will be a factor of 2-3 more accurate than the ERBE-like fluxes

The second method incorporates geostationary radiances similar to the process outlined for synoptic products in subsystem 7. We include this method to minimize problems during the initial flight with TRMM when we have only one spacecraft with two samples per day. As the number of satellites increases to 3, the geostationary data will have little impact on the results.

Because one of the major rationales for the Surface Data Products is to keep surface flux estimates as closely tied to the CERES direct observations as possible, this subsystem will not calculate in-atmosphere fluxes, and will derive its estimates of surface fluxes by the same methods discussed in subsystem 4.6.

Subsystem 11: Update Clear Reflectance, Temperature History

This subsystem keeps a database of the narrowband SW and LW radiances used by the cloud detection algorithms discussed in subsystem 4.1. The database is updated daily and is saved in Release 1 at a 10 minute or 18-km spatial resolution. This database is similar to that kept by the ISCCP system for cloud detection. Improvements over the ISCCP methodology include:

- Elimination of noise due to subsampling
- Elimination of noise from large geolocation errors (VIRS and MODIS have a nominal navigation error of less than 1 km without use of ground control points)
- Elimination of the assumption of Lambertian reflectance from land surfaces

Subsystem 12: Regrid Humidity and Temperature Fields

This subsystem describes interpolation procedures used to convert temperature, water vapor, ozone, aerosols, and passive microwave column water vapor obtained from diverse sources to the spatial and temporal resolution required by various CERES subsystems. Most of the inputs come from NMC analysis products, although the subsystem accepts the inputs from many different sources on many different grids. The outputs consist of the same meteorological fields as the inputs, but at a uniform spatial and temporal resolution necessary to meet the requirements of the other CERES processing subsystems. Interpolation methods vary depending on the nature of the field.

Relationships to Other EOS Instruments and non-EOS Field Experiments: Algorithm Validation and Interdisciplinary Studies

While the ties to VIRS on TRMM and MODIS on EOS have been obvious throughout this overview, there are ties between the CERES data products and many of the EOS instruments.

We expect to greatly increase our ability to detect cloud overlap by using the passive microwave retrievals of cloud liquid water path from the TMI (TRMM Microwave Imager), as well as the MIMR (Multifrequency Imaging Microwave Radiometer) instrument on EOS-PM and ENVISAT (Environmental Satellite). ENVISAT is the European morning sun-synchronous satellite which will provide passive microwave data in the same orbit as the EOS-AM platform. This constellation of instruments will allow a 3-satellite system with CERES/cloud imager/passive microwave instruments on each spacecraft. This suite provides both adequate diurnal coverage as well as greatly increased ability to detect the presence of multi-layer clouds, even beneath a thick cirrus shield. Passive microwave liquid water path will be included in the CERES algorithms in Release 2.

The MISR (Multiangle Imaging Spectroradiometer) and ASTER (Advanced Spaceborne Thermal Emission and Reflection Radiometer) onboard the EOS-AM platform will provide key validation data for the CERES experiment. MISR can view 300-km wide targets on the earth nearly simultaneously (within 10 minutes) from 9 viewing zenith angles using 9 separate CCD (charged coupled device) array cameras. This capability provides independent verification of CERES bidirectional reflectance models, as well as stereo cloud height observations. For broadband radiative fluxes, MISR has better angular sampling than CERES, but at the price of poorer time and spectral information (narrowband instead of broadband). The POLDER (Polarization of Directionality of Earth's Reflectances) instrument planned for launch on the ADEOS (Advanced Earth Observing System) platform in 1996 will also allow tests of CERES anisotropic models using narrowband models. ASTER on the EOS-AM platform will provide Landsat-like very high spatial resolution data to test the effect of MODIS and VIRS coarser resolution data (i.e., beam filling problems) on the derivation of cloud properties.

In September 1994 the LITE (Lidar In-Space Technology Experiment) provided the first high-quality global lidar observations of cloud height from space. These data should be a key source to determine the spatial scale of cloud height variations around the globe, as well as verification of AVHRR/HIRS analysis during NOAA satellite underpasses. In 2002, the NASA GLAS (Geoscience Laser Altimetry System) will provide 3 years of global nadir pointing lidar data for validating CERES derived cloud heights.

A major missing element in the spaceborne measurements is a cloud profiling radar (3-mm or 8-mm wavelength) to be able to measure multiple cloud level cloud base and cloud top heights. Spaceborne cloud radar has been requested as a high priority need by the GEWEX (Global Energy and Water Cycle Experiment) of the World Climate Research Program.

Finally, validation of satellite observations of cloud properties and surface fluxes can be best accomplished using surface and aircraft field experiment data. CERES does not have its own validation program and relies on its science team participation in appropriate field experiments. Members are currently part of the FIRE, GEWEX, and ARM programs. The ARM program of tropical, midlatitude and

polar instrumented sites for 10-year periods will be especially critical for validation of surface fluxes. Aircraft measurements as part of ARM, FIRE, and GCIP (GEWEX Continental-Scale International Project) will be critical to validation of in-cloud properties.

References

- Barkstrom, B. R. 1984: The Earth Radiation Budget Experiment (ERBE). *Bull. Am. Meteorol. Soc.*, vol. 65, pp. 1170–1185.
- Barkstrom, B. R.; and Smith, G. L. 1986: The Earth Radiation Budget Experiment: Science and Implementation. *Rev. Geophys.*, vol. 24, pp. 379–390.
- Baum, Bryan A.; Arduini, Robert F.; Wielicki, Bruce A.; Minnis, Patrick; and Si-Chee, Tsay 1994: Multilevel Cloud Retrieval Using Multispectral HIRS and AVHRR Data: Nighttime Oceanic Analysis. *J. Geophys. Res.*, vol. 99, no. D3, pp. 5499–5514.
- Brooks, D. R.; Harrison, E. F.; Minnis, P.; Suttles, J. T.; and Kandel, R. S. 1986: Development of algorithms for Understanding the Temporal and Spatial Variability of the Earth's Radiation Balance. *Rev. Geophys.*, vol. 24, pp. 422–438.
- Cahalan, Robert F.; Ridgway, William; Wiscombe, Warren J.; Gollmer, Steven; and Harshvardhan 1994: Independent Pixel and Monte Carlo Estimates of Stratocumulus Albedo. *J. Atmos. Sci.*, vol. 51, no. 24, pp. 3776–3790.
- CEES 1994: Our Changing Planet. The FY 1994 U.S. Global Change Research Program. National Science Foundation, Washington, DC, p. 84.
- Cess, Robert D.; Jiang, Feng; Dutton, Ellsworth G.; and Deluisi, John J. 1991: Determining Surface Solar Absorption From Broadband Satellite Measurements for Clear Skies—Comparison With Surface Measurements. *J. Climat.*, vol. 4, pp. 236–247.
- Cess, R. D.; Zhang, M. H.; Minnis, P.; Corsetti, L.; Dutton, E. G.; Forgan, B. W.; Garber, D. P.; Gates, W. L.; Hack, J. J.; and Harrison, E. F. 1995: Absorption of Solar Radiation by Clouds: Observations Versus Models. *Science*, vol. 267, no. 5197, pp. 496–498.
- Charlock, T. P.; Rose, F. G.; Yang, S.-K.; Alberta, T.; and Smith, G. L. 1993: An Observational Study of the Interaction of Clouds, Radiation, and the General Circulation. *Proceedings of IRS 92: Current Problems in Atmospheric Radiation*, A. Deepak Publ., 151–154.
- Coakley, J. A., Jr.; and Bretherton, F. P. 1982: Cloud Cover From High-Resolution Scanner Data—Detecting and Allowing for Partially Filled Fields of View. *J. Geophys. Res.*, vol. 87, pp. 4917–4932.
- Darnell, Wayne L.; Staylor, W. Frank; Gupta, Shashi K.; Ritchey, Nancy A.; and Wilber, Anne C. 1992: Seasonal Variation of Surface Radiation Budget Derived From International Satellite Cloud Climatology Project C1 Data. *J. Geophys. Res.*, vol. 97, no. D14, pp. 15741–15760.
- Gupta, Shashi K. 1989: A Parameterization for Longwave Surface Radiation From Sun-Synchronous Satellite Data. *J. Climat.*, vol. 2, pp. 305–320.
- Gupta, Shashi K.; Darnell, Wayne L.; and Wilber, Anne C. 1992: A Parameterization for Longwave Surface Radiation From Satellite Data—Recent Improvements. *J. Appl. Meteorol.*, vol. 31, no. 12, pp. 1361–1367.
- Hansen, James; Lacis, Andrew; Ruedy, Reto; Sato, Makito; and Wilson, Helene 1993: How Sensitive is the World's Climate? *Natl. Geogr. Res. & Explor.*, vol. 9, no. 2, pp. 142–158.
- Hiedinger, A.; and Cox, S. 1994: Radiative Surface Forcing of Boundary Layer Clouds. *Eighth Conference on Atmospheric Radiation*, pp. 246–248.
- Intergovernmental Panel on Climate Change, 1992: *Scientific Assessment of Climate Change—1992 IPCC Supplement*. Cambridge Univ. Press, p. 24.
- King, Michael D.; Kaufman, Yoram J.; Menzel, W. Paul; and Tanre, Didier D. 1992: Remote Sensing of Cloud, Aerosol, and Water Vapor Properties From the Moderate Resolution Imaging Spectrometer (MODIS). *IEEE Trans. Geosci. & Remote Sens.*, vol. 30, pp. 2–27.
- Lee, R. B.; Barkstrom, B. R.; Carmen, S. L.; Cooper, J. E.; Folkman, M. A.; Jarecke, P. J.; Kopia, L. P.; and Wielicki, B. A. 1993: The CERES Experiment, EOS Instrument and Calibrations. *SPIE*, vol. 1939, pp. 61–71.
- Li, Zhanqing; and Leighton, H. G. 1993: Global Climatologies of Solar Radiation Budgets at the Surface and in the Atmosphere From 5 Years of ERBE Data. *J. Geophys. Res.*, vol. 98, no. D3, pp. 4919–4930.

- Li, Zhanqing; Leighton, H. G.; Masuda, Kazuhiko; and Takashima, Tsutomu 1993: Estimation of SW Flux Absorbed at the Surface From TOA Reflected Flux—Top of Atmosphere. *J. Climat.*, vol. 6, no. 2, pp. 317–330.
- Menzel, W. P.; Wylie, D. P.; and Strabala, K. L. 1992: Seasonal and Diurnal Changes in Cirrus Clouds as Seen in Four Years of Observations With the VAS. *J. Appl. Meteorol.*, vol. 31, pp. 370–385.
- Minnis, Patrick; Kuo-Nan, Liou; and Young, D. F. 1993: Inference of Cirrus Cloud Properties Using Satellite-Observed Visible and Infrared Radiances. II—Verification of Theoretical Radiative Properties. *J. Atmos. Sci.*, vol. 50, pp. 1305–1322.
- Pinker, R. T.; and Laszlo, I. 1992: Modeling Surface Solar Irradiance for Satellite Applications on a Global Scale. *J. Appl. Meteorol.*, vol. 31, pp. 194–211.
- Ramanathan, V.; Subasilar, B.; Zhang, G. J.; Conant, W.; Cess, R. D.; Kiehl, J. T.; Grassl, H.; and Shi, L. 1995: Warm Pool Heat Budget and Shortwave Cloud Forcing—A Missing Physics? *Science*, vol. 267, pp. 499–503.
- Ramanathan, V.; Cess, R. D.; Harrison, E. F.; Minnis, P.; and Barkstrom, B. R. 1989: Cloud-Radiative Forcing and Climate—Results From the Earth Radiation Budget Experiment. *Science*, vol. 243, pp. 57–63.
- Randall, David A.; Harshvardhan; Dazlich, Donald A.; and Corsetti, Thomas G. 1989: Interactions Among Radiation, Convection, and Large-Scale Dynamics in a General Circulation Model. *J. Atmos. Sci.*, vol. 46, pp. 1943–1970.
- Rossow, W.; Garder, L.; Lu, P.; and Walker, A. 1991: International Satellite Cloud Climatology Project (ISCCP) Documentation of Cloud Data. In WMO/TD-No. 266 (Revised), *World Meteorol. Org.*, p. 76.
- Rossow, William B.; and Garder, Leonid C. 1993: Cloud Detection Using Satellite Measurements of Infrared and Visible Radiances for ISCCP. *J. Climat.*, vol. 6, no. 12, pp. 2341–2369.
- Schmetz, J. 1984: On the Parameterization of the Radiative Properties of Broken Clouds. *Tellus*, vol. 36A, pp. 417–432.
- Smith, G. Louis; Green, Richard N.; Raschke, Ehrhard; Avis, Lee M.; Suttles, John T.; Wielicki, Bruce A.; and Davies, Roger 1986: Inversion Methods for Satellite Studies of the Earth Radiation Budget: Development of Algorithms for the ERBE Mission. *Rev. Geophys.*, vol. 24, pp. 407–421.
- Stephens, Graeme L.; and Tsay, Si-Chee 1990: On the Cloud Absorption Anomaly. *R. Meteorol. Soc.*, vol. 116, pp. 671–704.
- Stowe, L. L.; McClain, E. P.; Carey, R.; Pellegrino, P.; and Gutman, G. G. 1991: Global Distribution of Cloud Cover Derived From NOAA/AVHRR Operational Satellite Data. *Adv. Space Res.*, vol. 11, no. 3, pp. 51–54.
- Stuhlmann, R.; Raschke, E.; and Schmid, U. 1993: *Cloud Generated Radiative Heating From METEOSAT Data. Proceedings of IRS 92: Current Problems in Atmospheric Radiation.* A. Deepak Publ., pp. 69–75.
- Suttles, John T.; Wielicki, Bruce A.; and Vemury, Sastri 1992: Top-of-Atmosphere Radiative Fluxes—Validation of ERBE Scanner Inversion Algorithm Using Nimbus-7 ERB Data. *J. Appl. Meteorol.*, vol. 31, no. 7, pp. 784–796.
- Welch, R. M.; Sengupta, S. K.; Goroch, A. K.; Rabindra, P.; Rangaraj, N.; and Navar, M. S. 1992: Polar Cloud and Surface Classification Using AVHRR Imagery—An Intercomparison of Methods. *J. Appl. Meteorol.*, vol. 31, no. 5, pp. 405–420.
- Wielicki, Bruce A.; and Green, Richard N. 1989: Cloud Identification for ERBE Radiative Flux Retrieval. *J. Appl. Meteorol.*, vol. 28, no. 11, pp. 1133–1146.
- Wu, Man L. C.; and Chang, Lang-Ping 1992: Longwave Radiation Budget Parameters Computed From ISCCP and HIRS2/MSU Products. *J. Geophys. Res.*, vol. 97, no. D9, pp. 10083–10101.

Clouds and the Earth's Radiant Energy System (CERES)
Algorithm Theoretical Basis Document

CERES Data Processing System Objectives and Architecture
(Subsystem 0)

CERES Principal Investigators

Bruce R. Barkstrom¹
Bruce A. Wielicki¹

¹Atmospheric Sciences Division, NASA Langley Research Center, Hampton, Virginia 23681-0001

Preface

The investigation of Clouds and the Earth's Radiant Energy System (CERES) is a key part of the Earth Observing System (EOS). This investigation grows from the experience and knowledge gained by the Earth Radiation Budget Experiment (ERBE). The CERES instruments are improved models of the ERBE scanners. The strategy of flying instruments on Sun-synchronous, polar orbiting satellites simultaneously with instruments whose satellites have precessing orbits in lower inclinations was successfully developed on ERBE to reduce time sampling errors. To preserve historical continuity, some parts of the CERES data reduction will use algorithms identical with the algorithms we used in ERBE.

At the same time, much that we do on CERES is new, even though it grows directly from the ERBE experience. To improve the calibration of the instruments, CERES has a much more extensive program of instrument characterization than did ERBE and adds several new components to the ground calibration system. To reduce the errors arising from Angular Distribution Models, CERES will measure these critical parameters by operating the CERES radiometers in a Rotating Azimuth Plane scan mode. To increase the certainty of the data interpretation and to improve the consistency between the cloud parameters and the radiation fields, CERES will include cloud imager data and other atmospheric parameters. Such interpretations are particularly important for testing and improving the General Circulation Models that provide our primary tool for estimating the probable consequences of global warming. CERES will include time interpolation based on observations of time variability observed with Geostationary data. Finally, because clouds are the primary modulator of all of the radiation fields to which the Earth-atmosphere system responds, CERES will produce radiation fluxes at the Earth's surface and at various levels within the atmosphere.

This Algorithm Theoretical Basis Document (ATBD) is one of thirteen volumes that describe the scientific and mathematical basis for the CERES data products. Because of the complexity of the CERES data processing system and the requirements for developing clearly defined interfaces, we have broken the theoretical basis material into separate volumes that correspond with a decomposition of the CERES data processing system. At the top level of this decomposition, the total CERES data processing system is composed of twelve major subsystems. Each of these subsystems produces data products, which are traditionally files, that EOSDIS will have to store, catalog, and disseminate. The subsystems are complex enough that they must be further decomposed in order to avoid misunderstandings. In each of the volumes after this, we have provided a system Data Flow Diagram (DFD) that shows how the other subsystem ATBD's fit into the context of the top-level decomposition. Where we are dealing with the ATBD of a major subsystem, that DFD shows the top-level decomposition, allowing the reader to relate this subsystem to other subsystems in the CERES data processing system. Where we are dealing with the ATBD of one of the components of a decomposed subsystem, the first few pages will contain a DFD that shows the relationship of this process to the other processes at the same level of decomposition.

In the long run, we expect to provide this material to the user community through the NASA Langley Research Center Distributed Active Archive Center (DAAC). With current developments in electronic distribution of information, it is highly likely that when the CERES data flows from the DAAC, the material in this document will be available electronically, perhaps with various hyper-linked access methods. These Release 1.2 ATBD's represent a major step in this direction.

It is clear that the work we have assembled in these volumes is not the work of our hands alone. In addition to the work of the individual authors whose names appear on the title page of each ATBD, these volumes represent contributions from members of the CERES Science Team who are not explicitly identified as authors and from members of the CERES Data Management Team. We are particularly grateful for the work of Peg Snyder and Carol Tolson. These two individuals have suffered through the critical task of shepherding the Data Flow Diagram through what must now be more than fifty versions. They, together with Troy Anselmo and Denise Cooper, have placed it into the CASE tool we are using

for more detailed design work, and from which we can now extract it for publication here. As usual, if this Diagram is not correct, it is our fault, not theirs. Kathryn Bush has provided cheerful help in assembling and coordinating the lists of Acronyms, Abbreviations, and Symbols. Larry Matthias provided the figures showing individual satellite swaths and the synoptic image. Finally, we express our thanks to Von Seaman for being willing to accommodate our willful suggestions on document formatting and for cheerfully helping to copy, collate, and distribute many copies of many versions of these documents.

Bruce R. Barkstrom
Bruce A. Wielicki

Hampton, VA
Nov. 1994

Abstract

The investigation of Clouds and the Earth's Radiant Energy System (CERES) has three major objectives:

- 1. To provide a continuation of the Earth Radiation Budget Experiment (ERBE) record of radiative fluxes at the Top of the Atmosphere (TOA) and of cloud radiative forcing.*
- 2. To produce the lowest error climatology of consistent cloud properties and radiation fields through the atmosphere that we can, based on a practical fusion of available observations.*
- 3. To improve our knowledge of the Earth's surface radiation budget (SRB) by providing a long term climatology of surface radiation fluxes based on better calibrated satellite observations and better algorithms than those currently in use.*

To fulfill these objectives, the CERES data processing system will use four major types of input data:

- 1. Radiance observations from CERES scanning radiometers flying on several satellites over the next 15 years.*
- 2. Radiance data from higher spatial and spectral resolution imagers on the same satellites as the CERES scanners. These imager data are required in order to accurately identify cloud properties, since the CERES scanners have spatial resolutions of about 30 kilometers.*
- 3. Meteorological analysis fields of temperature and humidity from NOAA.*
- 4. Geostationary radiances similar to those of the International Satellite Cloud Climatology Project (ISCCP). We will use these geostationary radiances for improving the CERES time interpolation process.*

The output from the CERES processing system falls into three major types of archival products:

- 1. ERBE-like products which are nearly identical to those produced by the ERBE, including instantaneous footprint fluxes with ERBE-like scene identification, as well as monthly averaged regional TOA fluxes and cloud radiative forcing.*
- 2. Atmosphere products with consistent cloud properties and radiative fluxes, including instantaneous CERES footprint fluxes and imager cloud properties, instantaneous regional average fluxes and cloud properties, 3-hour synoptic radiation and clouds, and monthly average fluxes and clouds.*
- 3. Surface radiation products concentrating on surface radiation budget components with vertically integrated cloud properties, including both instantaneous measurements and monthly averages over 1.25° regions.*

To transform the input data to output, we put the data through twelve major processes:

CERES Instrument Subsystem

- 1. Geolocate and calibrate earth radiances from the CERES instrument*

ERBE-like Subsystems

- 2. Perform an ERBE-like inversion to instantaneous TOA and surface fluxes*
- 3. Perform an ERBE-like averaging to monthly TOA and surface fluxes*

Cloud and Radiation Subsystems

- 4. Determine instantaneous cloud properties, TOA, and surface fluxes*
- 5. Compute surface and atmospheric radiative fluxes*
- 6. Grid single satellite radiative fluxes and clouds into regional averages*
- 7. Merge satellites, time interpolate, and compute fluxes for synoptic view*
- 8. Compute regional, zonal, and global monthly averages*

Surface Radiation Subsystems

- 9. Grid TOA and surface fluxes into regions*
- 10. Compute monthly regional TOA and SRB averages*

Utility Subsystems

- 11. Update the cloud radiance history*
- 12. Regrid humidity and temperature fields*

CERES Data Processing System Objectives and Architecture

0.2. CERES Historical Context

Humankind is engaged in a great and uncontrolled alteration of his habitat. Most scientists expect fossil fuel burning and releases of other trace gases to have long-term climatic consequences. Likewise, some experts have postulated that agriculture and forestry alter the Earth's surface in ways that irreversibly change the climate. In these and many other examples, we understand some of the immediate impacts of man's activities, yet we cannot predict the long-term consequences. One of the major sources of uncertainty lies in the impact of clouds upon the radiative energy flow through the Earth-atmosphere system. The investigation of Clouds and the Earth's Radiant Energy System (CERES) is intended to substantially improve our understanding of these energy flows, clouds, and the interaction between the two. The CERES investigation concentrates on four primary areas: Earth radiation budget and cloud radiative forcing, cloud properties, surface radiation budget, and radiative components of the atmosphere's energy budget. In the four subsections that follow, we provide a more detailed description of our current understanding and data sources in each of these areas.

0.2.1. Earth's Radiation Budget and Cloud Radiative Forcing

The flux of energy from the Sun is nearly constant. The flux of reflected sunlight is much less constant, depending on both surface and atmospheric conditions. The third major component of the energy flow through the top of the atmosphere, the outgoing flux of emitted terrestrial radiation, or longwave flux, is moderately constant. Over very long periods of time, these three components of the radiation budget need to balance. If there is a net flux of energy into the Earth-atmosphere system, the temperature of the planet's surface should increase; if the net flux flows out of the system, it should cool

(Hartmann, et al. 1986). In addition, long-term energy balance of latitudinal bands allows us to place constraints on the energy transfer of the oceans and the atmosphere from the latitudinal distribution of net radiation at the top of the atmosphere (Oort and Vonder Haar, 1976; Barkstrom, et al. 1990). Thus, measuring these three components of the Earth's radiation budget has been a goal of satellite meteorology almost since man began to dream of Earth satellites (Hunt, et al. 1986; London, 1957; House, et al. 1986; Vonder Haar and Suomi, 1971; Raschke, et al. 1973; Jacobowitz, et al. 1984a, b).

With the Earth Radiation Budget Experiment (ERBE) (Barkstrom, 1984; Barkstrom and Smith, 1986), we began to measure this energy flow at the top of the atmosphere (TOA), not just as an undifferentiated field, but with a reasonable separation between clear-sky fluxes and cloudy ones. ERBE measured both the clear-sky fluxes at the top of the atmosphere as well as the fluxes under all other conditions of cloudiness. The difference between the total-sky and clear-sky fields is known as the cloud-radiative forcing (Ramanathan, et al. 1989a, b), or CRF. The CRF is a direct measure of the impact of clouds upon the Earth's radiation budget, and is formally equivalent to the climate forcings caused by other perturbations, such as the increased greenhouse effect of CO₂ or atmospheric aerosols. Based on the ERBE observations, we can separate the CRF into longwave (LW) and shortwave (SW) components. The ERBE observations show that the longwave CRF is positive, demonstrating that in the flow of thermal energy, clouds increase the greenhouse effect. At the same time, the shortwave CRF is negative, more than offsetting the positive longwave forcing. Thus, clouds act to cool the current climate.

With cloud forcing, there are initial hints of unexpected cloud effects. For example, the LW cloud forcing of tropical thunderstorms nearly offsets their SW forcing, a surprising cancellation. Also remarkable is the fact that low-level cloud systems dominate the impact of clouds at all seasons because these systems increase the reflection above what the clear-sky background would give. Perhaps even more surprising is the fact that the shortwave cloud forcing overpowers the longwave for all seasons of the year (Harrison, et al. 1990). It has become clear through a number of studies with General Circulation Models (GCM's) that cloud radiative forcing is the single largest uncertainty in predicting how the Earth's climate will respond to changes in the energy flow through the Earth-atmosphere system (e.g., Cess, et al. 1989 and 1990).

The clear-sky fluxes are also useful by themselves. With them, we can begin to provide an observational baseline for assessing the impact of changes in the Earth's surface and in atmospheric conditions. For example, it may be possible to check if a long-term trend in aerosol concentration has increased the background albedo by comparing clear-sky albedo measurements from ERBE with similar measurements from CERES. Likewise, suspicions that changes in land surface properties have changed the planet's energy budget can be checked by comparing the clear-sky fluxes over the affected portions of the Earth.

Although the ERBE measurements have been very useful to the community, they are far from perfect. Work by the ERBE Science Team during the course of validation suggests that there are four major sources of uncertainty in the radiation budget and CRF measurements:

1. Instrument calibration and characterization
2. Angular Distribution Models (ADM's), which we use to produce flux from radiance measurements
3. Clear-sky identification, which sets the limit on CRF accuracy
4. Time sampling and interpolation

In section 0.6 of this document, we provide a more detailed and quantitative description of the influence of each of these uncertainty sources upon the CERES data products. It is important to understand how

these error sources have influenced the design of the overall CERES approach to producing radiation and cloud products.

The first source of error in TOA fluxes is instrument characterization and calibration. As the reader will find in section 0.6.1, this error source is particularly important in monthly and longer measurements of TOA energy balance. For example, we suspect that shortwave calibration uncertainty is one of the major contributors to the ERBE annual average net flux imbalance of the planet. In CERES, a substantial amount of work has gone into improving the instrument characterization, particularly of our knowledge of the spectral characteristics of the detector optical train and of the calibration equipment. In addition, the shortwave CERES calibration will benefit substantially from replacing the ERBE integrating sphere with a much better understood shortwave source. ATBD subsystem 1.0 is devoted to the CERES instrument subsystem and describes the substantial improvements CERES has made over ERBE.

The second major error source in TOA fluxes is the set of parameters we call Angular Distribution Models. The ADM's enter directly into most uses of the CERES data, because the ERBE and CERES algorithms use the ADM values R directly to produce upwelling TOA fluxes F^\uparrow from the observed radiances I

$$F^\uparrow = \frac{\pi I}{R} \quad (0-1)$$

If the Earth were Lambertian, R would be 1. Unfortunately for the production of fluxes from radiances, the Earth is not Lambertian. Early in the history of radiation budget measurements, investigators used this assumption. However, because the longwave ADM's systematically differ from Lambertian by several percent and because shortwave ADM's differ by factors of four or more, no one would accept this assumption as a useful approximation. Raschke, et al. (1973) introduced ADM's with dependences upon ocean, land, and cloud. The Nimbus 7 ERB scanner made the first systematic angular sampling of broadband radiances. Suttles, et al. (1988, 1989) combined the Nimbus 7 measurements with a cloud categorization based on cloud cover from THIR and TOMS to produce the current generation of ADM's.

During the course of ERBE validation, investigators found several items of concern for the ADM's. For the longwave limb-darkening models, several lines of evidence suggested that the ERBE models had insufficient limb-darkening. For the shortwave models, it appears that better results would be obtained if the models were more limb-brightened. As a result of these considerations, CERES will use a Rotating Azimuth Plane scan mode to resample the angular distribution of broadband radiance. Until we rebuild the ADM's, we will be unable to reduce the systematic errors arising from these critical sets of parameters.

The third source of error in TOA fluxes and cloud radiative forcing arises from scene identification. The ERBE ADM choice is made on the basis of the broadband radiances alone, using a maximum likelihood estimator (Wielicki and Green, 1989). Production of the ADM's is intimately connected with the scene-identification process. The THIR instrument used in the 11- μm window is a reasonable source of information for separating opaque, black clouds high in the atmosphere from the surface. However, THIR is not an ideal data source for more refined questions that the scientific community now considers important in dealing with radiation-cloud interactions. Likewise, the TOMS instrument strongly weighted the blue end of the reflected spectrum. Such a weighting does not give as strong a contrast between clear skies and clouds, nor does it give as much information as narrower spectral bands. CERES requires information obtained from higher spatial and spectral resolution instruments for ADM building, so that the error from these sets of parameters can be reduced. In addition, because of the rapid variations in clouds and radiation, we require nearly simultaneous observations from the same spacecraft. ATBD subsystems 4.1, 4.2, and 4.3 describe the algorithms we need for obtaining a better

physical understanding of the cloud properties from imager data. ATBD subsystem 4.5 describes our current understanding of the ADM construction process.

The fourth source of error that CERES is designed to reduce is that of time interpolation. For the radiation budget fluxes, the most accurate measurements we know how to make are those using broadband scanning radiometers with empirical ADM's. Thus, we require as many of these measurements as we can make. The combination of precessing orbits, such as the equatorial sampling we obtain from the TRMM satellite, with Sun-synchronous polar orbits, such as those we obtain from the EOS-AM1 and EOS-PM spacecraft, provide sufficient sampling to reduce the time interpolation for TOA fluxes to acceptable limits. To reduce the reliance upon mathematical interpolation, we plan for CERES to incorporate geostationary radiances, like those used by the International Satellite Cloud Climatology Project (ISCCP). Such data allow us to reduce the errors in the radiation budget measurements, and provide help in reducing our dependence upon mathematical assumptions about time variability. Subsystem ATBD subsystem 7.0 provides a description of the way in which the geostationary radiances will be used.

0.2.2. Cloud Properties

Although ERBE made the first measurements of cloud radiative forcing, that experiment was not designed to measure cloud properties. The most reliable current measurements of these parameters come from the International Satellite Cloud Climatology Project (ISCCP) (Rossow, et al. 1991). This ambitious project is currently analyzing data from all of the geostationary imagers (except for India's) and using AVHRR data to fill in the polar regions and the Indian gap. The ISCCP algorithms use visible channels (near $0.68 \mu\text{m}$) and window channels (near $11 \mu\text{m}$) from these satellites together with meteorological temperature and humidity fields as input. The ISCCP algorithms infer such cloud properties as regional cloud amount, cloud top altitude and pressure, cloud optical depth, and cloud emissivity. ISCCP also provides a classification of their retrieved clouds, which we show in figure 0-1. As this figure shows, the classification uses cloud top pressure for segregating the cloud types vertically and log of visible optical depth for segregating the cloud types according to reflectivity.

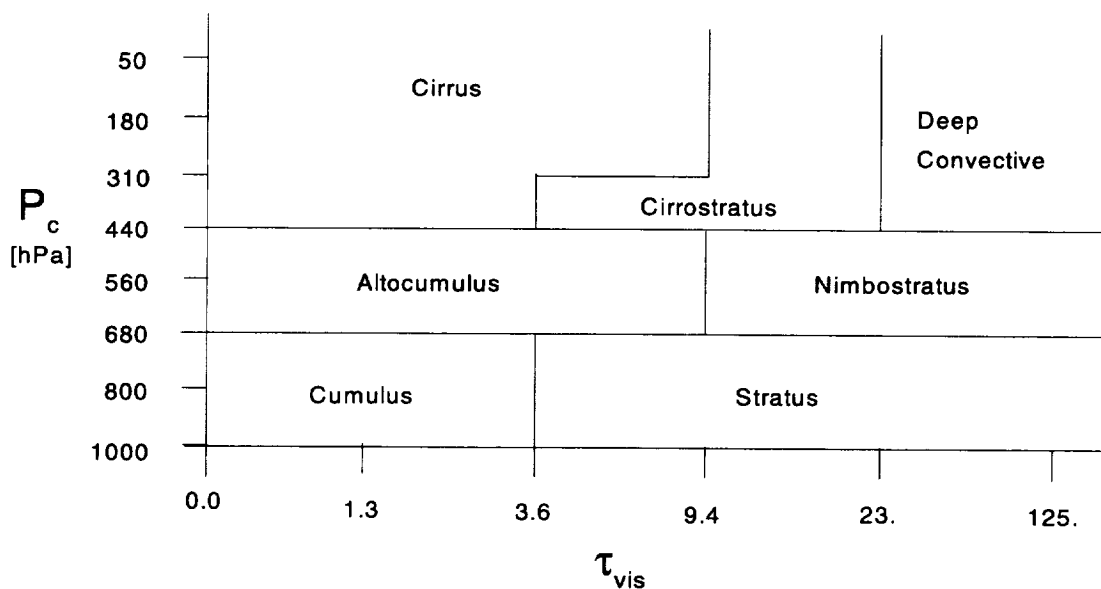


Figure 0-1. ISCCP cloud classification in optical depth, τ_{vis} , and cloud top pressure, P_c (after figure 2.2 in Rossow, et al. 1991). High clouds are those above 440 hPa; middle clouds are those between 680 hPa and 440 hPa; low clouds are those between the surface (1000 hPa) and 680 hPa. The names are traditional.

Table 0-1. ISCCP Cloud Property Retrieval Advances

1. First long-term (>10 year) cloud climatology
2. First global τ_{vis} retrievals
3. First global attempt to correct for nonblack cloud ϵ using τ_{vis} (although HIRS can account for $\epsilon \neq 1$, no previous imager has taken this into account)
4. First global attempt at cloud type classification based on τ_{vis} and p_c
5. First global cloud climatology to input $T(z)$ and $q(z)$
6. First global cloud climatology to use a single consistent radiative model to convert narrowband radiances to cloud properties
7. First global cloud climatology to use the concept of a moving time window to separate clouds from background by using cloud variability
8. First good global cloud diurnal sampling with geostationary samples every 3 hours
9. First attempt to time average cloud properties in a way that attempted to conserve radiative fluxes by using $\ln \tau_{vis}$ weighting

Table 0-1 shows nine areas in which ISCCP made significant advances in cloud property retrievals within the context of a global climatology based on operational satellite measurements. In many cases, the ISCCP algorithms had been tried on a case study basis by other investigators. Due to the difficulties relating to accurate radiometric calibration of spectral radiometers on operational satellites, ISCCP has had to spend significant resources on developing methods of vicarious calibration, calibration stability monitoring, and “drift correction.” Radiative transfer modeling also plays a much more significant role in the ISCCP algorithms than it does in the ERBE measurements for a number of reasons. Particularly important is the fact that there are no empirical ADM’s available for the narrowband radiance measurements that form the core of the ISCCP input data. All of the difficulties associated with accurately modeling radiative transfer in the Earth’s atmosphere appear in the ISCCP algorithms.

To better understand the details of *in situ* cloud properties and their relationship to satellite derived cloud properties, many of the CERES Science Team members have participated in the First ISCCP Regional Experiment (FIRE). FIRE has conducted a series of field campaigns that made surface and aircraft platform measurements of cloud microphysical parameters, liquid water and ice content, lidar and radar cloud height/thickness, as well as surface and atmospheric broadband radiative fluxes. The results of these campaigns has emphasized the importance of a number of ISCCP assumptions and has pushed the community to begin to find ways of improving the cloud property retrievals.

Table 0-2 shows 17 of the most important ISCCP assumptions. In the second column of this table, we show which cloud properties are most likely to be affected by the assumptions. The ISCCP experience and assumptions represent the current basis for cloud climatological work with satellites. Much of the work we do in the CERES cloud retrieval algorithms will be devoted to trying to remove these assumptions. The ATBD volumes associated with subsystem 4, i.e., volumes 4.0, and 4.1 through 4.3 are devoted particularly to the details of how CERES will remove as many of these assumptions as possible. One of the most important impacts of the ISCCP experience is the need to account for the extended spatial scales over which cloud properties are correlated. By using continuity of layering in space, we should be able to distinguish overlapping cloud layers. The cost of removing the limitation of having only a single cloud layer in a pixel is that we have to group many imager pixels together at once to retrieve cloud properties. In CERES, we will account for continuity of cloud layer altitude in time when we interpolate between observations. By doing so, we can substantially improve the physical basis for understanding how clouds interact with the physical climate system.

Table 0-2. ISCCP Cloud Property Assumptions

1. (C_{pixel}) All 4–8 km pixels (AVHRR, Geostationary Satellites) are either totally clear or totally cloud filled, i.e., $C_{pixel} = (0|1)$.
2. All clouds are plane-parallel.
3. (T_c, P_c) Cloud layers have a single temperature.
4. (T_c) All clouds are colder than the surface by 3 K for oceans, 3.5 K for coasts, 6 K for land, and 8 K for polar snow and ice, or mountains;
OR
they are brighter in radiance (specified as a percent of overhead-Sun Lambertian reflectance) by 3% for oceans, and coasts, 6% for land, polar snow and ice, or mountains.
If the brightness temperature or visible radiance exceeds the specified threshold, the pixel is assumed cloud-filled.
5. All surface and cloud properties are constant over the 25 km region represented by each sampled imager pixel.
6. (τ_{vis}) All land and sea ice surfaces are Lambertian in shortwave; ocean surfaces follow the Minnis and Harrison GOES ADM.
7. (ϵ_{win}) All surfaces are black in the longwave.
8. Radiance is too variable for solar zenith angles $> 70^\circ$ to retrieve reliably.
9. (r_e) All clouds are composed of 10 μm effective radius spherical water droplets and come from a Gamma distribution with $\nu = 0.1$.
10. ($\tau_{vis}, \epsilon_{win}$) The 10 μm sphere model gives a relationship $\tau_{vis}^{ext} = 2.704 \times \tau_{LW}^{abs}$.
11. Visible channel radiance radiative transfer includes Rayleigh scattering and O_3 absorption.
12. In the visible, clouds are conservative scatterers, with no water or gas absorption.
13. (τ_{vis}) Aerosols are not explicitly included in visible radiative transfer; they add to the surface reflectance.
14. Window channel radiance radiative transfer includes only water vapor lines and continuum.
15. (ϵ_{win}) Cloud retrievals do not use near IR information at night to correct for $\epsilon_{win} < 1$.
16. IR radiative transfer calculations use $T(z)$ and $q(z)$.
17. Clouds do not scatter in the IR.

0.2.3. Surface Radiation Budget

The surface radiation budget has long been recognized as a fundamental component of our understanding of the way in which the climate system operates. This subject has often been included in studies of micrometeorology (Geiger, 1965; Munn, 1966), as well as in standard works in physical climatology (Budyko, 1982; Budyko, 1974; Sellers, 1965). Because of this importance, there has been a history of establishing ground stations to monitor the radiation budget. However, such programs are not easy to carry over long periods of time. Calibration of field instruments is difficult because of the operating environment, as well as because of the nature of the instruments themselves. In addition, vast portions of the Earth's surface have no fixed facilities. As a result, surface radiation budget climatologies suffer from both measurement difficulties and from spatial and temporal sampling difficulties.

The situation has begun to change in recent years. The World Climate Research Program (WCRP) has established a Global Energy and Water Cycle Experiment (GEWEX) (Chahine, 1992). Under this umbrella, there is a network of surface stations with high quality instruments and well established calibrations called the Baseline Surface Radiation Network (BSRN). The data from this network are being archived at the Swiss Federal Institute as a Global Energy Balance Archive (GEBA) (Ohmura and Gilgen, 1993). In addition, the GEWEX program has established a program to retrieve the surface radiation budget from satellite data. The results from this program are being archived at the EOSDIS Distributed Active Archive Center (DAAC) at NASA's Langley Research Center (Whitlock, et al. 1995).

The algorithms used in this latter effort start with ISCCP data and work with carefully tuned regressions to derive longwave radiative fluxes at the Earth's surface (Darnell, et al. 1992).

There are also new developments in algorithms to derive the surface budget. Cess, et al. (1991) have investigated an algorithm that ties measurements of shortwave flux at the Earth's surface directly to measurements of net shortwave flux at the top of the atmosphere. They have also obtained a moderate number of ERBE measurements that are coincident with measurements of net flux at the Earth's surface. Li and Leighton (1993) have gone on to extend the direct tie between broadband net shortwave flux at the top of the atmosphere and at the surface to a broader range of conditions. They have used this extension to build a climatology of net shortwave flux at the surface over the five years of ERBE scanner data. Likewise, there have been suggestions by Inamdar and Ramanathan (1994) (see subsystem 4.6.2), as well as Stephens, et al. (1994) that similar algorithms can be constructed for longwave surface fluxes.

As with the TOA radiation budget and cloud properties, CERES algorithms for surface radiation budget are the recipient of a considerable body of knowledge and experience in the community. ATBD subsystem 5.0, particularly sections 5.2 and 5.3, provides more detailed discussions of the algorithms, as do portions of ATBD subsystems 4.7 and 2.0. There are two main streams of surface radiation budget in the CERES data processing system. In the "surface budget" portion, we expect to record the results of algorithms that depend most heavily upon the broadband CERES measurements, using the Li-Leighton and Inamdar-Ramanathan algorithms. We will also include these algorithms in the "ERBE-like" processing stream. In the "atmosphere" portion of the stream, we will include more sophisticated radiative transfer calculations. The simpler algorithms produce net flux or limited versions of the flux components at the surface. The radiative transfer algorithms produce all of the flux components, but do require more input information regarding the atmosphere and the surface.

0.2.4. Radiative Components of the Atmospheric Energy Budget

This section contains a substantial contribution of A. J. Miller of NOAA's National Centers for Environmental Prediction, whose contribution is gratefully acknowledged.

The fourth and final component of scientific background that bears on the CERES data processing is the energy budget of the Earth's atmosphere. This subject was a classic study of post-World War II meteorology. Figure 0-2 shows an estimate of three components of the atmospheric energy budget taken from figure 2.2 of Palmén and Newton's (1969) widely known book on atmospheric circulation. This figure shows the radiative energy loss, the latent heat source, and the resulting atmospheric kinetic energy that must be expended to hold the atmosphere in energy balance over the latitude belt from 32°N latitude to the North Pole. The values in this figure are stated as energy flux differences [in $\text{W}\cdot\text{m}^{-2}$] between the top and bottom of atmospheric layers with pressure differences of hPa. We can see that radiation serves as an energy loss at all altitudes, and declines less rapidly with altitude than does the latent heat source. This early work was brought to a classic summary in the work of Lorenz (1967) which emphasized the role of such energy flows in generating and dissipating kinetic energy of the general circulation.

Studies of the energetics of atmospheric circulation have often been used as diagnostics of atmospheric circulation models (Piexoto and Oort, 1992). The concept of atmospheric potential energy was first put forth by Lorenz (1955). Physically, he explained that the atmosphere, by virtue of its temperature structure, contains potential energy that can never be transferred into kinetic energy. It is only when this basic state is perturbed that the deviations can be transformed into the wind fields. As an example, the general heating in the tropics and cooling in high latitudes perturbs the basic state of zonal potential energy, creating zonal available potential energy which is then converted into zonal kinetic energy.

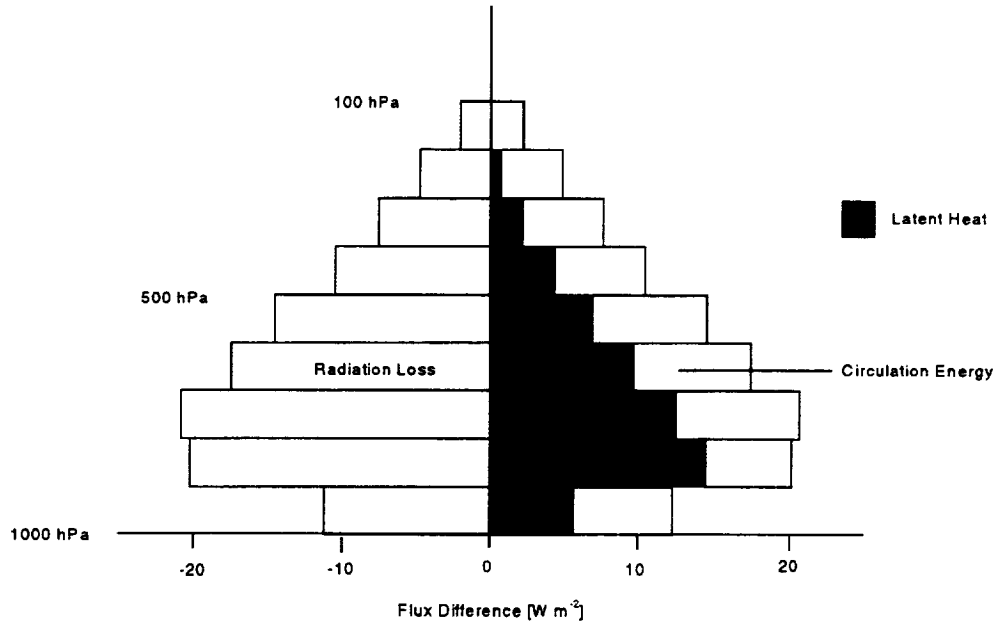


Figure 0-2. Classic picture of the atmospheric energy balance in winter from 32°N to the North Pole following Figure 2.11 of Palmén and Newton (1969). The atmosphere is divided into 100 hPa layers, with the surface at 1000 hPa. Radiation removes energy from all layers of the atmosphere, as shown by the negative values of flux difference. The total energy removed from the atmosphere by this sink of energy is about 110 W·m⁻² that emerges as longwave flux from the top of the atmosphere comes directly by transmission from the surface. The filled rectangles indicate the contribution latent heat was believed to make to each layer's energy balance. The remaining energy needed to make up the deficit between the radiative loss and the latent heat gain must come from atmospheric circulation energy, which is shown by the unfilled rectangles on the right side of the vertical axis.

Mathematically, the relationship of zonal and eddy available potential energy A_Z and A_E respectively to the generation terms is written in the following form

$$\frac{dA_Z}{dt} \approx \overline{[Q]''[T]''} \quad (0-2)$$

and

$$\frac{dA_E}{dt} \approx \overline{[Q^*T^*]} \quad (0-3)$$

Here, Q is the local heating rate and T is the atmospheric temperature. The square brackets represent zonal averages of the assigned quantities, the asterisks represent the deviations from the zonal average, and the double primes represent the deviations from the overall average. Thus, we see that available potential energy is generated when a positive correlation exists between the heating and the temperature. Physically, of course, this makes sense, if warm air is being heated it is being driven away from the mean state and vice-versa.

From the perspective of the influence of clouds on the generation of available potential energy, one can consider the effect of clouds to be a perturbation on the clear-sky heating. In such a case, the radiation part of the local heating rate in the above equation Q_r can be written as:

$$Q_r = Q_c + Q_w \quad (0-4)$$

where Q_c is the clear-sky heating and Q_w is the perturbation from clouds, which is a function of the cloud properties (Stuhlmann and Smith, 1988a or 1988b). Overall, clouds redistribute the vertical

heating profile, with the longwave greenhouse effect competing with the shortwave albedo effect. Thus, clouds can have strong localized impacts on the generation of available potential energy.

Q_w is a complex function of location, cloud type, and optical thickness. As an example, Stuhlmann and Smith (1988a or 1988b) present the following scenario to demonstrate how Q_w impacts the available potential energy during an El Niño episode. During the cold episode, the longwave greenhouse effect of the stratus is dominated by the albedo effect off the west coast of South America, and Q_w is negative. This results in a reduction of the generation of A_Z and the Hadley Cell. In the warm episode, the stratus off the west coast of South America transforms to thick cumulus and increases Q_w and A_Z . At the same time, the warm sea surface temperature on the subsiding branch of the Walker circulation is still higher than that over the Eastern Pacific and out of phase with the strong convective heating over the Eastern Pacific. The generation of A_E is weakened and is a stabilizing feedback in reducing the Walker circulation.

There have been many studies of the effects of changes in cloud properties upon atmospheric circulation. Section 5.2.2 of ATBD subsystem 5.0 discusses several such studies. However, there appear to have been relatively few quantitative studies of the influence of clouds on atmospheric energetics. The papers by Stuhlmann and Smith (1988a and 1988b) appear to be two most directly related to this study. In dealing with the question of atmospheric energetics, it is important to distinguish between Cloud Radiative Forcing and energetics of the circulation (Barkstrom, 1992). CRF refers to the relationship between clear and cloudy sky fluxes averaged over the entire Earth and used in understanding the potential for changing the Earth's surface temperature. The relationship between cloud changes and atmospheric energetics relates to the way in which clouds change the atmospheric heating and cooling that drives the circulation. As Stuhlmann and Smith note, "It is the vertical and horizontal distribution of the total diabatic heating which determines the energy conversion and the dynamic structure of the atmosphere. To understand how a change in cloudiness will affect the general circulation and therefore [. . . changes in the general circulation], it is necessary to estimate the structure of the cloud-generated diabatic heating field. The field then can be related to the concept of available potential energy. . . which is generated by the distribution of the diabatic heating field and is then converted to kinetic energy. The cloud-generated available potential energy is a measure of the intensity of the general circulation due to cloudiness, and a change in cloudiness can be related to a change in that intensity."

Stuhlman and Smith's study was theoretical in nature and used the zonal structure of the temperature and diabatic heating fields. However, we know that there are important variations in cloud and heating fields with both longitude and latitude. The usual studies of atmospheric energetics depend upon radiative calculations that use many of the same assumptions we have already listed for ISCCP. Because of the sensitivity of the atmospheric circulation to the assumptions in these calculations, it is of fundamental importance to provide empirical guidance regarding the true state of the atmosphere. It is particularly important to recognize that the layering of cloud properties and the variability of cloud optical properties are not well represented in current operational or climate models of the atmospheric circulation. Thus, the new information CERES will provide about the spatial and temporal structure of the cloud fields and the corresponding radiative heating is important. In this regard, the most important field to understand correctly is probably the field of longwave radiative flux. The vertical variations in this field are currently thought to be dominated by the discontinuity in net flux at the tops of cloud layers (particularly for optically thick clouds). CERES data should identify these cloud tops well, and will provide a very useful start to improvements in understanding atmospheric energetics.

0.3. CERES Objectives

As we have seen, there is a fundamental need to ensure that radiation budget measurements and cloud properties are measured simultaneously and that they remain consistent at all the scales of time and space at which we produce the data. ERBE, ISCCP, and the SRB Project as well as numerous other

attempts to produce climatologies of clouds and their radiative impact have so far not been able to reach a single consistent picture of clouds and their impact on radiation. ERBE produced a highly reliable, consistent, and accurate measure of the radiation fields. It also used empirical observations of the Angular Distribution Models, circumventing difficulties associated with relying on theoretical angular distributions. However, ERBE was forced to rely on a scene identification algorithm that used instruments with insufficient spectral and spatial resolution to provide reliable cloud properties. The ISCCP measurements are better designed for cloud retrievals. However, they do not include highly accurate radiation measurements. The SRB Project relies on instruments that do not have absolute calibration and do not have measurements of the ADM's that would directly relate the measured radiances to fluxes. In short, the current radiation and cloud projects fall short of producing the consistent ties between radiation and clouds that the community needs in order to advance the understanding of how to properly include these parameters in the models we use to estimate how the climate will respond to various forcings.

To remedy these shortcomings, the investigation of Clouds and the Earth's Radiant Energy System (CERES) has three major objectives:

1. To provide a continuation of the ERBE record of radiative fluxes at the Top of the Atmosphere and of TOA cloud radiative forcing
2. To produce the lowest error climatology of consistent cloud properties and radiation fields (TOA, surface, and within the atmosphere) that we can based on a practical fusion of available observations
3. To improve our knowledge of the Earth's surface radiation budget by providing an additional long term climatology of surface radiation fluxes based on better calibrated satellite observations and better algorithms than those currently in use

Let us briefly discuss the meaning and implication of each of these objectives.

First, CERES will continue the ERBE measurement record. This objective is important because it will allow the scientific community to look for changes in three fundamental fields: the field of total-sky fluxes, the field of clear-sky fluxes, and the fields of cloud radiative forcing. From the total-sky flux, we can examine the constraint on total energy flux transport in the Earth-atmosphere system. With the clear-sky field, we can look for possible changes from ERBE in the radiative impact of changes in surface properties and in aerosol radiative forcing. With the cloud radiative forcing, we can look for possible changes associated with cloud feedback, as well as the overall stability of the CRF established by ERBE. Such a continuation places considerable emphasis on monthly and regionally averaged data products. It also requires that we maximize the homogeneity of the CERES ERBE-like products in terms of calibration, time-sampling, and algorithms.

Second, CERES will produce data products that maximize the consistency between the cloud properties and the radiation fluxes throughout the atmosphere. Such data products will do much to improve GCM parameterizations of clouds and radiation. They will provide many instances of particular kinds of clouds that have consistent measurements of radiative fluxes. These data will also provide the ability to study the evolution of cloud properties and radiative perturbations, where the clouds and radiation act together on such systems. The long-term climatology of such systems will help diagnose the forcing and response behavior of the climate system. Finally, these products will contribute to a more accurate energy balance diagnosis of the atmospheric circulation, wherein we may hope to improve our understanding of the relative roles of radiation and latent heat.

For this second major portion of the CERES investigation objectives, there are four major sources of input data:

1. CERES instrument data which will provide the fundamental radiometric calibration and the empirical Angular Distribution Models we use to deduce flux from radiance
2. VIRS and MODIS cloud imager data that we use to determine cloud properties
3. NOAA meteorological analysis fields of temperature and humidity that provide an underlying background of information, although we expect to bring these fields into agreement with the radiative observations
4. Geostationary radiances, which will provide fundamental data on time variations in the field after suitable calibration with the CERES instruments and being interpreted with the help of the CERES ADM's

We expect to enforce consistency between the clouds and radiation at several points in the processing of the data: at the instantaneous CERES footprints, where we insist on consistency between the cloud properties and the CERES fluxes; at the hourly regional average, where we insist on the same kind of consistency, but over a more extended spatial scale; and in time interpolation and temporal averaging, where we want to ensure that the cloud properties and radiative fluxes are sensitive to the time variations disclosed by the geostationary observations. Later in this ATBD, we will discuss the specifics of the kinds of data we will produce in this part of the CERES processing system.

Third, CERES will improve the record of surface radiation budget using the CERES instrument radiometry and improved algorithms based on the use of the TOA fluxes from the CERES instruments. Such improvements are very important for improving our understanding of the energy and latent heat budgets at the Earth's surface.

0.4. CERES Processing System Architecture—Overview

A system to implement the CERES objectives represents a major step forward, yet does not involve fundamentally new principles. Rather, such a system requires close integration of the parts and careful attention to the logistics of data processing. In the next few sections of this ATBD, we want to describe our current understanding of the architecture of a system that will produce data products meeting the objectives. We may think of this system as having three major functions:

1. Producing ERBE-like products
2. Producing atmosphere products
3. Producing products for surface radiation budget and cloud feedback studies

Shortly, we will describe the working decomposition of CERES data processing into 12 subsystems. We usually represent this decomposition in the form of a Data Flow Diagram, which shows the relationship between the data products and the subsystems that produce them.

Individuals with particular interests can find which of the ATBD subsystem volumes contains the material they want to see. However, because there are common threads to various aspects of the processing that are not integrated within the individual ATBD subsystems, this document provides a summary description of the way in which the system works as a system. For example, the data products are systematically arranged according to time and space intervals to make working with the data easier when we get into operations. By describing these features of the products in this volume, we hope to provide better comprehension of what the CERES processing system does. Similarly, we provide a more detailed description of the ERBE-like algorithms which lays out the fundamental structure of inversion and scene identification we have used in the past. Then, we go on to describe how this set of concerns is modified and extended in the more complex CERES cloud identification context. In the

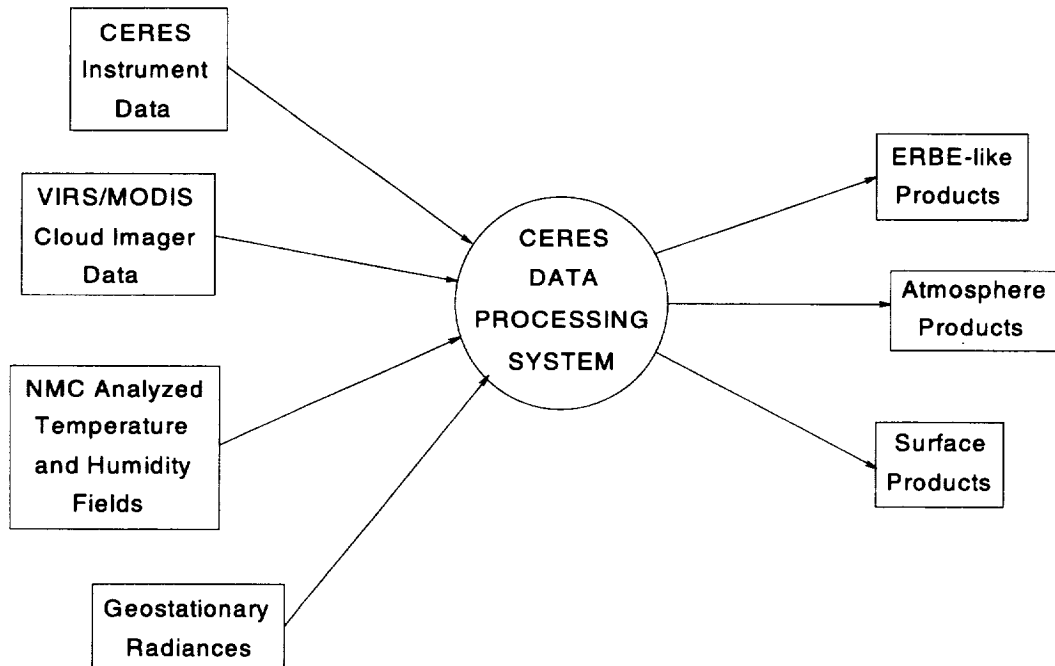


Figure 0-3. Overall context of CERES data processing. The four major kinds of input data appear on the left; the three major kinds of output products appear on the right.

same way, we describe the ERBE-like time averaging algorithms to lay the groundwork for the extension into the CERES context, where we need to preserve consistency between the TOA radiation fluxes and the cloud properties. In addition to the scientific concerns that we have to deal with in fitting disparate algorithms together, we also describe some of the operational considerations that have shaped both the data products and the functional decomposition. In the last major sections of this ATBD, we provide a more explicit description of the implementation issues, including a summary of data product sizing, quality control products, and data processing operations.

0.4.1. Processing System Context

Figure 0-3 shows the overall context of the CERES data processing system. This system accepts four major kinds of input data:

1. CERES instrument data, including radiometric, housekeeping, ephemeris, and attitude data
2. VIRS and MODIS cloud imager data, calibrated and Earth located
3. NMC analyzed fields of temperature and humidity, providing vertical profiles of these fields over the entire Earth at least once every 12 hours
4. Geostationary radiances in visible and window channels every three hours

The CERES processing system carefully calibrates, Earth locates, and interprets these data to yield the desired output products.

We can categorize each of the output products as falling into one of three categories:

1. ERBE-like products, which are primarily shortwave and longwave radiative fluxes at the top of the Earth's atmosphere. These products supply continuity with the historic ERBE record of TOA fluxes and cloud radiative forcing.

2. Atmosphere products, which include instantaneous, synoptic, and monthly averaged radiative fluxes and consistent cloud properties on spatial scales that range from CERES footprints to global averages. These products supply the most detailed information we can produce on the interaction between radiation and clouds. With the instantaneous CERES footprint data, we provide the simplest connection between radiation and clouds. With regional data, we provide modelers with the ability to check parameterizations against particular kinds of cloud situations. With monthly average products, we provide data for diagnosing the radiative contribution to the atmospheric energy balance.
3. Surface products, which contain shortwave and longwave radiative fluxes at the Earth's surface, together with vertically averaged cloud properties. These less voluminous products supply data with homogeneous sampling and data reduction, from which investigators can build reliable climatologies of the Earth's surface radiation budget.

With this context, we will describe the functional decomposition of the system. As a basic design philosophy, we decomposed the scientific functions into more manageable subsystems with clearly defined data product interfaces. Each subsystem then deals with data having relatively homogeneous space and time scales. A subsystem also makes a smaller set of transformations than does the overall system. Thus, by providing a careful functional decomposition, we make the system design work easier. By assigning data products to be the interfaces between the functions and by defining these interfaces in full detail as early as possible, we markedly increase the probability of having a stable and robust design.

0.4.2. CERES Data Product Summary

Table 0-3 summarizes the properties of the CERES data products as individual logical files. The product identifier is provided in more detail in the description of the major portions of the processing subsystems described below. We can see that there are a relatively small number of spatial organizations: 24-hour satellite swaths, 1-hour satellite swaths, geographic regions, and global data sets. One of the most important distinctions we will discuss in more detail here and in the other ATBD subsystem descriptions lies in the differences between the spatial scale of imager pixels (about 1 km), CERES footprints (about 25 km), ERBE-like geographic regions (about 250 km), and CERES geographic regions (about 140 km). In most of the single hour data products, we have data organized within CERES footprints along the satellite swath. The data product *FSW* is an anomaly in that it is organized by Earth-fixed geographic regions (about 1.25° in latitude and longitude) that were visible in a single hour's satellite swath. These data products also have a temporal organization that is broken into a small number of categories: 1-hour data products, 24-hour data products, 3-hour synoptic products, and 1-month products. As we examine the data flow diagram, we will see that small spatial scales tend to occur with data products that cover small intervals of time. For example, monthly products cover the globe at a fairly coarse spatial scale. The data product file (or granule) size is not a clear function of the space or time organization, and varies widely.

0.4.3. Processing System Decomposition

There are several reasons why we need to provide a more detailed breakdown of the CERES functions. Certainly, there is a need to segregate activities and data structures to a greater degree than what we have available in the context diagram. A more important rationale is that we want to match the space and time scale of the algorithms to the data on which they operate. Some functions apply only to the highest resolution instantaneous data; others are only appropriately applied when we are trying to understand the larger space and time characteristics of the cloud and radiation fields.

Table 0-3. Properties of Major CERES Data Products

Product	Spatial Organization	Time Coverage	Product Size, MB
CERES Instrument Subsystem Products			
INSTR: CERES Instrument Packets	N/A	24 Hours	87.0
EPHANC: CERES Ephemeris and Attitude Data	S/C Orbit	24 Hours	0.1
BDS	Satellite Swath	24 Hours	240.8
IES	Satellite Swath	1 Hour	15.0
ERBE-Like Products			
EDDB	Regional	1 Month	29.3
ES8	Satellite Swath	24 Hours	217.8
ES9	Regional	1 Month	104.2
ES4	Regional	1 Month	27.6
ES4G	Global	1 Month	24.5
Atmosphere Products			
TRMM CID	Satellite Swath	1 Hour	71.1
MODIS ID	Satellite Swath	1 Hour	1992.8
MWP	Global	1 Day	3.6
ASTR	Global	1 Hour	10.5
SURFMAP	Global	1 Day	82.8
CRH	Global	7 Days	92.0
CRHDB	Global	7 Days	92.0
SSF	Satellite Swath	1 Hour	154.0
CRS	Satellite Swath	1 Hour	216.8
FSW	Satellite Regional	1 Hour	4.0
GEO	Global	15 Days	5.1
SYN	Global	3 Hours	35.2
AVG	Global	1 Month	283.7
ZAVG	Global	1 Month	3.0
Surface Radiation Products			
SFC	Satellite Swath	1 Hour	2.3
SRBAVG	Global	1 Month	533.7
Atmospheric Property Inputs			
MWH	Global	1 Day	TBD
APD	Global	1 Day	TBD
GAP	Global	6 Hours	TBD
OPD	Global	1 Day	TBD

0.4.3.1. CERES time intervals. One of the continuing themes that we find operating across the entire CERES processing system is the need to describe the time variability of the fields with three major spans of attention. At the shortest time, we have the sampling time of individual measurements. This time scale is about 10 msec for the CERES scanner sampling and two orders of magnitude smaller for the imager data. For these kind of sampling times, what matters to us is not the time difference from

one sample to the next, but the spatial separation between the measurements. We refer to such short time intervals as “instantaneous.”

At the next level of time discrimination, we have time divided into 1-hour intervals. There are several reasons for considering data at this time resolution. First, it is a reasonable portion of a day for contributing to a daily average. Second, it is a small enough time that the large scale features of the cloud and radiation fields do not change too much over the interval. Thus, we are able to correct for the motion of the Sun while still bringing the observations to a common time half-way through the hour. Third, an hour interval allows us to create “image-like” data structures in which the CERES footprints are arrayed over the Earth without having to worry about overlapping data from one orbit to the next. Finally, an hour interval provides a direct tie to the averaging interval we used in ERBE, enhancing the comparability of the new data set with the old.

The CERES data products introduce a new interval of time that was not present in the ERBE data: a uniform synoptic time spacing of 3 hours. This new time interval allows us to make the time averaging algorithms more regular. It also provides us with a chance to inform the time interpolation algorithms of the time variations found in the geostationary radiances. Thus, the CERES time interpolation will take advantage of new data about time variations, rather than relying wholly upon simple mathematical interpolation formulas or upon complex integrations of the equations of motion. Both of these interpolations have adherents in the community. In ERBE, we used simple mathematical interpolations with some corrections for systematic temporal behavior. Other members of the community prefer the confidence that comes from applying formulations derived from mass and energy continuity. For CERES, we prefer to rely on observations, avoiding overly simple mathematics or upon derivations that rely on physics that may not describe the formation, evolution, and dissipation of cloud systems.

The CERES processing system also recognizes the importance of a 24-hour diurnal interval, particularly for dealing with the variation in incident sunlight. Systematic diurnal cycles are also possible for the longwave field, particularly in the ERBE-like processing portion of the CERES system. There, the time interpolation and averaging algorithms allow the time variation to adjust to a time variation similar to one inferred from geostationary observations.

Finally, all three “branches” of the CERES processing system produce monthly averages. Such level 3 products are important to the atmospheric community for several reasons. First, they provide a sufficiently long time period that the radiative influence on the atmosphere can be fully included in summaries of the data. Second, they provide a useful climatology, being substantially reduced in data volume from the original data sources. Indeed, a substantial portion of the work done with the ERBE data so far has been done with monthly averages.

0.4.3.2. CERES spatial sampling. The CERES processing system also contains several discrete spatial scales. One of the most important considerations in the decomposition of the total processing system has been to identify the point at which we move from one spatial scale to another.

At the shortest spatial interval, we have the resolution of the cloud imager pixels. MODIS has a finer resolution, 0.25 km in the shortwave part of the spectrum, than does VIRS with about 2 km. Although clouds do have significant structure at scales down to perhaps km, we believe that the VIRS/MODIS spatial resolution is sufficient to account for most of the features that influence the radiation fields.

The next larger spatial scale that interests us is the CERES footprint size. This spatial scale varies with the viewing zenith of the scanner footprint. At nadir, the half-power point of the footprint on the EOS-AM1 spacecraft will be about 20 km. As the footprint approaches the limb, that size increases to about 125 kilometers before it becomes impractical to invert the data. As we will see later, the connection between the CERES radiances and the imager data is mediated by the CERES Point Spread Function (PSF). This function gives us the angular sensitivity of the CERES measurement to a radiating

object in the field of view. The PSF is not rectangular or circular; rather it is roughly Gaussian, showing the effect of the time delay and smoothing of heat transfer in the detector and electronic filtering of the analog signals in the detector signal processing. ATBD subsystem 4.4 section 4.4.2.1 contains a description and derivation of the PSF. In ATBD subsystem 4.4, we are very careful in our description of how to maintain consistency between the CERES data and the cloud properties at all spatial scales as large as or larger than the CERES footprints.

To make the data useful for large-scale climate purposes, we cannot stop at the CERES footprint spatial scale. The next largest scale of interest to us is a 1.25° (or 140 km) region of latitude and longitude. For the ERBE-like processing, we will retain a region size about a factor of two larger. However, the philosophy of spatial averaging remains the same. We make a clear transition at the *FSW* product from data organized with respect to the satellite scan sampling pattern to data organized with respect to the Earth. In the ERBE-like part of the processing, this transition occurs in the inversion subsystem (process 2 of the main Data Flow Diagram), where the input data are organized by scan lines and the output in the ERBE-like Daily Database (EDDB) is organized by Earth-fixed regions with a spatial scale of 2.5° in latitude and longitude. The regional spatial organization is the fundamental one for the monthly averaging portion of the system. The largest scales that we use in the CERES data processing are those in the summary monthly averages that go from regions to zonal and global averages.

0.4.3.3. The CERES processing system data flow diagram. Figure 0-4, is the top level data flow diagram for the CERES processing system. It shows the major processes as labeled circles and the basic data products as either rectangles or pairs of horizontal lines. In this figure, we show all of the processes that must operate to produce monthly averaged data products and processes whose data files must be updated within a month to derive these products.

For example, to produce a monthly average ERBE-like product, ES4, we need CERES instrument data that goes through processes 1, 2, and 3. To produce a monthly average radiation and cloud product, we have to receive CERES instrument data, imager data, NMC temperatures and humidities, and geostationary data. As part of the cloud property determination, we have to update the clear-sky radiance history once a week.

In this figure, we do not show processes that occur on a sporadic basis, such as updating calibration coefficients or producing ADM's. Although each CERES instrument will have a calibration sequence about once every two weeks, the ERBE experience strongly suggests that we plan not to make routine updates to the instrument gains or offsets. In the case of the ADM's, we will only update these coefficients once, after several years of observations. Such an update is NOT a part of the routine monthly processing, which is what we show in this figure.

We also do not show the subsidiary files, such as calibration coefficients, ADM's, DM's, spectral correction coefficients, etc. In many cases, we need to coordinate the configuration management of these files. However, they are updated only occasionally. The section of this ATBD dealing with implementation issues suggests our philosophy of handling configuration management of these files.

0.5. CERES Processing System Architecture Detailed Systems Engineering

In this section of the CERES System ATBD, we describe the processing system products and processes in a moderate level of detail. Here, we want to provide a systems engineering overview of these products and processes. In other words, we want to ensure that we have arranged the subsystems so that they will accept the input data and create the proper data products. When we move to semiautomated production, we do not want to miss the major portions of the processes that we need. We also want to be sure that we have not designed inconsistent interfaces.

In doing this detailed examination, we also have a chance to identify and follow some common threads through the system. The detailed ATBD descriptions are not easy to follow. The authors deal

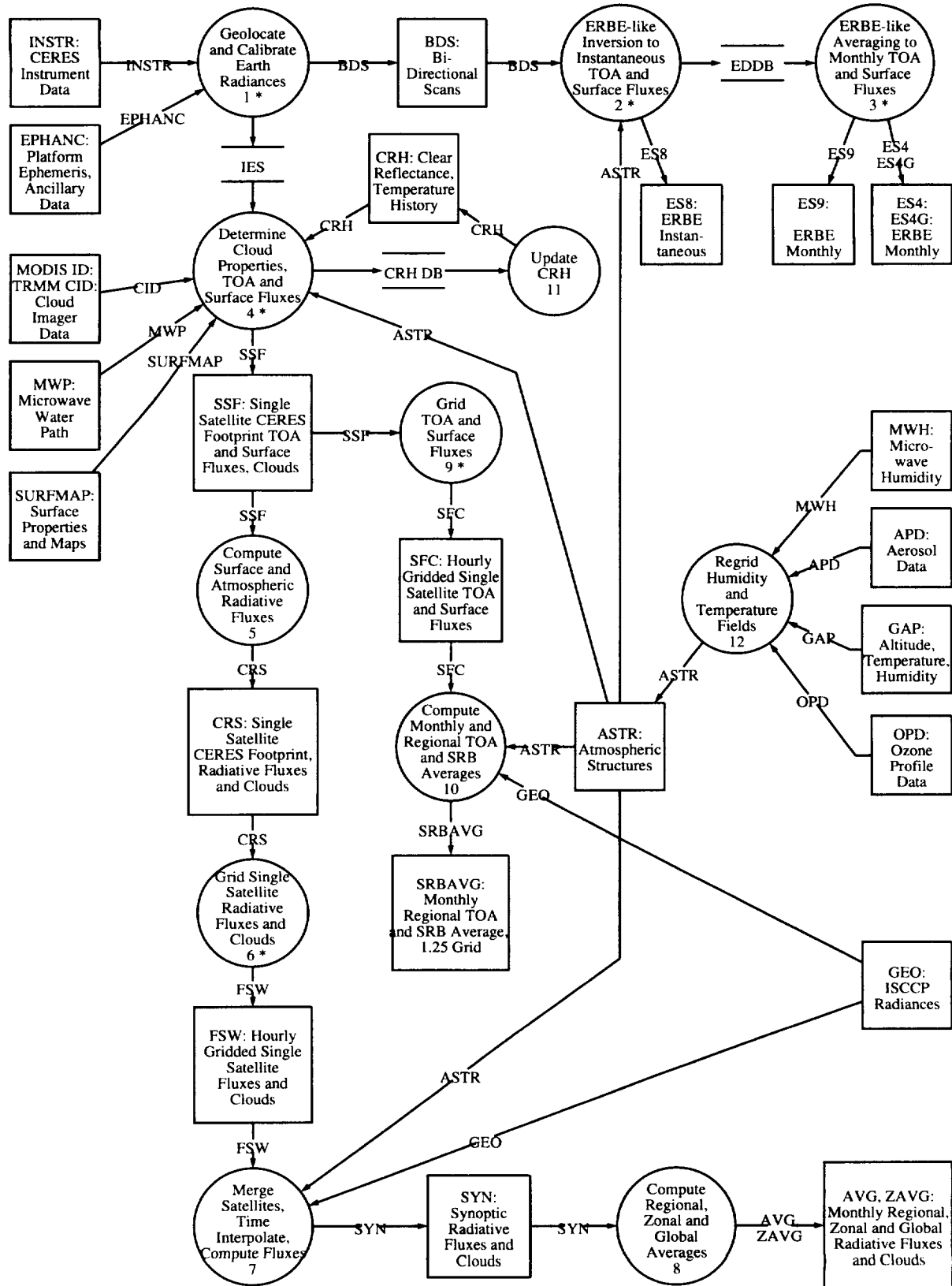


Figure 0-4. CERES top level data flow diagram.

with a specialized area of endeavor—instrument calibration or cloud property determination or time averaging. Here, we use figures to show the sequence of processes, since they make it easier to envision the structure of the data products. Visualization also decreases the probability of errors in designing these data products.

We start with the instrument subsystem, at the extreme upper left of the data flow diagram (figure 0-5). For this subsystem, we describe the major input data sources and then the major output data products. After this is done, we discuss the core features of the algorithms in this area. This structure of discussion is common to all of the subsystems:

- CERES Instrument Subsystem
- ERBE-like Subsystems
- Atmosphere Subsystems
- Surface Radiation Subsystems

A much fuller description of the algorithms and data products is in the appropriate sections of the ATBD's.

0.5.1. CERES Instrument Subsystem

The CERES instrument subsystem is the precursor to all parts of the CERES processing system. The input data are organized in packets which we process in time order. We require this time ordering because we must remove instrument drift by interpolating between observations of space. Once we have produced filtered radiances, we reorder the spatial organization of the footprints.

0.5.1.1. Major inputs. The INSTR (CERES Instrument Packets) product is a 24-hour collection of data packets from a single CERES instrument. The first packet in this product is the first packet whose beginning time started after 0^{HR}U.T. of a given day. The last packet is the last packet for the instrument that started before 24^{HR} of that day. These packets are ordered in increasing time sequence during the day. The packets may contain housekeeping data, radiometric data, scan position data (such as the elevation or azimuth of the scanning mechanism), or other kinds of status information.

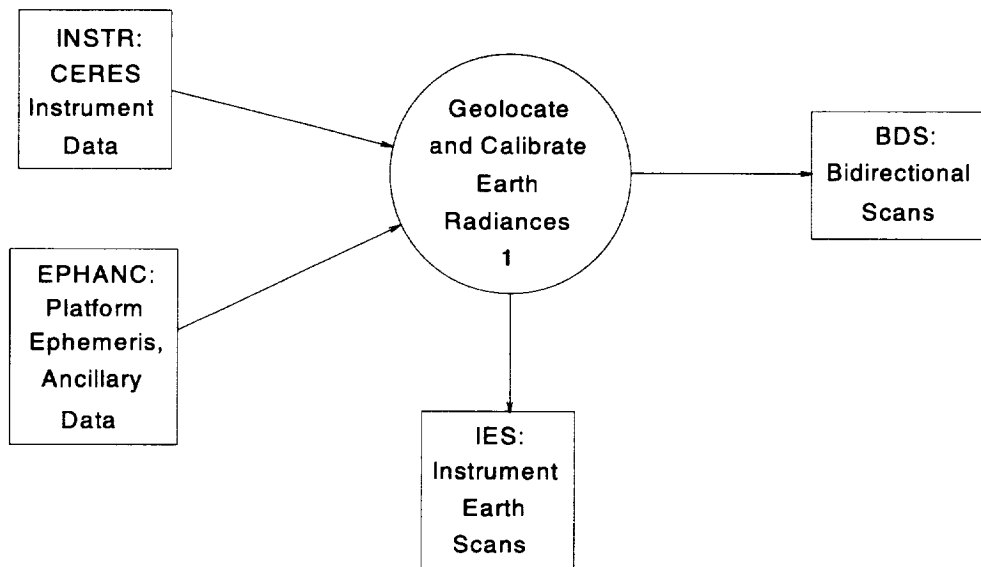


Figure 0-5. Major data products and processes for CERES instrument subsystem.

The EPHANC (CERES Ephemeris and Attitude Data) product is also a 24-hour collection of spacecraft position and attitude. Again, the day starts at 0^{HR}U.T. and ends at 24^{HR}U.T. The ephemeris gives the spacecraft position as X , Y , and Z and with appropriate orbital elements at fixed time intervals during the day. The attitude data give the spacecraft roll, pitch, and yaw, as well as the time derivatives of these three quantities, at the same time intervals. If these data are like ERBE's, they will be provided by the Flight Dynamics Facility at Goddard Space Flight Center (GSFC) at a time interval of one minute.

0.5.1.2. Major outputs. The BDS (Bidirectional Scans) product is a 24-hour collection of raw and converted CERES data from a single CERES instrument. This product is intended as a restart data source, so BDS contains all of the data in INSTR. In addition, the BDS product carries filtered radiances and their locations in colatitude and longitude. The data are ordered into second scans that allow us to easily find the space observations that give the zero radiance reference for the radiometric data.

The IES (Instrument Earth Scan) product is a set of CERES footprint values whose organization is spatially ordered. Because the CERES data have a much lower resolution than the cloud imager data, it is useful to preorder the CERES footprints before attempting to merge that data with the imager information. Even when the CERES scanner operates in a cross-track mode, the CERES scan lines are not necessarily orthogonal to the suborbital track. In the rotating azimuth plane scan (RAPS) mode, temporally ordered data are not spatially contiguous; spatially contiguous data are not temporally close together. We sort the CERES pixels according to their distance along the orbit. Then, we take all of the pixels whose field-of-view axis has an equivalent longitude (along the orbit) that falls within the equivalent longitude covered by the cloud imager data for one hour of Universal Time. A rough way of characterizing the spatial ordering of the IES pixels is that they fall within a standard one hour time interval with respect to the cloud imager data.

0.5.1.3. Processing description. The radiometric part of the incoming data stream consists of 12-bit digital "counts," m_s , that contain a digitization of the analog signals output from the detectors. The CERES instrument subsystem must convert these counts to more useful information. The subscript s refers to the particular sample number in the scan pattern. If we take the full second scan cycle, then there are 660 such samples in a cycle.

It is important to note that the instrument subsystem produces filtered radiances \tilde{I} . By this term, we mean that the output from the CERES instrument subsystem contains a wavelength integrated product of spectral radiance, I_λ , and the spectral sensitivity of the channel, S_λ :

$$\tilde{I} = \int_0^\infty d_\lambda S_\lambda I_\lambda \quad (0-5)$$

With ERBE, we prefer to retain the flexibility of improving the measurement accuracy by a separate "unfiltering" process that includes an identification of the scene being measured. We provide a simple description of this unfiltering in the ERBE-like inversion portion of this volume. The ERBE-like inversion ATBD subsystem 2.0 contains details and other references for this process.

To determine the drift of the CERES sensors, these instruments observe space at least once every 6.6 seconds. Most of the time, they observe space twice as often. The scan pattern also holds the scanning part of the instrument at the space observation position for about 20 samples, in order to reduce the random component of the system noise by averaging. Figure 0-6 illustrates a hypothetical scan with four space clamps and an internal calibration observation.

Between space observations, we estimate the instrument drift by linear interpolation:

$$m_{space}(t) = \frac{t_{after} - t}{t_{after} - t_{before}} \bar{m}_{before} + \frac{t - t_{before}}{t_{after} - t_{before}} \bar{m}_{after} \quad (0-6)$$

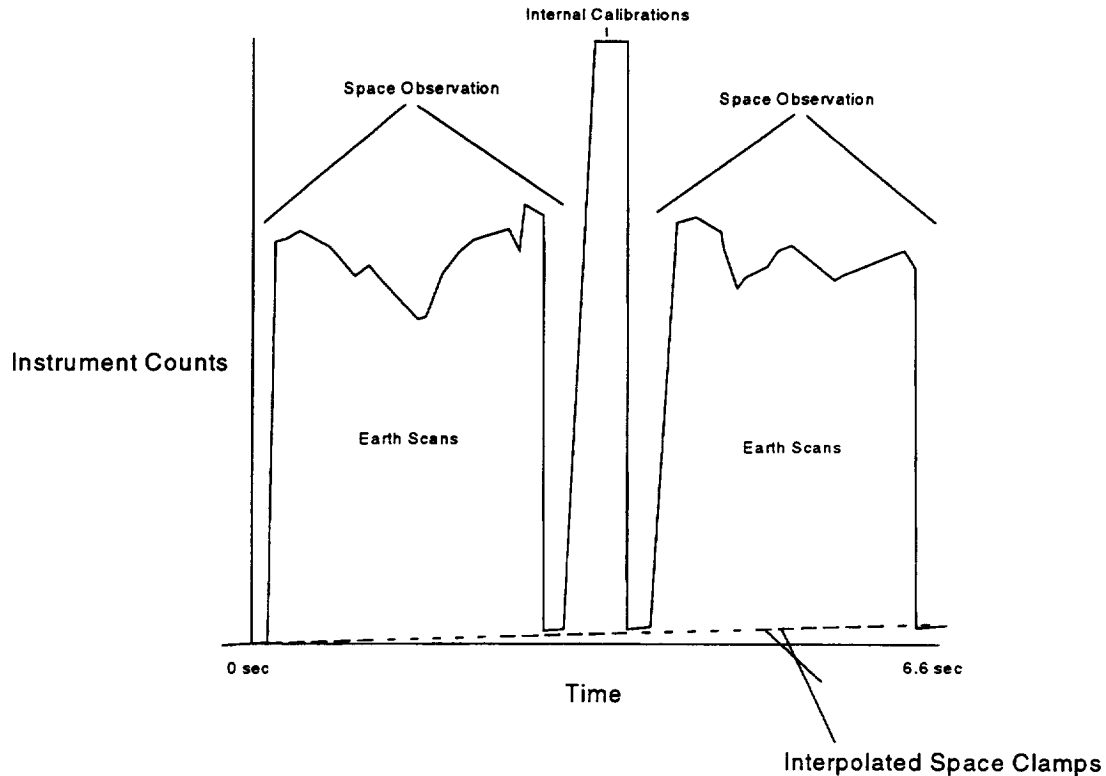


Figure 0-6. Hypothetical CERES instrument data from one bidirectional scan. The scanner in this hypothetical scan observes space four times in a 6.6 sec scan. Between the two middle space observations, the scanner observes the internal calibration source up inside the instrument. The dotted line shows the required interpolation between space clamps.

In this expression, $m_{space}(t)$ is the interpolated estimate of what we would have had with no detectable radiance. The times defined by the overbar are the average time of the space sample averages. The samples defined by the overbar are the average space sample counts.

The working equation for producing calibrated, filtered radiances from the raw telemetry data is

$$\bar{I}_s = \frac{A_v}{V_{bias}}(m(t_s) - m_{space}(t_s) - O_s) \quad (0-7)$$

In this equation, A_v is the calibration coefficient of the particular channel, V_{bias} is the bias voltage applied across the active detector flake, and O_s is a sample dependent offset. Although we hope to minimize offsets in the flight instruments, it appears wisest now to leave in this term. Each spectral channel uses this equation, with separate values of A_v and of the offsets O_s .

Geolocation of the filtered radiances is done similarly for either ERBE-like processing or CERES processing. In each case, we start by finding where the center of the footprint optical axis was at the time of the sample. Because of the time delay introduced by the thermal characteristics of the detector and the electronic filtering, the location of the Point Spread Function's center is not identical with the elevation and azimuth we receive from the telemetry. Once we know where the optical axis was pointing with respect to the instrument, we need to relate the instrument coordinates to spacecraft coordinates using alignment coefficients determined during the instrument integration onto the spacecraft. Then, we find the spacecraft location and attitude at the time of measurement. With this information, we can finally obtain the colatitude and longitude where the field of view intersects the appropriate description of the Earth.

CERES needs two models of the Earth's geoid. The first model applies to ERBE-like data products, where we focused on the top of the atmosphere. To preserve continuity, we chose a simple, oblate spheroid, and place the top of the atmosphere 30 km above this geoid. This model is likely to be unique to the CERES historical ties to ERBE, and is perhaps not applicable to the broader EOS community's needs.

The second model of the Earth is needed to maximize the consistency with the MODIS data products. What we want is an Earth location for which CERES and MODIS produce data coming from the same position in space. We would observe that to some extent the model we choose for Earth location is arbitrary: what we observe is radiance emerging from an arbitrarily chosen surface. However, we do recognize that collocation of CERES and MODIS will be easier if both use the same Earth model.

0.5.2. ERBE-Like Processing

The ERBE-like processing constitutes the first of the major scientific processing branches of the CERES processing system. It is the branch in which we provide ties between the CERES measurements and the historic data from ERBE. As we show in figure 0-7, the ERBE-like processing branch includes two major processes: ERBE-like inversion and ERBE-like time averaging.

0.5.2.1. Major inputs. The input data for this subsystem are created by the CERES instrument subsystem and reside in the BDS data product.

0.5.2.2. Major outputs. The EDDB (ERBE Daily Data Base) is a collection of data from a month of operation by CERES instruments on all of the satellites in orbit within that month. The data elements contained in EDDB are $2.5^\circ \times 2.5^\circ$ regional averages of longwave and shortwave fluxes categorized by scene identification. This data storage product also contains statistics from the CERES pixels that go into making up the regional average. At the start of a given month, EDDB will be empty. At the end of the first day of observations input in a month, EDDB will contain the observations from a single CERES scanner. By the end of the month, it will contain all of the cross-track scanner observations that have been analyzed with the ERBE algorithms. The data in the EDDB product is organized by geographic region, starting at the North Pole and winding around the Earth in a spiral pattern to the South Pole. For each geographic region, the observations are organized by hour within the month.

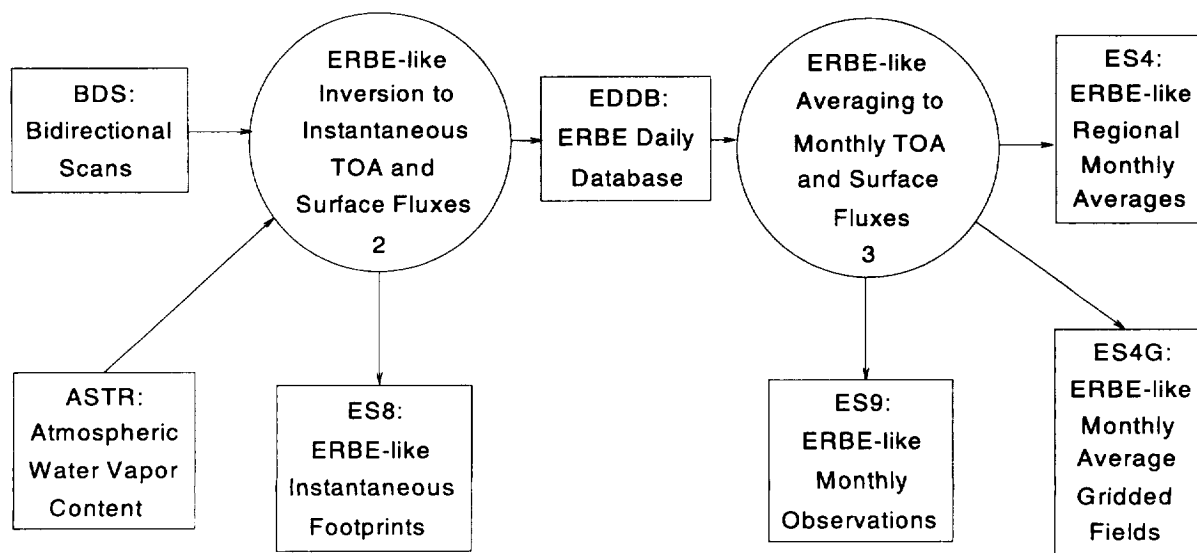


Figure 0-7. Major data products and processes for the ERBE-like processing subsystems.

The ES8 (ERBE-like Science Product 8) product is a 24-hour collection of Earth observations from a single CERES scanner operated in cross-track mode. The ES8 product contains individual pixels of filtered radiance, unfiltered longwave and shortwave radiance, colatitude and longitude, ERBE scene identification, and longwave and shortwave flux. This product is based on the same universal time basis as the CERES Instrument Packets data product.

The ES9 (ERBE-like Science Product 9) product contains the final data record of the individual, regional averages for a month. The ES9 product for archival will contain all of the satellite observations that were made in that month. However, it is possible that versions of this product will be made that include only a single scanner. The data in this product contain observations from the first hour of the first day of the month to the last hour of the last day of the month. The data in this product are organized like the EDDB internal product: by region, and within a region by hour within the month. We show a sample of this organization in the subsection on monthly ERBE-like processing below.

The ES4 (ERBE-like Science Product 4) product is a summary of the monthly averages of fluxes organized by region. The data in this product are time averages for a single month. This archival product contains as much of the Earth as is seen from the full satellite coverage for that month. Versions of this product may be available for less than the full coverage. This product basically records the data for the regions in the EDDB, together with the monthly averages that can be produced from that data in a single product.

The ES4G (ERBE-like Science Product 4, Gridded) product is a rearranged version of the ES4 product. Whereas the ES4 product is one that contains a variety of fields for each region, the ES4G product is organized into a group of fields, such as shortwave flux, longwave flux, clear-sky longwave flux, etc. Each field covers as much of the globe as is available to the entire suite of satellites available during the month.

0.5.2.3. Processing description. We start this branch with Bidirectional Scan Data (BDS) from one of the CERES instruments that operates in cross-track mode. This data product contains CERES filtered radiances organized into 6.6 second scans with about 200 footprints in each scan. The ERBE-like inversion process produces unfiltered longwave and shortwave radiances and Top of Atmosphere (TOA) fluxes for these two spectral divisions, categorized by ERBE scene types. In their archival form, these data are preserved in the ES8 data product. The individual footprint measurements are then averaged into Earth-fixed geographic regions and placed into the ERBE Daily Database (EDDB).

From this database, the ERBE-like Averaging subsystem extracts the regional observations for the month and produces a monthly average. The observations and monthly averages are available in the ES9 data product, while a summary of just the monthly averages appears in the ES4 and ES4G products. The latter two products contain the same data, but are organized differently. S4 is organized by region, where each geographic region contains the fields of reflected solar flux, emitted terrestrial flux, and statistics related to scene identification. The ES4G is organized by field, where each field can be visualized as an image of the entire Earth on an equal-area grid.

In understanding the algorithms for this branch, we also encounter several concepts that carry directly into the more advanced CERES processing:

- a. Inversion from Radiance to Flux
- b. Angular Distribution Models (ADM's)
- c. Directional Models (DM's)
- d. Scene Identification Index
- e. Spectral Unfiltering
- f. Regional Averages
- g. Time Interpolation Models

The first five of these concepts appear in the ERBE-like inversion subsystem. The Directional Models are very closely tied to the models for time interpolation that we need for the third major subsystem of CERES processing.

The first three of these concepts: *Inversion from Radiance to Flux*, *Angular Distribution Models*, and *Directional Models* are tied intimately together. We relate (monochromatic or broad-band) flux to radiance with the integral relationship

$$F^{\uparrow} = \int_0^{2\pi} d\phi \int_0^{\pi/2} d\theta \sin\theta \cos\theta I(\theta, \phi) \quad (0-8)$$

Here, F^{\uparrow} represents the upwelling flux, while $I(\theta, \phi)$ represents the radiance emerging from the top of the atmosphere at a viewing zenith, θ , and viewing azimuth, ϕ . This relationship is a definition, found in any standard textbook on atmospheric radiation.

For practical purposes, we turn the relationship around and relate radiance to flux with an ADM, R , where

$$R(\theta, \phi) \equiv \frac{\pi I(\theta, \phi)}{F^{\uparrow}} \quad (0-9)$$

If the radiance were isotropic, so that I were independent of θ and ϕ , then we would find that R was 1. This fact gives us the normalization factor π . However, this Lambertian approximation is not sufficiently accurate for use in inverting data. ADM's are not generally discussed in textbooks on atmospheric radiation, although they are critical components to satisfactory data reduction in any project attempting to measure the Earth's radiation budget. In principle, the ADM's contain variations due to both vertical and horizontal structure in the atmosphere or surface optical properties. However, we can only measure average models based on statistically sampling the angular variations of the radiation field.

Directional models apply to the shortwave part of the spectrum. These models describe the variation of albedo with solar position. Specifically, we normalize the albedo variation by forming the ratio

$$\delta(\mu_0) \equiv \frac{a(\mu_0)}{a(1)} \quad (0-10)$$

The *Directional Model* for the particular scene is $\delta(\mu_0)$. The albedo is $a(\mu_0)$, which is related to the reflected solar flux as

$$a(\mu_0) \equiv \frac{F^{\uparrow}}{E_0 \mu_0} \quad (0-11)$$

Throughout these expressions, μ_0 is the cosine of the solar zenith angle, and $a(1)$ is the albedo for overhead Sun. The solar irradiance at the top of the atmosphere is E_0 , and it is the "solar constant" (typically measured at about $1365 \text{ W}\cdot\text{m}^{-2}$) adjusted by the inverse square of the Earth-Sun distance at the time of reflection.

The ADM's and DM's are both empirical data structures—they are based on observations rather than theory. To develop them, we observe similar parts of the Earth under a variety of solar illumination and meteorological conditions. The observations must include a wide sampling of the angles in the outgoing hemisphere of radiation above the set of ADM targets. The samples have typically been collected in angular bins. The average radiances then provide the fundamental data that are normalized to produce a "statistical average" flux. By dividing the average radiances by the average flux, we derive the ADM directly from the observations. By also using the fact that we have to collect reflected sunlight over a variety of solar zenith angles, we can directly obtain the directional models as part of this process.

Volume 4.5 of these ATBD's provides a more detailed discussion of the ADM and DM development for CERES, as well as discussing some new ways of developing these models.

The ADM's and DM's are not divorced from the question of what kind of scenes the scanners are observing. For ERBE, we broke the Earth into a five underlying geographic types: ocean, vegetated land, desert, snow, and coast. Over each type we typically had four categories of cloudiness: clear, partly cloudy, mostly cloudy, and overcast. These verbally descriptive categories were based on observations with the Nimbus 7 THIR and TOMS instruments, as well as the hemispherical angular sampling of the Nimbus 7 ERB broadband radiometers. We may categorize scenes with whatever information we choose. However, to keep storage within bounds, we must limit the number of categories. The scene identification algorithm provides an index to the ADM and DM database that lets us invert radiance to flux.

Spectral unfiltering is another important concept that we carry forward from ERBE. By separating the instrument interpretation into a step including the spectral throughput of the instrument and another step where we remove that response using scene information, we gain in at least two important ways. First, we can use a count conversion algorithm that treats the absorbed radiation independently of the spectral content of the incident radiation. The quantity A_v is truly independent of spectral content and corresponds to "absorbed radiant power per count." Second, by using information about the scene in correcting for the instrument spectral coloration, we gain accuracy and flexibility.

Regional averaging is the sixth concept we carry forward from ERBE. While level 2 products are of some interest, they are still organized in terms of individual footprints. However, it is much easier to deal with Earth-fixed data, particularly if we want to look at time series of the energy budget over particular parts of the Earth. Thus, at an intermediate stage in the processing, we want to average footprints together. With most other research groups, we prefer to align our regions with parallels of colatitude and meridians of longitude.

Finally, we want to produce monthly averaged fields of radiation. Since the observations occur on a discrete basis, we need some form of time interpolation to produce a monthly average. For ERBE-line averaging, we use a simple linear interpolation in the longwave part of the problem. The shortwave time interpolation is more complex and involves the scene identification and directional models.

0.5.2.3.1. ERBE-like inversion. The fundamental purpose of ERBE-like inversion is to produce longwave and shortwave flux from longwave and shortwave radiance using ADM's:

$$F^\uparrow = \frac{\pi I}{R} \quad (0-12)$$

Before we can get to this point, however, we need to get the longwave and shortwave radiances from the three channels of filtered radiance. We also need to select the appropriate ADM, R for each spectral band. There are five major steps in this process:

1. Perform a rough scene identification
2. Perform spectral unfiltering
3. Choose the final scene ID
4. Perform final spectral unfiltering
5. Invert radiances to fluxes

In addition, the ERBE-like inversion subsystem also performs a regional averaging before placing the regional averages in the ERBE Daily Database.

Rough scene ID

Based on the fact that cloudy areas tend to be more reflective than clear areas and that the longwave radiances of cloudy areas are lower (colder) than clear ones, we can perform a rough scene identification based on the total and shortwave channels before we make a definitive scene identification.

Spectral unfiltering

With the rough scene identification, we can choose appropriate coefficients that will give us the best fit to a range of estimates for the best fit to spectrally correct the three-channels to longwave and shortwave radiances. In a simple approach, we might be tempted to approximate

$$I_{SW} = \frac{1}{\bar{S}_{SW}} \tilde{I}_{SW} \quad \text{and} \quad I_{LW} = \frac{1}{\bar{S}_{TOT}} \tilde{I}_{TOT} - I_{SW} \quad (0-13)$$

However, if we contemplate this type of relationship for long, we are likely to conclude that there is some difficulty in choosing the appropriate average spectral throughput factors (represented by the symbols of the type \bar{S}_{SW} as the spectral throughput of the shortwave channel). Thus, in practice, we use

$$\begin{pmatrix} I_{LW} \\ I_{SW} \end{pmatrix} = \begin{pmatrix} C_{LT} C_{LW} C_{LS} \\ C_{ST} C_{SW} C_{SS} \end{pmatrix} \cdot \begin{pmatrix} \tilde{I}_{Tot} \\ \tilde{I}_{Win} \\ \tilde{I}_{SW} \end{pmatrix} \quad (0-14)$$

The matrix elements, C_{ij} , are based on radiative transfer models, knowledge of discrete values of the instrument channel spectral sensitivity, S_λ , and on an estimated population of Earth scenes.

Final scene ID

The final ERBE scene identification uses a maximum likelihood estimator based on the observed radiance statistics from the Nimbus 7 data. Figure 0-8 shows a schematic representation of such statistics. There is data for one such diagram for each bin in viewing zenith, azimuth, and geographic type. In each bin, there are average values for shortwave and longwave radiance, as well as appropriate standard deviations. An observed radiance will appear as a single point in this diagram. The algorithm computes the radiance distance from each of the means, thereby obtaining a measure of the likelihood of the observation belonging to the scene type. It then chooses the most likely.

Inversion

With the scene ID index available, the inversion algorithm simply chooses the appropriate longwave and shortwave models from a table. In vectorial form,

$$\begin{pmatrix} F_{LW}^\uparrow \\ F_{SW}^\uparrow \end{pmatrix} = \pi \begin{pmatrix} R_{LW}^{-1} & 0 \\ 0 & R_{SW}^{-1} \end{pmatrix} \cdot \begin{pmatrix} I_{LW} \\ I_{SW} \end{pmatrix} \quad (0-15)$$

At this point, we have completed the basic inversion steps and can produce the ES8 data product. This product contains the following fundamental data for each footprint:

- Geometry, view zenith, view azimuth, solar zenith
- Filtered radiances, \tilde{I}_{TOT} , \tilde{I}_{Win} , and \tilde{I}_{SW}
- Unfiltered radiances, I_{LW} , and I_{SW}
- Scene ID index, clear, partly cloudy, mostly cloudy, or overcast
- Broadband fluxes, F_{LW}^\uparrow , and F_{SW}^\uparrow

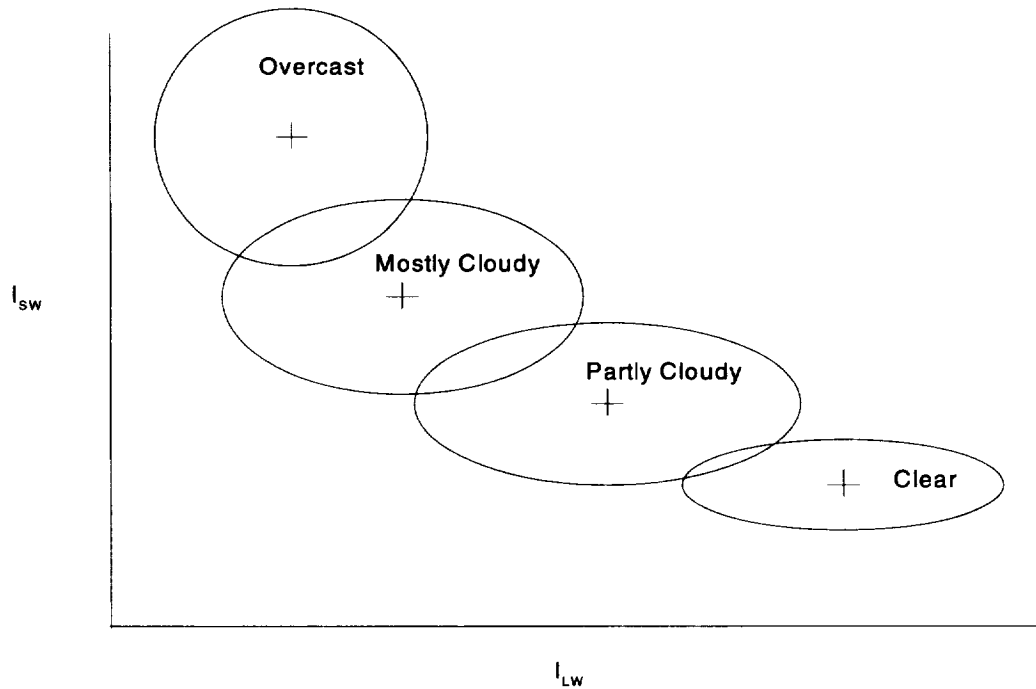


Figure 0-8. Schematic ERBE-like scene ID diagram. The radiances used in the ERBE ADM construction for a given viewing geometry have a range of values for a given scene ID type. We show the mean longwave and shortwave radiance for each scene type as the crosses and the standard deviation of the distribution about the mean as the ellipses. In making the scene identification, we locate a radiance with the appropriate viewing geometry in this diagram and then judge which scene type is most likely.

Regional averaging

The final step in the ERBE-like inversion processing is to average fluxes within geographic regions that occur within a particular hour of the day. For ERBE, this process included all footprints whose PSF fell within the given region.

0.5.2.3.2. ERBE-like averaging. ERBE approaches time averaging from the standpoint of allowing each region to have its own time series. Thus, once all of the observations for a month are in the ERBE Daily Database, we proceed through the regions. The advantage is that the database allows us to take data that come in ordered only by time and convert the algorithm that operates first on space and then on time.

Within the time sequence for a given region, the ERBE-like algorithm uses a basic strategy of piecewise linear interpolation. However, the algorithm modifies its behavior over land and deserts when it is dealing with longwave fluxes and uses a more complex variant for all of the shortwave time interpolation.

It will help us to set the time interpolation algorithm in context if we consider figure 0-9. In this figure, we show how we break up time within a month. Each day has 24 hours; each month has the appropriate number of days. When we have an observation within a given day-hour box, we indicate that in the figure with an 'X'. With this structure, we can compute a monthly average in several ways (see Brooks, et al. 1986).

		Hour in Day																												
		1	2	3	4	5	6	7	8	9	10	11							23	24	Monthly									
Day in Month	1			X								X																	X	
	2			X								X	X																	X
	3			X								X	X																	X
	4			X								X																		X
	5			X							X	X																		X
	6			X							X																			X
	7			X						X	X																			X
	8			X					X	X	X																			X
	9			X					X	X																				X
Hourly	30			X																							X	X	X	
				X				X	X	X	X	X															X	X	X	

Figure 0-9. Time samples that enter the ERBE-like monthly average processing and its data structure. A month is divided into days of 24 hours. Each hour and day receives an hour-day bin. If there is an observation by one of the satellites, we indicate a contribution to the monthly average by an ‘X’ in this figure. If we add observed values vertically, keeping the hour fixed, we have ‘hourly averages’; if we add horizontally to get the numbers in the right column, we have ‘daily averages.’ The monthly averages placed in the ES4 and ES4G products come from the lower right entries in this data structure.

The most commonly used monthly average is one that we find by stretching out the days end-to-end. Now, where we have observations at time t_{i-1} and t_i , we interpolate between as

$$F^\uparrow(t) = \frac{t_i - t}{t_i - t_{i-1}} F^\uparrow(t_{i-1}) + \frac{t - t_{i-1}}{t_i - t_{i-1}} F^\uparrow(t_i) \tag{0-16}$$

The average of this interpolation is then

$$F^\uparrow \equiv \frac{1}{\Delta t} \int_{\Delta t} dt F^\uparrow(t) \doteq \sum_{\substack{\text{Observations} \\ \text{in Month}}} \frac{1}{2} \frac{t_{i+1} - t_{i-1}}{\Delta t} F^\uparrow(t_i) \tag{0-17}$$

Longwave modifications for desert and land

The longwave flux responds to the surface temperature and atmospheric temperature profiles quite directly. As a result, over deserts and over vegetated land, we want to account for this effect to minimize potential biases that may not be properly taken into account by the piecewise linear averaging algorithm. Rather than introduce a complex algorithm, we simply fit a half-sine curve to the data.

Shortwave modifications to use directional models

Shortwave time averaging is more complex. For each scene ID type, we expect the reflected flux to follow the diurnal model:

$$F^\uparrow_{ID}(t) = E_0 \mu_0(t) a_{obs} (\mu_0 = 1) \delta_{ID}(\mu_0(t)) \tag{0-18}$$

as long as $\mu_0 > 0$, i.e., daylight.

In practice, we have to deal with multiple scene types in a given region. We can represent the observations with the fraction of the footprints that were observed at a given time. In vectorial form, we can write

$$\mathbf{f}(t) \equiv \begin{pmatrix} f_{CLR}(t) \\ f_{PC}(t) \\ f_{MC}(t) \\ f_{OVC}(t) \end{pmatrix} \quad (0-19)$$

Then, we can linearly interpolate in scene fraction:

$$\mathbf{f}(t) = \frac{t_i - t}{t_i - t_{i-1}} \mathbf{f}(t_{i-1}) + \frac{t - t_{i-1}}{t_i - t_{i-1}} \mathbf{f}(t_i) \quad (0-20)$$

The same approach applies to the variation of overhead sun albedo:

$$\mathbf{a}_0(t) = \frac{t_i - t}{t_i - t_{i-1}} \mathbf{a}_0(t_{i-1}) + \frac{t - t_{i-1}}{t_i - t_{i-1}} \mathbf{a}_0(t_i) \quad (0-21)$$

where

$$\mathbf{a}_0(t_i) \equiv \begin{pmatrix} a_{CLR}(\mu_0 = 1, t_i) \\ a_{PC}(\mu_0 = 1, t_i) \\ a_{MC}(\mu_0 = 1, t_i) \\ a_{OVC}(\mu_0 = 1, t_i) \end{pmatrix} \quad (0-22)$$

If we now use the diagonal matrix with the directional models:

$$\Delta(t) \equiv \begin{pmatrix} \delta_{CLR}(\mu_0(t))\mu_0(t) & 0 & 0 & 0 \\ 0 & \delta_{PC}(\mu_0(t))\mu_0(t) & 0 & 0 \\ 0 & 0 & \delta_{MC}(\mu_0(t))\mu_0(t) & 0 \\ 0 & 0 & 0 & \delta_{CLR}(\mu_0(t))\mu_0(t) \end{pmatrix} \quad (0-23)$$

we can now write

$$F^\uparrow(t) = \mathbf{a}_0^T(t) \cdot \Delta(t) \cdot \mathbf{f}(t) \quad (0-24)$$

There are some additional fine points of time interpolation near the beginning and end of a day that we may want to take into account elsewhere.

As before, we time integrate this interpolation form over the month to arrive at the proper monthly average. It should be clear at this point that the monthly average process for the shortwave TOA fluxes is not simply a sum of the observed values.

0.5.3. Atmosphere Processing

The atmosphere processing constitutes the second of the major scientific branches of the CERES processing system. It is the branch where we obtain measurements of cloud properties that are consistent with the CERES broadband fluxes. This branch also has the largest number of processes. As we show in figure 0-10, the atmosphere processing branch includes five major processes:

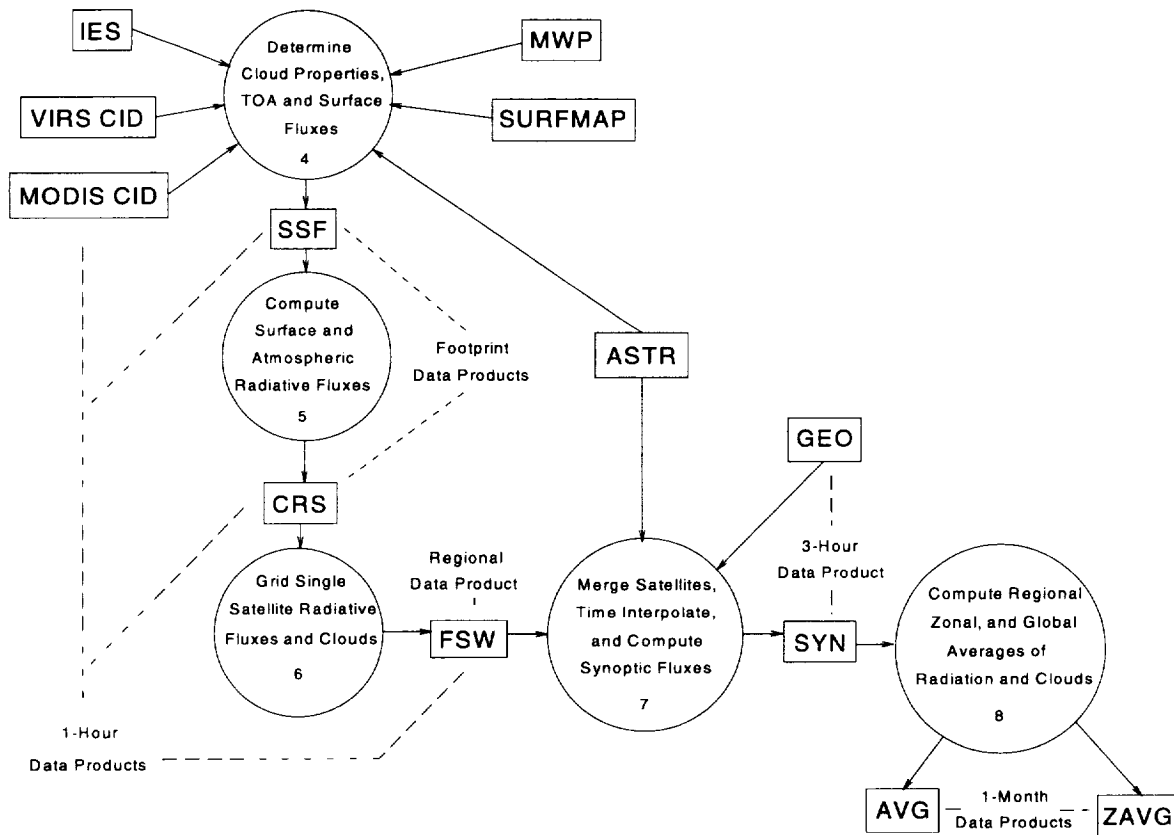


Figure 0-10. Major data products and processes for the atmosphere processing subsystems.

1. Determine cloud properties
2. Compute radiation fields within the atmosphere
3. Grid the footprint data to regional averages
4. Interpolate in time to compute synoptic radiation and cloud fields
5. Average over time to get monthly zonal and global averages

0.5.3.1. Major inputs. The following products are the major inputs to the atmosphere processing:

The *TRMM CID* product is an hourly satellite swath of VIRS pixels. We expect this product to be a set of VIRS scan lines, where each scan line is made of a fixed number of multispectral pixels.

The *MODIS CID* product is an hourly satellite swath of MODIS pixels. We expect this product to be a set of scan lines. These scan lines are spectral subsamples of the MODIS pixels.

The *GEO* (GEOstationary) product is the synoptic window and visible channel radiances of the geostationary satellites, like that used by the International Satellite Cloud Climatology Project (ISCCP). This product covers as much of the Earth as is available through the two channels of geostationary (and sometimes AVHRR) data; in short, it is intended to be global in scope. The spatial resolution is about 8 kilometers. This form of geostationary data has one map each hour.

The following products are required to make up the standard atmospheric profile (ASTR) data product that is used in several of the subsystems:

The *MWH* (MicroWave Humidity) product is a satellite derived product, covering a single day. The instrument from which this data derives is a microwave radiometer. Each measurement comes as a pixel, which is composited into a global data set.

The *APD* (Aerosol Profile Data) product may come from satellite measurements (particularly MODIS, MISR, or AVHRR) or from a climatology. This data provides an aerosol loading and some vertical profile information for a time scale that covers a week, although Saharan dust outbreaks and other short time scale phenomena need to be included in this data product.

The *GAP* (Global Atmospheric Profiles) product is the basic set of analyzed temperature and humidity fields produced by the National Oceanic and Atmospheric Administration (NOAA) as an operational product. The products from NOAA currently include temperature, humidity, and winds at nine standard pressure levels once every twelve hours. The spatial resolution is currently about 2° in latitude and longitude. Because of its operational nature, this product will be routinely available during the CERES data processing.

The *OPD* (Ozone Profile Data) may be either an operational satellite derived product or an ozone climatology. Because the ozone concentration changes relatively slowly, we expect this data product to be updated once a month, to cover the globe at about 2.5° to 5° spatial resolution, and to have moderate vertical resolution.

0.5.3.2. Major outputs. The *ASTR* (Atmospheric Structures) product contains the standardized input to the rest of the CERES processing. *ASTR* will have a spatial resolution of 1.25° in latitude and longitude. This product's time resolution will be one product every hour. The vertical resolution will include 38 standard pressure levels.

The *CRH* (Clear-sky Reflectance and temperature History) product is a collection of cloud imager radiance values that can be used to set thresholds for cloud detection. This product will be updated about every seven days and to have a spatial scale of collection of about 18 km in latitude and longitude, as described in ATBD subsystem 4.1.

The *SSF* (Single Satellite Flux) product contains a single hour of single satellite measurements of TOA fluxes and cloud properties for single CERES pixels. The spatial organization is still a satellite swath of CERES pixel resolution data. This product does not contain the radiation field within the atmosphere for each CERES pixel.

The *CRS* (Cloud and Radiation Swath) product contains the instantaneous CERES pixel values of TOA fluxes, cloud properties, and radiation fluxes within the atmosphere and at the Earth's surface. The *CRS* product includes one hour of Universal Time and all of the data from one CERES instrument over the spatial swath beneath the instrument.

The *FSW* (Flux and clouds regional SWath) product contains regional averages and other statistics for a single hour of Universal Time from a single CERES instrument swath. The data are like the *CRS* product, in that the *FSW* regional values include TOA fluxes, cloud properties, and radiation fluxes within the atmosphere and at the Earth's surface. The *FSW* product covers one hour of Universal Time and all of the regions included in the spatial swath seen by the CERES instrument from any one of the satellites carrying that instrument. The *SYN* (Synoptic) product is a synoptic, three-hour view of consistent cloud and radiation properties with a spatial resolution of 1.25° in latitude and longitude.

The *AVG* (Average) product is a complete, global monthly average at 1.25° resolution in latitude and longitude. This data product includes TOA shortwave and LW flux, cloud properties, and radiation within the atmosphere.

The *ZAVG* (Zonal Average) product provides zonal averages (i.e., averages over longitude) of the cloud and radiation data in *AVG*. This product is at 1.25° resolution in latitude, and is likely to include various statistical distinctions, such as clear-sky fluxes, land, ocean, etc.

0.5.3.3. Processing description. We start this branch with the combination of CERES data, in the form of the *IES* product, and of cloud imager data, either *VIRS* data or *MODIS* data. Both the CERES

data and the imager data have the same single hour time interval. When we record the results in the SSF data product, we have a single hour swath of data organized within CERES footprints. The next step in the processing is to compute the radiation fields within the atmosphere for each footprint. The CRS data product is the last of the data organized at this spatial resolution.

Thereafter, we go to regions fixed with respect to the Earth. The gridding process carefully accounts for the fact that often some part of the CERES footprint falls outside of the region, but is still influenced by that region's radiance. The FSW data product is thus organized on the basis of a single hour of observations with a 1.25° colatitude and longitude resolution. This spatial organization gives us regions about 140km in size placed in an equal-area grid that has one-half the size of the ISCCP grid boxes.

The next major step in processing merges the single satellite FSW products into one-hour regional observations, time interpolates between the observations, and then supplements the CERES observation times with geostationary data. Once this set of observations has filled as many regions as possible, we recompute the atmospheric radiative fluxes to produce the SYN data product. This product represents our best estimate of the radiation and cloud fields that we can obtain from the complement of instruments carried on satellites with EOS instruments. The production of a synoptic data product is a critical component of time averaging for three reasons: synoptic views form an essential step in understanding the atmosphere's meteorology with particular emphasis on the life cycle of cloud systems; synoptic views are a major step in validating the CERES data processing, particularly of time interpolation; and the synoptic data product provides a more regular data structure than other alternatives and thereby eases the work of designing algorithms and operating the data processing system.

The final processing subsystem in this branch of the CERES processing is the time averaging step that ingests a number of SYN products and combines them to produce the AVG and ZAVG data products. In a sense, these last two products parallel the ES9 and ES4 data products of the ERBE-like branch of processing.

In understanding the algorithms for this branch of processing, we need to record four fundamental kinds of cloud properties:

- a. Cloud physical and optical properties
- b. Cloud height categories
- c. Cloud overlap conditions
- d. CERES scene ID index

Although the last of these items is an extension of the ERBE Scene ID index, the previous three kinds of cloud information are new and perhaps unique to the CERES processing. As we will see, we can follow these properties from their determination in the highest resolution imager data through their summary in properties of clouds within a CERES footprint. Finally, we will see them contribute to average properties of clouds on a regional basis, both instantaneously in FSW and in the SYN and monthly averages.

The *cloud physical and optical properties* are fundamental pieces of information we obtain from the high spatial and spectral resolution imager data. We can break these properties into several categories. First, there is vertical position information: p_c , cloud top pressure; p_e , effective cloud pressure (which becomes different from p_c where the emissivity deviates from 1); cloud effective temperature, T_e ; effective cloud altitude, Z_e ; and p_b , cloud base pressure. Second, there is horizontal coverage information: C , cloud fraction, usually thought of as the fraction of an underlying area covered by the projection of cloud elements in a layer having a markedly larger optical depth than the clear atmosphere. Third, there is information on the optical properties, particularly τ_{vis} , the visible optical depth, and ϵ_{win} , the window emissivity. Fourth, there is information on the form and content of condensed water in the cloud. These variables include W_{liq} , the liquid water path [kg m^{-2}], and W_{ice} , the ice water path [kg m^{-2}]. Fifth, there

is r_e , the average particle radius of condensed water. Sixth, and finally, we carry $\langle v/h \rangle$, the aspect ratio of the clouds, i.e., the ratio of the vertical extent to horizontal size.

$$\text{CP} \equiv \left[\begin{array}{l|l} p_c & \text{cloud top pressure} \\ p_e & \text{effective cloud pressure} \\ T_e & \text{cloud effective temperature} \\ Z_e & \text{effective cloud altitude} \\ p_b & \text{cloud base pressure} \\ C & \text{cloud fraction} \\ \tau_{vis} & \text{visible optical depth} \\ \epsilon_{win} & \text{window emissivity} \\ W_{liq} & \text{liquid water path} \\ W_{ice} & \text{ice water path} \\ r_e & \text{water particle effective radius} \\ D_e & \text{ice particle effective diameter} \\ \langle v/h \rangle & \text{aspect ratio of the clouds} \end{array} \right] \quad (0-25)$$

We can represent these properties in the form of a cloud property vector (CP) as shown in equation (0-25). When we first encounter this vector, we are dealing with the cloud properties retrieved from the high resolution imager pixels. Later, when we make the cloud properties consistent with the CERES fluxes, we need to consider averages of these properties over the CERES point spread function. Finally, when we grid radiation fields and cloud properties, we need additional averaging of this vector. To the regional average, we also add a histogram of visible optical depth during the day or of window emissivity at night. This histogram provides us with a useful summary when we start dealing with averages of cloud properties over a CERES footprint or a geographic region.

The *cloud height category* is the second important concept that ties together the atmospheric processing branch. Briefly, for each layer we see, we use the effective pressure p_e to categorize the cloud heights:

$$\text{CHC} \equiv \left\{ \begin{array}{ll} H(\text{High}) & \text{if } p_e \leq 300 \text{ hPa} \\ UM(\text{Upper Middle}) & \text{if } 300 \text{ hPa} < p_e \leq 500 \text{ hPa} \\ LM(\text{Lower Middle}) & \text{if } 500 \text{ hPa} < p_e \leq 700 \text{ hPa} \\ L(\text{Low}) & \text{if } (p_e > 700 \text{ hPa}) \end{array} \right. \quad (0-26)$$

CHC provides us with a single index. We increase the reliability of our layering estimates by using the statistical properties of pixels in conjunction with the common observation that clouds occur in layers. Indeed, under most circumstances, the cloud effective pressure is likely to be one of the variables that has the largest horizontal correlation length of any of the cloud property variables.

We use the expectation of long horizontal correlations of cloud height in several different ways. When we start determining cloud properties with the imager data, we use average altitudes of cloud layers to segregate imager pixel properties into two layers. These average properties are a major help when we encounter overlapping layers in a single pixel. Later in the aggregation of pixel properties into CERES footprint averages, we use layering to reduce the variations in cloud categories within a footprint. The same variance reduction also holds when we work with regional averages. In time averaging,

we separately interpolate the regional cloud properties (at least for Release 1 of the software) on grounds that clouds in each of the *CHC* categories are likely to be influenced by different physical conditions in the atmosphere. In other words, quite different cloud systems can advect over one another without physically interacting.

The *cloud overlap condition* is the third major concept for the CERES atmospheric processing. Because CERES builds data products involving the vertical profile of atmospheric radiation, we need to keep track of the simultaneous vertical overlap of cloud layers. At present, this information usually is not saved following GCM runs. However, because of the way in which radiant energy flows, the interposition of cloud layers that insulate layers above the cloud from layers below can cause large changes in the energy balance and heating or cooling rates of the atmosphere.

In many cases, more than two layers can overlap. However, it is very difficult for satellite retrieval algorithms to discern such cases. Accordingly, we choose to bundle all conditions of cloud overlap into the following eleven conditions:

$OVLP \equiv$	{	<i>CLR</i>	if there are no clouds	(0-27)
		<i>H</i> (High)	if there is only an H category	
		<i>UM</i> (Upper Middle)	if there is only a UM	
		<i>LM</i> (Lower Middle)	if there is only a LM	
		<i>L</i> (Low)	if there is only an L category	
		<i>H/UM</i> (High over Upper Middle)	if there are both H and UM	
		<i>H/LM</i> (High over Lower Middle)	if there are both H and LM	
		<i>H/L</i> (High over Low)	if there both H and L categories	
		<i>UM/LM</i> (Upper Middle over Lower Middle)	if there are both UM and LM	
		<i>UM/L</i> (Upper Middle over Low)	if there are both UM and L	
		<i>LM/L</i> (Lower Middle over Low)	if there both LM and L	

We can apply these labels for overlap conditions to imager pixels, to CERES footprints, and to regional averages. In the latter cases, we need to account for the statistics of the occurring conditions.

The *CERES Scene ID index* is the fourth major concept for the atmospheric processing for CERES. As we have seen, this concept was a critical component of the ERBE processing. During the first release of the CERES software, we will continue to use the old ERBE ADM's. In this case, the choice of ADM hinges primarily upon the fractional cloud cover, which is part of the information carried by the cloud property vector. Thus, we have a data structure with which we can improve our inversion process, even if we do not change our cloud retrieval algorithms. A critical use of the CERES rotating azimuth plane scan mode is to produce improved ADM's to reduce the large ERBE angular sampling errors. These new models will include the variation with cloud visible optical depth, infrared emittance, cloud particle phase, and cloud height.

0.5.3.3.1. Cloud property determination. EOS offers a critical opportunity to improve the consistency between measurements of radiation and of cloud properties. Initially, we will continue to use the ERBE ADM's. However, when we have collected several years of data, we will produce a new set of ADM's that will markedly reduce the systematic errors in the ERBE data.

Cloud property input geometry

To understand the manner in which we propose to deal with cloud property determination, it will help to work our way through a sequence of figures that can show how the imager data and the CERES footprint data must play together to produce consistent measurements of radiation and clouds.

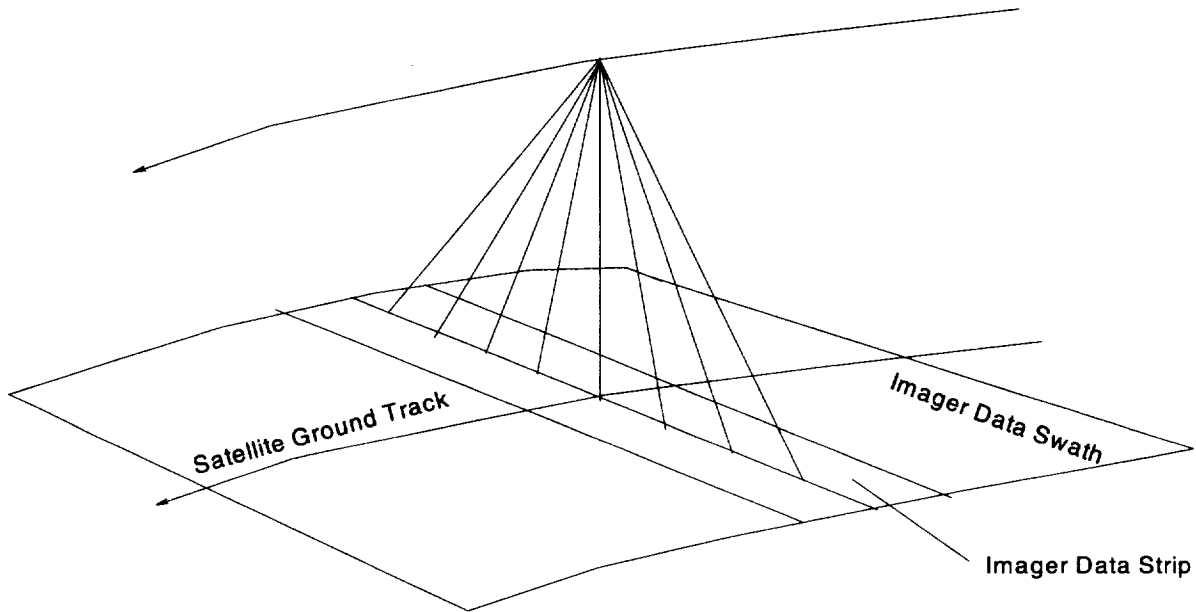


Figure 0-11. General geometry of cloud imager data swath and the image data strip CERES will work with. Here we show a small portion of a single hour of imager data. To keep this image in perspective, the swath of data from MODIS is about 2000 km across. The image data chunk that the CERES algorithms will use is about 500 km wide in the along-track direction.

We can start with the swath of data taken by the imager. Figure 0-11 provides a schematic perspective view of this swath. We can see the orbital path of the satellite and the ground track under it. The data taken by the imager is designed to align perpendicular to the ground track, with all of the pixels in a given scan being in a single line. The fan-shaped sampling in this figure represents light rays from some of the points on the Earth's surface. For the initial part of CERES processing for cloud property determination, we expect to read in a strip of the swath that is the full width, but only about 500 km long. We refer to this as the image data strip in figure 0-11.

Imager clear-sky determination and cloud detection

Figure 0-12 shows the first part of building up the cloud properties over the Earth. We start by taking the imager data strip and overlying the geographic type that we obtain from the SURFMAP input product. This product is expected to have ten arc minute, or 18 km spatial resolution. The geographic type will include distinctions between oceans, various land ecosystem types, various desert types, and some indication of the snow or ice conditions. The geotypes are not intended as scientific categorizations for purposes of ecosystem or ocean color or cryosphere research; rather, these types need to provide a sufficient characterization of the surface that we can choose appropriate spectral and angular models of the reflection and emission from the surface.

The next data structure to interact with the Imager Data Strip is the Cloud-No Cloud Mask. ATBD subsystem 4.1 contains a description of the algorithms CERES uses to produce this mask. To a substantial degree, we use an extension of the ISCCP time history approach with several key improvements. First, of course, we expect the MODIS and VIRS data to be better located and calibrated than such imager data has been in the past. Second, we will use a number of more sophisticated algorithms than have been used in the past, including spatial coherence information, multispectral clear and cloudy tests, texture measures, and artificial intelligence classification for complex backgrounds such as snow and mountains. Figure 0-13 shows how the Cloud-No Cloud mask overlays a portion of the Imager Data

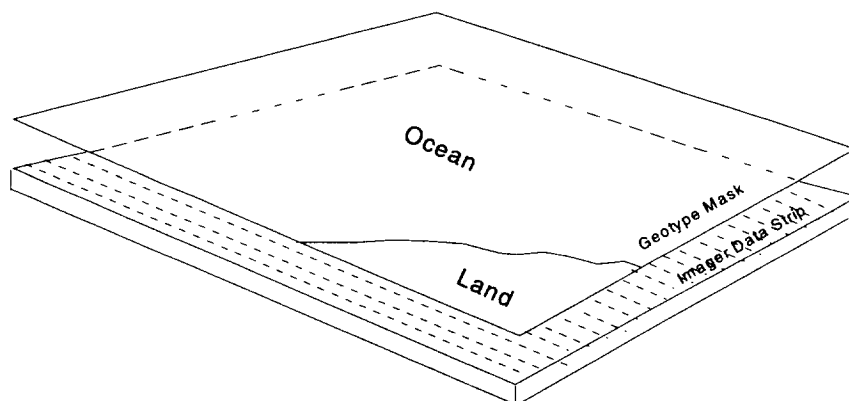


Figure 0-12. Portion of the imager data strip overlaid with the geotype mask. The imager data strip contains the radiances from selected bands of the imager. Here we show the geotype mask, which provides a categorization of the Earth's surface into such subdivisions as ocean or land for purposes of selecting appropriate surface reflectance models. The geotype mask is somewhat coarser than the pixels, with a resolution of 10 arc minutes, or about 18 km.

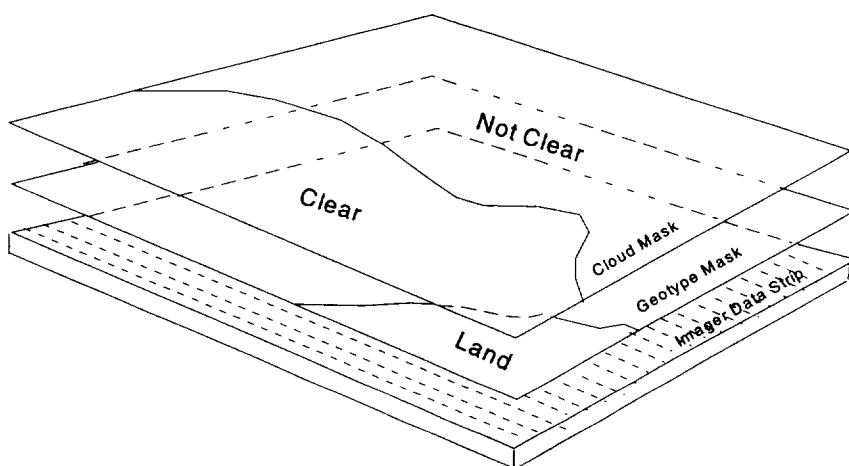


Figure 0-13. Portion of the imager data strip and geotype mask overlaid with the cloud-no cloud mask. Here, we overlay a mask indicating whether the pixels in the imager data strip are clear or cloudy. This mask is developed from CERES algorithms that extend the ISCCP time history approach.

Strip and the Geotype Mask. With the combination of the Geotype Mask and the Cloud-No Cloud Mask, we can identify whether pixels are clear ocean or cloudy land.

Identifying cloud height in imager pixels

Following overlaying both the geotype and cloud-no cloud masks, we determine the height of cloud layers in each pixel, using techniques described in the ATBD subsystem 4.2. This process gives us imager pixel columns that have clouds whose altitudes fit into our atmospheric height categories as illustrated in figure 0-14. ISCCP embedded this step within the cloud property determination steps that CERES will take after this height identification is completed. Here, we will apply 15- μm vertical sounding techniques, spatial coherence, and comparisons of multispectral histograms with theoretical calculations. Where the data suggest that there are several layers, the CERES algorithms will assign the height of the nearest well-defined cloud layer to the pixels. Because the downwelling LW flux at the Earth's surface is sensitive to low level clouds and cloud overlap conditions, identifying multilevel systems is

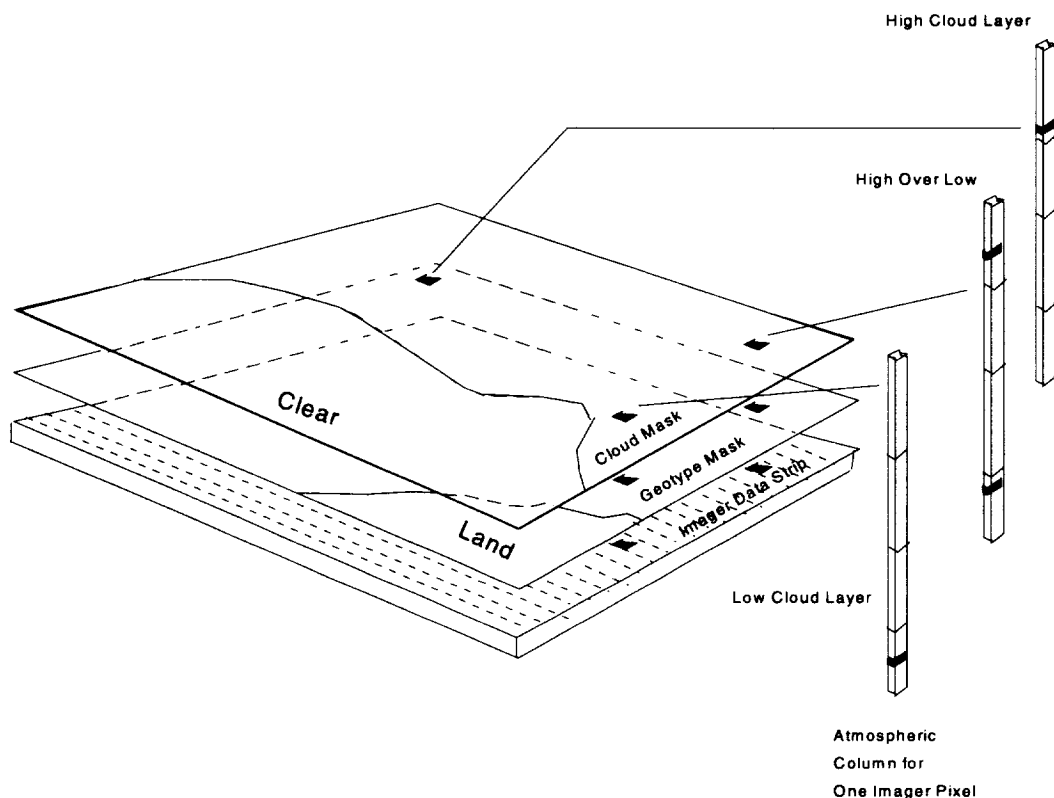


Figure 0-14. Sample atmospheric columns with identified cloud layers as they relate to the imager data strip and the geotype and cloud-no cloud masks. The columns illustrate the schematic structure of cloud layers within an atmospheric column. The regular horizontal markings on the columns indicate where the breaks between height categories occur. The column lowest on the right has a cloud layer only in the lowest height category, as the cloud overlap condition mask over the pixel where this column is located. Likewise, the atmospheric column highest on the right has a cloud layer only in the upper height category.

critical to advancing our understanding. Thus, we will examine how best to include this step in the Release 1 algorithms.

With the cloud altitude determined, even in multi-layer situations, we can readily develop the cloud overlap condition mask. Figure 0-15 illustrates this step. By coregistering the two data structures that we have overlaid on the imager data strip, we have a data structure that represents a major part of the preprocessing steps for this set of algorithms. Typical atmospheric columns with the identified cloud layers for selected imager pixels are shown in figure 0-16.

Determining cloud optical properties

With the cloud layers defined, we combine the full spectral information with theoretical calculations to obtain the cloud properties for each pixel. In most cases, we will use independent pixels with plane-parallel clouds as the basis for the theoretical calculations. An important input to these retrieval algorithms is a database of radiances from these calculations. While we used such a database on ERBE for spectral corrections to unfiltered radiances, here our use of theory is much more central to the appropriate retrieval of the cloud properties. CERES should be able to provide a much more sophisticated analysis than ISCCP has provided. ISCCP had to use a strong assumption relating visible optical depth to the microphysics of 10- μm water spheres. Also, during the day, ISCCP corrected the emitting temperature for an emittance less than 1. In contrast, CERES will determine the cloud particle size and phase using spectral channels at wavelengths of 1.6 μm and 2.1 μm during the day and 3.7 μm and 8.5 μm at night. Subsystem 4.3 of the ATBD's provides more detail on this step in the processing.

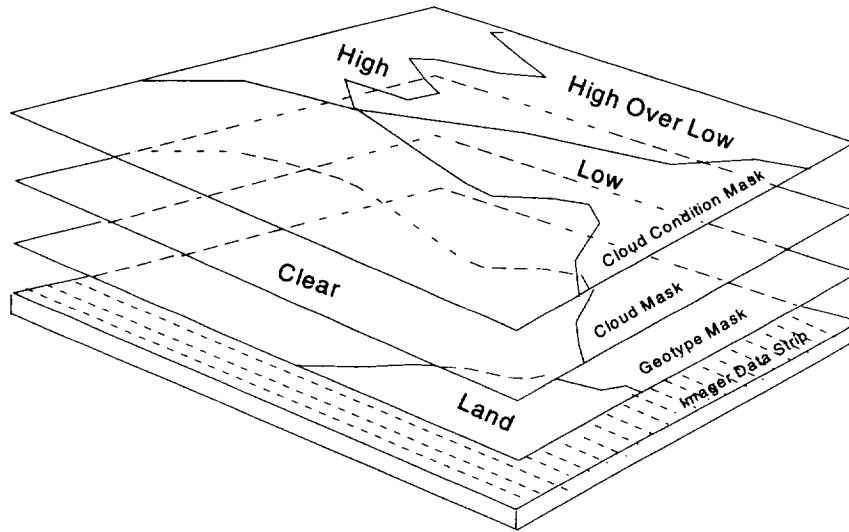


Figure 0-15. Portion of the imager data strip overlaid with cloud overlap condition mask. Following identification of cloud layers within the imager data strip, we expect to be able to separate pixels with only one layer from pixels with more than one cloud layer. The cloud overlap condition mask provides a single index for each imager pixel, identifying which of the 11 possible cloud overlap conditions occur in that pixel.

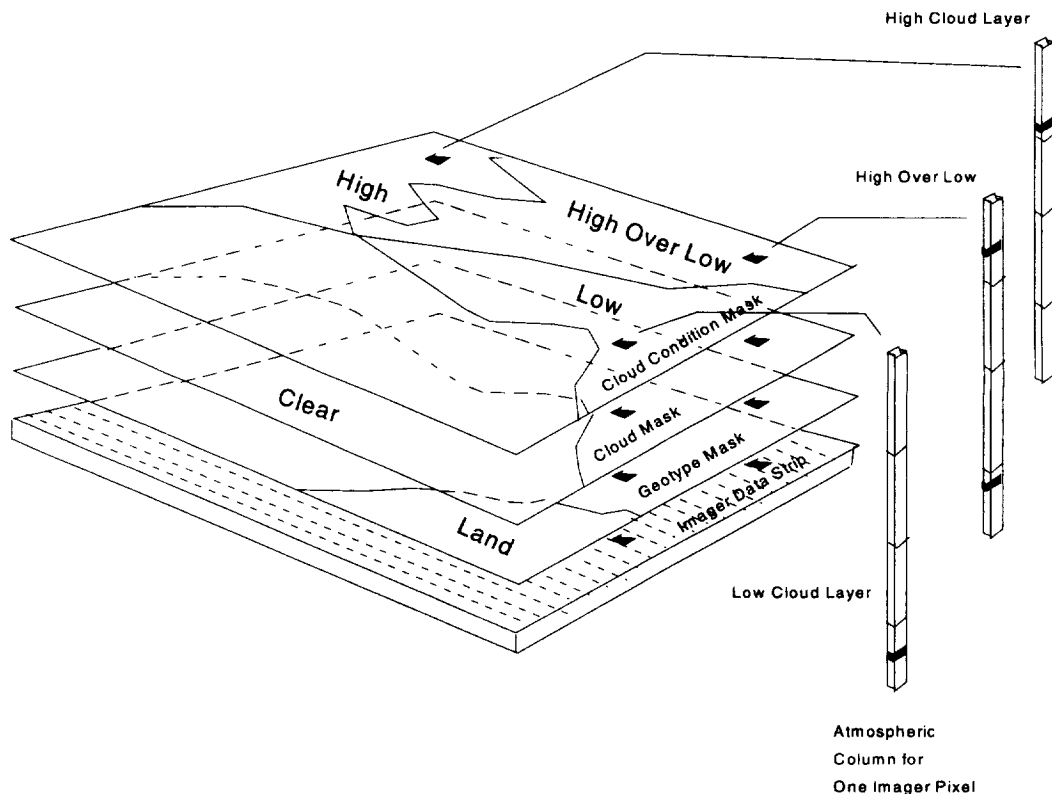


Figure 0-16. Sample atmospheric columns with identified cloud layers as they relate to the imager data strip and the overlying masks. The columns illustrate the schematic structure of cloud layers within an atmospheric column. The column lowest on the right has a cloud layer only in the lowest height category, as the cloud overlap condition mask over the pixel where this column is located. Likewise, the atmospheric column highest on the right has a cloud layer only in the upper height category. The regular horizontal markings on the columns indicate where the breaks between height categories occur.

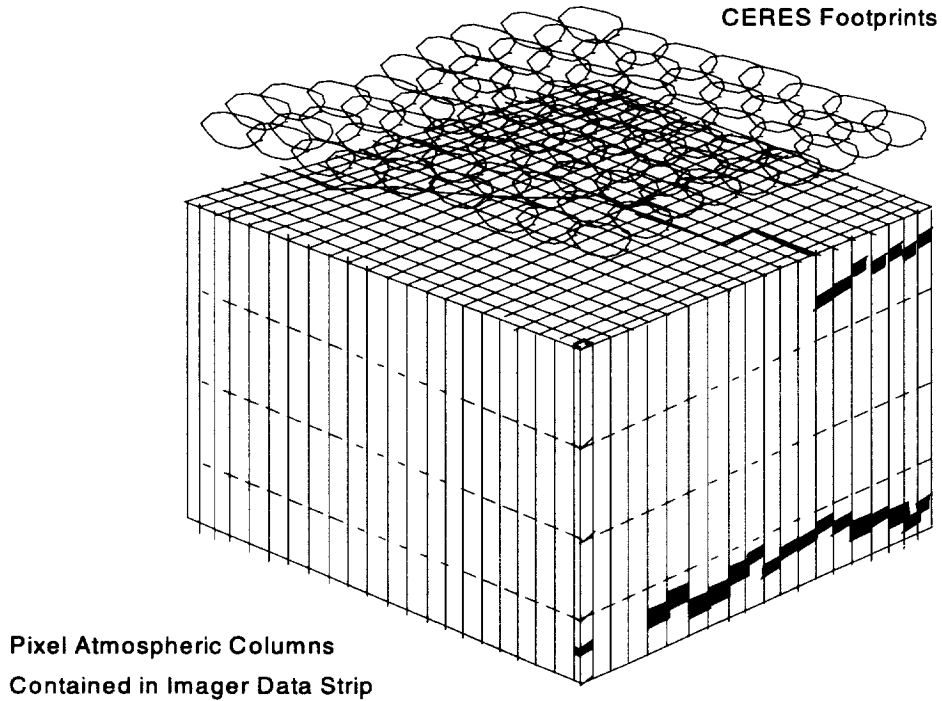


Figure 0-17. Arrangement of atmospheric columns in an imager data strip with respect to CERES footprints over the same strip. The atmospheric columns over the imager data strip are available as we enter the final stages of the cloud determination algorithms. Cloud layers in some of the columns appear as dark markings whose altitude varies from column to column. We also show a schematic representation of the relationship between these columns and the CERES footprints that contain them.

Placing clouds within the CERES footprint

When we have completed the cloud property determination we have just described, we can think of the geography in the Imager Data Strip as having an array of atmospheric columns over each pixel. Because the imagers use detectors etched into a block of semiconductor material, their pixels align themselves together, so that the atmospheric columns in the strip can be represented as a “block” of material, much like the lower structure in figure 0-17. In this figure, we can see markers delimiting the standard divisions between the cloud height categories. We can also see the cloud layers in some of the columns. Near the back, we have two layer columns; near the middle front, we can see the lower layer extending out below the high layer.

As the next step in processing, we need to summarize the cloud properties within a CERES footprint. To assist us in visualizing the relationship between the imager columns and the CERES footprints, figure 0-17 also shows a number of CERES footprints over the atmospheric columns. The elliptical outlines here are intended to represent the 95% level on the point spread function (PSF). These outlines are not to scale: each CERES footprint includes several hundred of the imager pixels. As we can see in the figure, the CERES footprints do overlap each other. To ensure maximum consistency between the cloud properties and the radiation fluxes, we have to carefully account for the quantitative structure of the PSF (see figure 0-18).

The PSF raises two important issues for consistency between the CERES radiative fluxes and the cloud properties: how to properly weight the contribution of various cloud properties to the CERES footprint and how to produce a proper average of values within a particular overlap condition. The answer to the first question is to weight the properties by the PSF contribution:

$$\langle f \rangle \equiv \int d\Omega P(\Omega) f(\Omega) \tag{0-28}$$

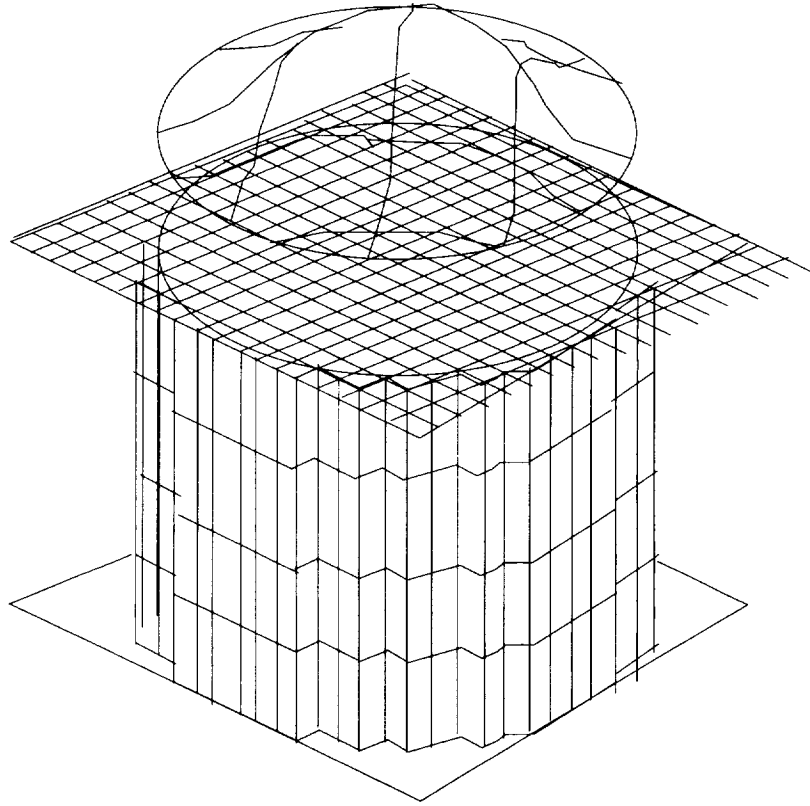


Figure 0-18. Relationship between CERES point spread function and pixel atmospheric columns.

In this expression, f is a quantity we want to average, Ω refers to a solid angle with respect to the optical axis, and P is the PSF. The PSF has units of inverse solid angle, so that if ΔA represents the area of an imager pixel located at a distance r from the CERES scanner, oriented with a viewing angle, θ , then the practical implementation of the previous equation is

$$\langle f \rangle = \sum_{\Delta A \text{ in FOV}} \frac{\Delta A \cos \theta}{r^2} P f \quad (0-29)$$

Because the contribution of a particular overlap condition may not be uniform, we need to allow each cloud layer to contribute properties to the layer average according to the relative contribution of the layer to the overall sum. Thus, we take

$$W(i|OVLP = Choice) \equiv \begin{cases} \frac{\Delta A \cos \theta}{r^2} P & \text{if } OVLP_i = Choice \\ 0 & \text{otherwise} \end{cases} \quad (0-30)$$

i refers to the i th pixel in the footprint. Then, for a particular cloud property, f , the appropriate average for this choice of overlap is

$$\langle f|OVLP = Choice \rangle = \frac{\sum_{i \in OVLP_i = Choice} W(i|OVLP = Choice) f_i}{\sum_{i \in OVLP_i = Choice} W(i|OVLP = Choice)} \quad (0-31)$$

This approach to averaging cloud properties to preserve consistency between the CERES radiative fluxes and the imager cloud properties is carefully laid out in ATBD subsystem 4.5.

Inverting the CERES data to TOA fluxes

We now have average cloud properties, overlap condition, and cloud height categories assigned to the CERES footprints. With this information, we choose an appropriate ADM for inversion. In addition to the inversion, ATBD subsystem 4.6 does the spectral correction and inversion from broadband radiances to TOA fluxes. There is no difference between the equations we use here and the equations we used for ERBE-like processing for either the spectral correction or the inversion. The major difference in detail lies in the choice of ADM. For the prelaunch and immediate post-TRMM launch releases of the CERES software, we will use the ERBE ADM's. Thus, the only choice we have in cloud parameters lies with the footprint averaged cloud fraction, C . However, when we have collected sufficient samples with the new cloud property identifications from the cloud imagers, we will make a new choice of ADM. ATBD subsystem 4.5 discusses new ways to determine ADM's and DM's.

Empirical surface flux algorithms

With the TOA fluxes available, we finally turn to the computation of the surface radiation budget with simple parameterizations. We will tie these parameterizations as closely to measurements of surface radiation budget as we can. ATBD subsystem 4.6 and the subsections 4.6.1–4.6.3 provide details of these algorithms for shortwave and longwave fluxes.

As in many other cases, there are advantages and disadvantages to this empirical formulation. On the one hand, there are three major points in favor of these ties:

1. The parameterizations are based on theoretical relationships but have coefficients that are tied directly to measurements of surface radiation budget
2. The careful calibration and characterization of the CERES instruments and the empirical source of the ADM's minimizes the chances of inadvertent biases appearing in the measurements because of incorrect theory
3. These relationships are computationally inexpensive

On the other hand, there are two major points against using these relationships:

1. Surface measurements are extremely sparse and may not be available at all when we need new measurements to derive coefficients
2. Not all radiative flux components at the surface may be available

0.5.3.3.2. Surface and atmospheric radiation budget determination. At this point in the processing system, we have the SSF data product that contains cloud properties and their statistics, as well as TOA fluxes for each CERES footprint. The next major process in the atmospheric branch of CERES processing determines the radiative fluxes through the atmosphere and at the Earth's surface for each of these footprints. Because the radiative transfer calculations also produce TOA fluxes with the retrieved atmospheric structure, this portion of the CERES processing will directly compute discrepancies between the directly derived CERES TOA flux and those that the transfer calculations derive. The algorithms in this portion of the system will then adjust the parameters that appear most likely to produce the discrepancy using a Lagrange multiplier technique. At the end of this process, the routine will recompute the internal and surface fields to produce the radiation fields within each of the CERES footprints and will write the results to the CRS data product. These algorithms are discussed in more detail in ATBD subsystem 5.0. At the end of this subsystem's processing, we will have an hour swath of CERES footprints with the full radiation fields and cloud properties, as consistently produced as possible. The product that contains this information is the CRS data product.

0.5.3.3.3. Gridding. The next subsystem in the CERES processing fixes the data with respect to the Earth and regularizes it in space and time. We start with the CERES footprints and suitably weight each one according to its contribution to a regional average. The regions are equal area, with a size about

1.25°, arranged in an ISCCP-like grid. For ERBE, we used a simple regional average scheme, in which a footprint contributes to the regional average if the center of its field-of-view was within the region. That approach has the disadvantage that it is moderately sensitive to spatial aliasing errors. Accordingly, for CERES, we will slightly modify the averaging weights of footprints falling in Earth-fixed geographic regions to produce consistent regional averages for both the radiative fluxes and the cloud properties. ATBD subsystem 6.0 discusses these algorithms in more detail. At the end of this process, we have regional averages of the radiation fields and of the cloud properties, as well as their statistics.

The FSW product that this subsystem produces contains only the regions observed within a given hour by a given satellite. It is true that we could combine several satellites together in producing regional averages, using the larger number of CERES footprints to improve the statistical sampling. However, there are likely to be many cases (particularly early in the processing) in which we will want to be able to examine how different satellites will contribute to the regional averages. For example, if we have concerns over the calibration of one scanner with respect to another, we may use the statistics of the differences in radiation from the two satellites as one objective measure of the discrepancy. Likewise, we will want to carefully examine the cloud properties of clouds retrieved from VIRS with those from MODIS, as well as those from the MODIS on the EOS-AM missions and on the MODIS-PM missions. By having separate granules for each satellite, we ease the operational burden on the CERES processing by allowing us to vary the parameters of each satellite's data reduction separately without forcing reprocessing of both to produce a new version of FSW.

Figure 0-19 illustrates the geometry of spatial sampling within a given hour, using data from ERBE. As with CERES, ERBE had a sun-synchronous satellite that covered the poles. We can see this satellite's swath in figure 0-19 as the fairly vertical track on the extreme right edge of the figure. ERBS provides an inclined orbit track, slightly to the left of the NOAA-9 track. One of the advantages of building FSW is illustrated in this figure in the region where the two swaths cross each other. When we want to merge the data from two or more satellites together, we already have the data fixed to the Earth and can spend much less time and computer resource sorting through the data. The gridding process also substantially reduces the volume of data we need to archive at this level of processing.

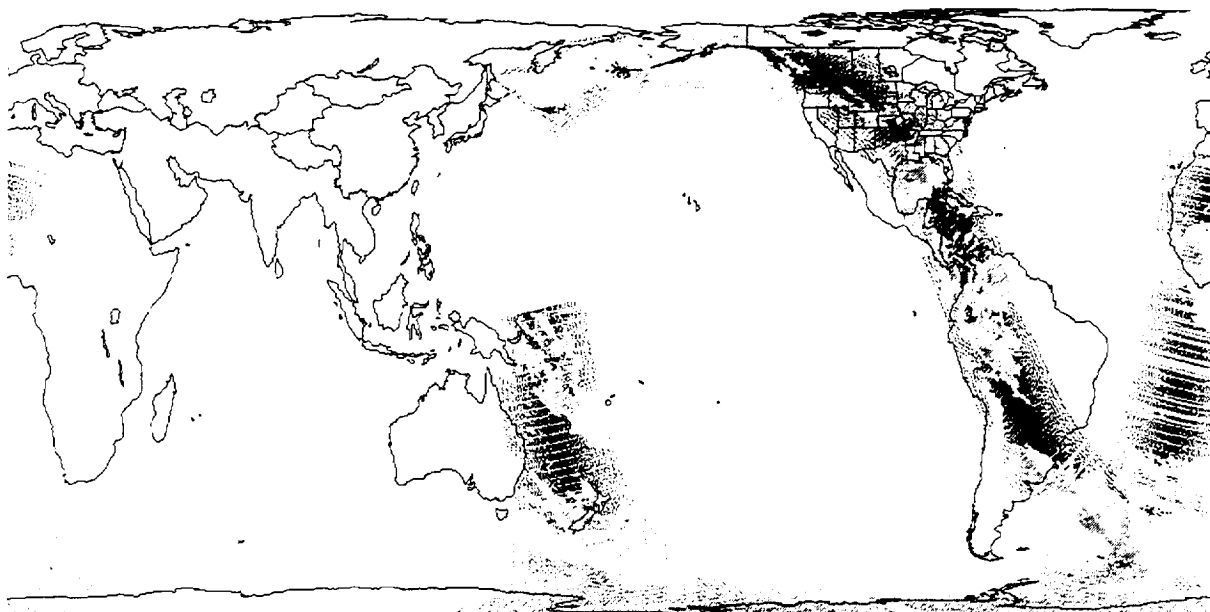


Figure 0-19. Longwave flux swaths from a single hour of ERBS and NOAA-9 data on July 2, 1985. High longwave fluxes appear as darker regions, while low longwave flux values appear as whiter regions. NOAA-9 provides the more vertical track on the extreme right of this figure, whereas the ERBS inclined orbit appears slightly to the left. The map projection is equal area.

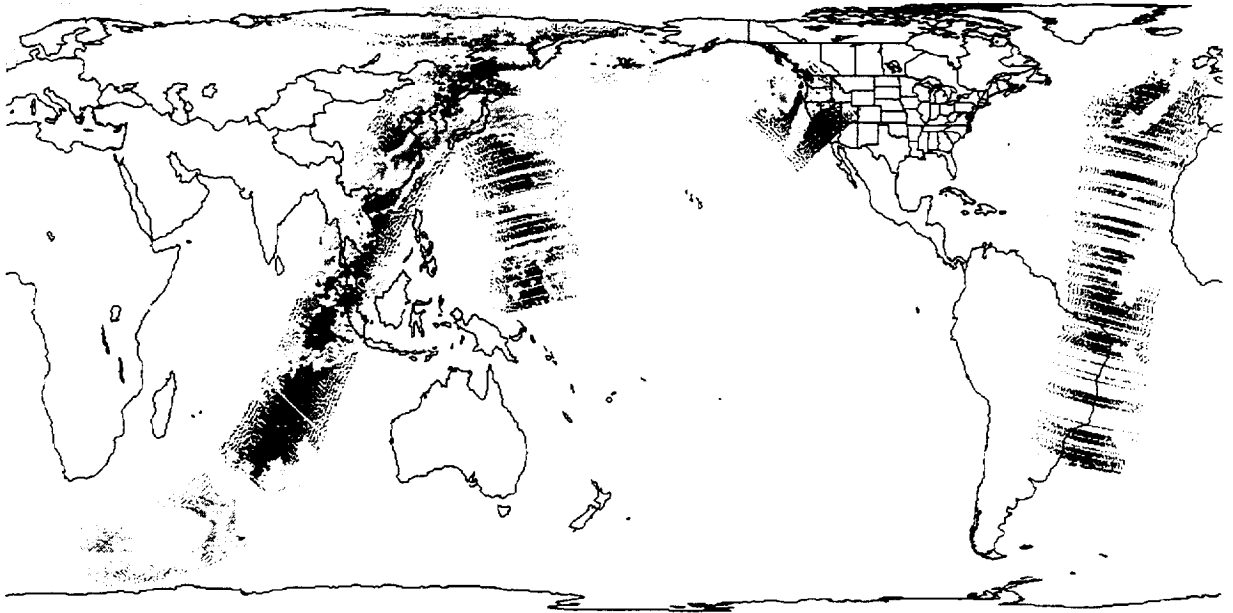


Figure 0-20. Longwave flux swaths from a single hour of ERBS and NOAA-9 data on July 2, 1985. Longwave flux and map projection are as in the previous figure.

0.5.3.3.4. Time interpolation to the synoptic product. Once we have the FSW data product, we can readily combine the data from several satellites in a single hour of the month. For TRMM, the swath of data within an hour will cover about eight percent of the Earth's area. When we combine the TRMM and the EOS-AM swaths of regions, we now observe about fifteen percent of the Earth's area in a given hour. Where these two swaths overlap, we need to combine the data together. Again, figure 0-20 shows overlapping satellite swaths on the same day. Because of precession, the two orbits now cover a different portion of the Earth, although their relative geometry on a given day is nearly fixed.

Next, because radiation interacts with the atmosphere and the Earth's surface in ways that require time scales of a week or longer to be fully felt, we generally require averages of the clouds and radiation over periods of about a month. To regularize the process of time interpolation, it will be much easier to work with even time intervals. Thus, bringing the radiation and cloud data together in a synoptic product eases the work of time averaging. Indeed, it makes visible the time interpolation. In addition, the synoptic view of the Earth makes it much easier to understand the spatial structure of such extended fields as those of cloud systems. The features that appear in these images are much more easily recognized than they are in asynoptic presentations of the data. The synoptic presentation also makes it easier to understand these features as physical phenomena than if we leave them with only a heavily smeared, time-averaged representation.

Figure 0-21 shows a longwave synoptic image obtained from data shown in the previous two figures, as well as other ERBE data spread over 24 hours on each side of the time shown here. Owing to the long spatial scale of cloud system correlations, as well as the fact that cloud systems do not appear to move extremely rapidly, this image shows the recognizable features, such as storms and fronts, that we just discussed.

Based on the ERBE approach, we can use a simple form of interpolation to go from one observation of a region to the next. Such a strategy will allow us to "fill in" the map in the areas where we are missing data. Interpolation of cloud properties is also straightforward, as suggested in ATBD subsystem 7.0. To base our knowledge of time variations on observations, we then need to bring in the geostationary satellites. The algorithm suggested in display 0-1 shows how we expect to bring this new information to bear on the time variability problem. When this algorithm requires geostationary data, the first three



Figure 0-21. Longwave flux synoptic image for July 2, 1985. Light areas are cold cloud-top regions; dark areas are hot, clear-sky regions. This image was built with simple linear interpolation between observations, very similar to the approach adopted for most of the ERBE time averaging algorithms.

steps pick up on the information already produced by the regional averaging process that gives us the FSW data product. In step 4 of this algorithm, we use the interpolated scene ID vector to give a single ADM for a region observed by the geostationary. By using regressions that relate the narrowband, geostationary radiance to the CERES broadband radiances, we can tie the calibration of the operational instrument to the accurate calibration of the CERES radiometers and also produce a surrogate, broadband flux. *We already have observational evidence (Minnis, et al. 1991) that such regressions are highly variable from one region of the Earth to another, and are quite variable with time, since they must account for both the calibration instability of the geostationary instruments and for atmospheric variability.* To then ensure consistency between the geostationary time-filling and the cloud properties, we adjust the cloud properties to agree with the geostationary interpretations of the time variations. Finally, we compute the fluxes within the atmosphere using the adjusted cloud properties. At the end of this process, we have the SYN product that contains both radiation and clouds on a regional basis every three hours.

0.5.3.3.5. Monthly atmospheric averaging. With the SYN product, we have a relatively straightforward start to time averaging. As suggested in ATBD subsystem 8.0, we operate with the time series for each region independently of the time series for other regions. We still need to ensure that the systematic time variations in thermal structure and in directional dependencies of the scenes that we observe are properly and consistently taken into account.

0.5.4. Surface Processing

The surface processing (figure 0-22) constitutes the third (and final) major branch of the CERES processing system that we will discuss here. What we hope to achieve with this branch is to improve the surface radiation budget data with information derived directly from the CERES TOA fluxes and to provide a much smaller set of data for climate investigations. In order to compress the data volume, we vertically average the cloud properties and weight them according to the contribution they make to various fluxes, such as longwave flux at the Earth's surface or shortwave net cloud forcing. To keep the data as consistent as possible with the atmospheric branch of CERES processing, we also introduce the geostationary radiances into the time averaging of the surface branch.

```

for regions on the Earth loop
    if CERES has an observation in the region at this hour
    then
        Synoptic Fieldsregion := CERES Fieldsregion;
    else
        Linearly Interpolate Cloud Layer Propertiesregion;
        Linearly Interpolate Cloud Overlap Fraction Vectorregion;
        Linearly Interpolate Scene ID Vectorregion;
        Choose ADM with Interpolated Scene Vector;
        Use broadband to narrowband regional,
            short-term regressions to estimate  $I_{GEO}$ ;
        Get  $F_{GEO}$  from  $\pi I_{GEO} R_{interpolated\ scene\ vector}$ ;
        Adjust Layer and Overlap Vectors to Agree with  $F_{GEO}$ ;
    end if;
end loop;

```

Display 0-1. Algorithm for time interpolation of TOA fluxes and clouds using geostationary data.

0.5.4.1. Major inputs. The surface processing branch starts with the SSF data already produced from the cloud determination process, subsystem 4.

0.5.4.2. Major outputs. The *SFC* (Surface Flux) product contains a single hour of single satellite measurements of clouds and TOA radiation fluxes, together with surface radiation budget fluxes of net shortwave and longwave radiation. The surface net fluxes are derived from the TOA fluxes by regression methods similar to those of Li and Leighton for the shortwave flux and from the work of Inamdar and Ramanathan for the longwave part of the spectrum. The data in this product are organized into the CERES footprint, spatially ordered data that we mentioned for the IES data product.

The *SRBAVG* (Surface Radiation Budget Average) product contains the monthly average of the net surface flux data at a spatial resolution of 1.25° in latitude and longitude. We expect routine production to have all of the satellites with CERES instruments included in this average. Some nonstandard production runs may not include all of the satellites or all of the instruments.

0.5.4.3. Processing description. The process here is considerably simpler than it is in the atmospheric branch. We start with the SSF data product and immediately average the data to horizontal regions, as well as compressing the vertical structure of the cloud properties to column averages. Such compression should aid GCM investigators who want simpler cloud property indicators. With the regional averages, this branch then activates the time averaging process. At the end, the system produces regional averages of TOA fluxes and surface radiation budget information using relatively simple algorithms.

This branch includes two relatively simple new concepts that influence the processing:

- a. Simplified algorithms to directly relate the TOA fluxes to surface fluxes
- b. Column averaged cloud properties

There are two types of *simplified algorithm for deducing surface fluxes from TOA fluxes*: shortwave net flux algorithms, such as the algorithm suggested by Li and Leighton (1993), and longwave net flux

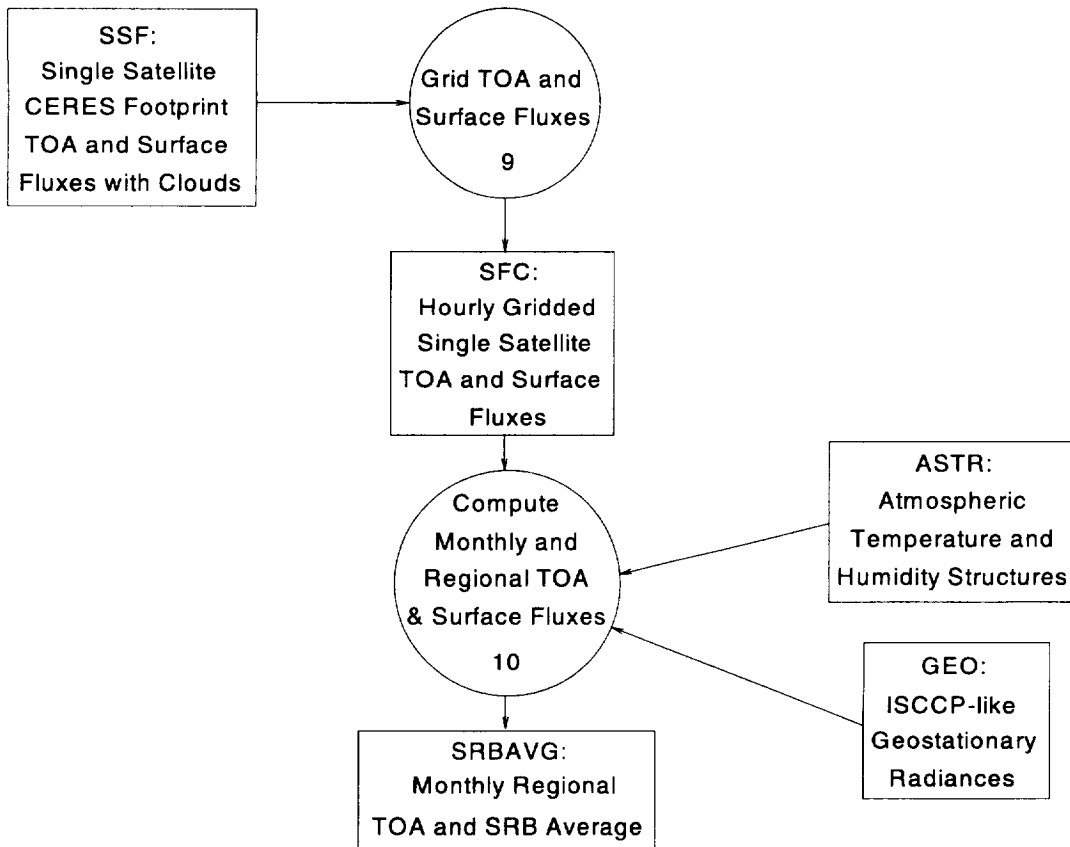


Figure 0-22. Major data products and processes for the surface processing subsystems.

algorithms, such as that suggested by Inamdar and Ramanathan (1994) in subsystem 4.6.2. For the first of these algorithms, we use the principle that the net flux of solar energy is absorbed by water vapor or by clouds in the same part of the spectrum. Therefore, the energy removed acts as a nearly constant offset (slightly dependent on the column amount of water vapor) and linearly proportional to the net flux at the top of the atmosphere. In the case of the longwave flux, the algorithm proceeds by using the surface temperature to derive a net upward flux from the surface and then computing the downward flux from a combination of window channel observations and some additional information from atmospheric water vapor column amount. Both of these algorithms are described in more detail in subsystem 10 of these ATBD's.

In order to provide a more useful data set to the modeling community, we also carry *column averaged cloud properties*. For purposes of simply summarizing the effect of clouds on the longwave TOA flux, we observe that simple parameterizations often approximate the effect of clouds as being proportional to $T_{sfc} - T_{cld}$. More carefully, we expect to construct such weightings as $C_e(T_{sfc} - T_{cld})$. In the products emerging from the surface branch of the CERES processing, we use five of these weightings to summarize the properties of the cloud fields.

0.5.4.3.1. Horizontal gridding and vertical averaging. The first subsystem in this branch of the CERES processing goes from the footprint values in SSF to the regional averages that are familiar to us from the atmospheric branch processing in subsystem 6 (cf. the ATBD subsystem 6.0 for details). The major change in the output lies in the vertically averaged cloud properties that we need to carry to reduce the data volume. Because different groups have different needs, there are different column averaged cloud properties that we carry into the SFC output product.

0.5.4.3.2. Monthly surface averaging. As with the horizontal gridding, the monthly averaging of the surface branch of CERES processing repeats much of what we did in the atmospheric branch. ATBD subsystem 10 describes the variations on the algorithms.

0.6. System Uncertainty Estimation

The estimation of uncertainties for the various data produced by any of the EOS instruments is a large and difficult problem. Although the desire for clearly and precisely stated estimates of uncertainty is a fundamental motivation for much of what we do, the practical development and application of such estimates is an area in which considerable research is required.

We can cite the ERBE experience as an example. Often, the community thinks of the radiation budget as being made of three numbers: a solar irradiance (about 341 W-m^{-2}), a reflected flux (about 30% of the solar irradiance), and an emitted flux (about 235 W-m^{-2}). Surely, the measurement providers should be able to provide a simple estimate of the uncertainty in those numbers. Why can't we just take the calibration uncertainty and carry that through to the final numbers?

The answer to that question requires a more detailed understanding of how the ERBE system actually produces the numbers. If we take the CERES ERBE-like processing as an illustration of what is involved, we find that there are at least three major steps in the processing:

1. Instrument calibration
2. Inversion, where we need the scene identification, spectral characterization of the instrument and of the Earth scene, and the relationship between the measured radiance and the flux leaving the top of the atmosphere
3. Averaging, where we need to account for the satellite sampling of the time variability of the TOA flux and systematic variations with time of day (LW) and with solar position (SW)

For each of these processes, there are many constants and some fairly complex algorithms. One measure of complexity is simply the number of constants the processing system needs to maintain. The number of constants for each part of the ERBE processing is roughly as follows:

1. About 300 offsets and 3 gains for each satellite
2. About 10000 ADM values, with an additional 10000 standard deviations, and 6000 spectral correction matrix elements
3. About 200 directional model values

For each system, there are complexities to calculating uncertainties.

For example, the scanning radiometers are instruments with gains and offsets. The standard error calculations that are often quoted in radiometry come from experience with instruments trying to observe single valued sources in a calibration chamber. In contrast, the Earth-viewing radiometers we use for radiation budget work use calibration to determine a gain through a linear regression. Although the equations for deriving uncertainties with regressions are well known, and involve calculating fidelity intervals (which seems a better nomenclature than inverse confidence intervals), this more rigorous approach is not commonly used in quoting uncertainties. If we are forced to think of the calibration as a "sum of squares," the individual measurement levels in the calibration should act as independent contributors to the gain and thereby reduce the amount of uncertainty. However, the uncertainty now varies with the radiance being measured, so that an appropriate numerical value for uncertainty must carefully state the population of Earth radiances being measured.

The other processes that enter the radiation budget measurements involve even more complex considerations. For example, the ADM's that enter directly into the calculation of TOA flux are subject to angular variations about the mean models we use in the data reduction. With the current sampling, we cannot distinguish between true variations in the ADM's (a source of perceived "scintillation") and high spatial frequency variations in the TOA flux (a source of true "scintillation" in the field). Indeed, the

two kinds of variation are correlated, and thus require careful mathematical and numerical treatment. It is also true that the scene identification and the variations in ADM's are correlated. This fact means that rigorous treatment of the uncertainty propagation needs to carefully account for the space and angle sampling that produces the actual measurements. Because angular sampling and latitude are far from independent in satellite experiments, computing the spatial pattern of both instantaneous and time averaged measurement errors is a far from trivial exercise. The nature of the problem is not too difficult to imagine: consider the fact that in July, a noon Sun-synchronous satellite will sample the terminator in the far Southern reaches of the Earth, while the Sun is nearly overhead in the top half of the Northern hemisphere.

In the subsections that follow, we attempt to provide a moderately quantitative picture of what we believe is a likely assessment of uncertainties. The assessment we provide is based on a simpler estimation process than the more rigorous assessment whose difficulties we have just described. Particularly for the TOA fluxes, we will assume that there are three dominant contributions to the uncertainty: instrument calibration, ADM variability and error, and time sampling. We treat these sources of error as independent of each other and try to assess their relative contribution to appropriate kinds of data products. For the other types of data with which CERES works, we provide uncertainty estimates based on a similar kind of understanding. In most cases, we have more detailed assessments of uncertainty for each of the subsystems. These assessments will be found within the ATBD's of the subsystem.

0.6.1. Top of Atmosphere (TOA) Radiative Fluxes

The measurement of TOA fluxes will enter its fourth generation with the CERES instruments on the TRMM and EOS AM and PM spacecraft. The most recent ERBE measurements provide the standard of comparison for global radiation data sets. This success was gained though extensive prelaunch work with a science team to

- a. Oversee instrument design, development, and testing
- b. Design data products
- c. Design analysis algorithms.

A final key element was an integrated data management team to execute two versions of the data system before launch. This is the same overall strategy being used by the EOS project for the EOS data products. Because there is no "ground truth" to test the accuracy of satellite TOA flux estimates, a comprehensive set of internal consistency checks is required to achieve high quality data (Barkstrom et al. 1990). As a result of the extensive ERBE, Nimbus 7, and Nimbus 3 experience, there is a good understanding of the sources of error in determining TOA radiative fluxes.

In essence, the measurement of TOA fluxes is a 7-dimensional sampling problem. The dimensions are listed in table 0-4, along with the sampling solution planned for the EOS observations:

Table 0-5 gives an estimated error budget for the CERES TOA fluxes as compared to the ERBE scanner data. Error estimates are taken from several studies of the Nimbus 7 and ERBE data (Suttles et al. 1992; Harrison et al. 1990; Green et al. 1990; Barkstrom et al. 1990; Suttles et al. 1988 and 1989). Table 0-5 considers error estimates for both the instantaneous TOA fluxes which might be useful for input to extended range forecast models, as well as errors for commonly used climate data products. The results indicate that for instantaneous measurements, the CERES TOA flux errors will be dominated by angular sampling errors. For monthly average regional observations, net TOA flux errors are roughly equally caused by calibration, angular sampling, and time sampling errors. For the equator-to-pole gradient of net radiative flux critical to the determination of net oceanic heat transport (Vonder Haar and Oort, 1973) angular sampling errors caused by systematic variation of solar zenith angle with latitude are dominant. For climate monitoring, (i.e. year-to-year variability) errors are dominated by calibration stability. Overall, the CERES measurement errors are expected to be a factor of 2 to 4 lower than the ERBE errors.

Table 0-4. Sampling Dimensions and Solutions

Number	Dimensions	Sampling Solution
1	Spectral	Broadband CERES spectral channels
2, 3	Spatial (Longitude, Latitude)	Cross-track scanning CERES radiometer
4, 5, 6	Angular: (View Zenith, View Azimuth, Solar Zenith)	Conversion of measured radiance to flux uses empirical angular models measured by a second CERES scanner which rotates in azimuth as it scans in elevation. Models require coincident cloud imager data.
7	Temporal	6 samples per day provided by a 3-satellite system: 2 Sun-synchronous orbits (EOS-AM, PM) and 1 precessing orbit (TRMM).

Table 0-5. CERES TOA Flux Error Budget

Field	Monthly Average Regional 5 yr. trend Solar Irrad. 340 W-m ⁻²		Monthly Zonal Average Equator to Pole Diff. Solar Irrad. 340 W-m ⁻²	
	ERBE	CERES	ERBE	CERES
Calibration	2.0	1.0	0.2	0.1
Angle Sampling	0.0	0.0	12.0	4.0
Time Sampling	0.0	0.0	2.6	1.0
Space Sampling	0.3	0.3	0.0	0.0
Total SW Error	2.0	1.1	12.3	4.1
Calibration	2.4	1.2	2.6	1.3
Angle Sampling	0.0	0.0	2.0	0.7
Time Sampling	0.0	0.0	0.9	0.7
Space Sampling	0.2	0.2	0.0	0.0
Total LW Error	2.4	1.2	3.4	1.6
Calibration	3.1	1.6	2.6	1.3
Angle Sampling	0.0	0.0	12.2	4.1
Time Sampling	0.0	0.0	2.8	1.2
Space Sampling	0.4	0.4	0.0	0.0
Total Net Error	3.1	1.6	12.7	4.4
Science Requirement	2 to 5	<1	10	1 to 3
Calibration	2.1	1.0	6.0	3.0
Angle Sampling	3.3	1.1	37.5	12.5
Time Sampling	2.6	1.0	0.0	0.0
Space Sampling	0.3	0.3	0.0	0.0
Total SW Error	4.7	1.8	38.0	12.9
Calibration	2.4	1.2	2.4	1.2
Angle Sampling	1.6	0.5	12.5	4.2
Time Sampling	0.9	0.7	0.0	0.0
Space Sampling	0.2	0.2	0.0	0.0
Total LW Error	3.0	1.5	12.7	4.3
Calibration	3.2	1.6	6.5	3.2
Angle Sampling	3.7	1.2	39.5	13.2

Table 0-5. Concluded

Field	Monthly Average Regional 1 Std. Dev. Solar Irrad. $340 \text{ W}\cdot\text{m}^{-2}$		Instantaneous footprint 1 Std. Dev. Solar Irrad. $1000 \text{ W}\cdot\text{m}^{-2}$	
	ERBE	CERES	ERBE	CERES
Time Sampling	2.8	1.2	0.0	0.0
Space Sampling	0.4	0.4	0.0	0.0
Total Net Error	5.6	2.4	40.1	13.6
Science Requirement	10	2 to 5	none	10

The improvements are realized from three major elements:

1. Factor of 2 improvement in instrument calibration by using more accurate ground and onboard calibration sources
2. Factor of 2 to 4 improvement in angular sampling errors by the use of the rotating azimuth plane CERES scanner to fully sample angular space combined with the use of advanced cloud imagers (VIRS, MODIS) to identify anisotropic targets as a function of cloud and surface properties
3. Factor of 2 to 3 improvement in time sampling errors by the use of a three satellite sampling system and the use of improved shortwave directional models

0.6.2. Surface Radiative Fluxes

Global satellite estimates of radiative fluxes at the surface (up, down, and net) are now becoming available (Darnell et al. 1992; Li and Leighton, 1993). In general, the intervening atmosphere complicates the measurement when compared to the more straightforward derivation of TOA fluxes. A major advantage, however, is the ability to test satellite-based surface flux estimates directly against surface-based measurements such as those currently provided by the Global Energy Balance Archive (GEBa) (Ohmura and Gilgen, 1991) and in the future against the Baseline Surface Radiation Network (BSRN), (WMO, 1991) now being established around the globe.

As a result of this ability, two independent approaches are desirable for determining surface radiative fluxes:

1. Calculation of surface fluxes using observed cloud and atmosphere parameters with measured TOA broadband fluxes acting as a constraint on the radiative calculation.
2. Parameterized relationships between simultaneously observed TOA fluxes (or radiances) and surface fluxes. These relationships are based on radiative transfer calculations and are validated empirically.

Work is progressing on a range of approaches between 1 and 2. Initial SRB estimates of SW up, down, and net fluxes use ISCCP narrowband radiances, but without a constraining broadband TOA flux measurement (Darnell et al. 1992; Pinker and Laszlo, 1992). Verification against GEBa data and FIRE field experiment data indicate monthly average 2.5° regional mean accuracies of about $20 \text{ W}\cdot\text{m}^{-2}$ (1s). While this is not as accurate as estimates of TOA fluxes using ERBE, much of this discrepancy may be caused by spatial mismatching of the scales of observations for the satellite (250 km) and the surface (30 km) observations. In the time frame of the EOS observations, calculated SW surface flux accuracies should increase greatly as more accurate cloud properties (VIRS, MODIS), atmospheric (AIRS), and surface properties (MISR, MODIS) become available, and as broadband measurements of TOA fluxes can be used to constrain the model calculations, including implicit corrections for 3-D radiative transfer effects. The MISR measurements of the BDRF of vegetation canopies will provide improved separation of net surface SW flux into upwelling and downwelling components.

The second approach to SW flux estimation is a direct linear relationship between net SW flux at the top of the atmosphere and net SW flux at the surface (Cess et al. 1991; Li and Leighton, 1993). This relationship is verified empirically as a function of solar zenith angle. The rationale for this method (Davies et al. 1984) is that water vapor absorption and absorption by liquid water and ice occur in the same portion of the spectrum. To first order, placing a cloud in the atmosphere simply changes the vertical distribution of solar absorption, but not the total. The dependence of the absorption on solar zenith angle can be understood as a change in path length. Because cloud particles can reflect a significant amount of radiation even at absorbing wavelengths, however, and because that reflection depends on particle size and shape, there are still questions about accuracy as a function of cloud type and height. The key for improvements in the empirical algorithm is to obtain more extensive surface observed net SW fluxes for validation as a function of varying cloud conditions and climate regimes. The FIRE, DOE ARM program, and the WCRP BSRN observations will be key to increasing the accuracy and confidence in this empirical approach.

The situation for LW surface fluxes is more complex, at least for downward LW flux at the surface. Calibration of surface LW flux pyrgeometer measurements is still questionable and downward flux radiative computations are dominated by low-level water vapor and cloud base altitude (Gupta, 1989; Gupta et al. 1992), two of the more difficult measurements to obtain from space. For clear-sky conditions, encouraging progress has been made on direct relationships to TOA LW fluxes (Inamdar and Ramanathan 1994; Stephens et al., 1994). In the EOS time frame, improved lower tropospheric water vapor will be available from the AIRS/MHS instruments. Tests are underway using FIRE observations to examine methods to relate satellite measurements of cloud temperature and optical depth to estimate cloud geometrical thickness (Minnis et al. 1990; Minnis et al. 1992). Recent sensitivity studies using ISCCP cloud data (Charlock et al. 1992), however, indicate that cloud overlap may in fact be the limiting source of information for calculations of downward longwave flux at the surface. Methods to derive multiple cloud layers from satellite data, however, have only recently begun and a great deal of additional emphasis is needed in this area. Two approaches appear promising. For optically thin high clouds, infrared sounding channels can isolate the high cloud, while visible and infrared window channels are used for the low level cloud (Baum et al. 1992). For optically thick high clouds, a combination of optical measurements for the upper (ice) cloud and microwave measurements for the low (water) cloud may help define cloud overlap. In the long term, active systems such as the GLAS lidar for optically thin cloud and a 94 GHz cloud radar for optically thick cloud offer the best solution (GEWEX, 1994). For surface LW emission, additional work is still required to improve models of land emissivity and directional thermal emission from vegetation canopies (Li and Becker, 1993; Sellers and Hall, 1992; Slingo and Webb, 1992).

0.6.3. Radiative Fluxes Within the Atmosphere

Determination of radiative fluxes within the atmosphere is necessary for the radiative components of the atmospheric energy balance and to estimate radiative heating rates within the atmosphere. Clearly, the most accurate measurement of radiative energy budget of the atmosphere will be for the total atmospheric column. This total column radiation budget can be simply obtained by differencing the TOA and surface radiative fluxes discussed in previous sections of this ATBD.

A second level of sophistication is required for determining the vertical structure of the atmospheric energy budget and of radiative heating rates within the atmosphere. Even for aircraft observations, this is an exceedingly difficult measurement, primarily because of the large spatial and temporal variability of cloud fields. Estimates from space will necessarily be a combination of observed atmospheric properties (temperature, water vapor, aerosols) and cloud properties used as input to radiative transfer calculations. One of the primary concerns will be the accuracy of these radiative models. However, during the EOS data period we will have the advantage of using broadband TOA flux observations to constrain the model solution. For example, if SW TOA fluxes calculated for a cloud field disagree with TOA

measurements, then the satellite derived cloud optical depth could be adjusted to get agreement. In this case, the error in both the satellite optical depth estimate and the radiative calculations could both be caused by the use of a 1-D radiative transfer model for a 3-D cumulus cloud field. Since the TOA flux measurement will use CERES measured anisotropic models appropriate for a 3-D cumulus cloud field, the TOA conversion of SW radiance to flux can in fact include the typical 3-D radiative properties of the cloud field, and thereby remove most of the bias in the radiative flux calculations of the effect of the cloud within the atmosphere. The bias is removed by adjusting the cloud optical depth to one which would give a 1-D equivalent albedo. In this way, the radiative flux profile within the atmosphere will be consistent with TOA observations, and the cloud optical depth estimation can be corrected for first order 3-D effects as well.

Even with TOA flux constraints, however, the ability to remotely sense cloud thickness, or cloud overlap is subject to serious question. As a result, the initial strategy for EOS is to phase in progressively more advanced estimates of radiative fluxes within the atmosphere, as indicated below:

At launch	TOA and Surface Fluxes only
18 months after launch:	Add Tropopause and 500 hPa levels
36 months after launch:	Add 4 to 12 levels as further study warrants

One of the key elements for testing within atmosphere flux calculations is likely to be the use of remotely piloted aircraft currently under development which are capable of gathering statistics over very long flight legs with accurately stacked flight tracks (ARM began test flights in spring, 1994). The remote sensing challenges for within atmosphere fluxes are similar to those for downward LW flux at the surface: profiles of water vapor, cloud thickness, and cloud overlap.

0.7. Implementation Issues

0.7.1. Strategic Concerns and Risks

There are three major strategic concerns for the CERES data processing system

- Managerial complexity during software development
- Logistic and scheduling complexity, particularly given the requirements for rapid validation of data products
- Requirements for early product sizing and algorithm compute power estimates

The first strategic concern is the managerial complexity during the design and construction of the processing system. Members of the CERES Science Team must provide the algorithm specifications; a combination of the Science Team and Data Management Team will construct the system and operate it. Each Team has its own skills and concerns, yet they must act as one body in producing and operating it. Science Team members are often reluctant to specify exception handling. Data Management Team members may work with tools that do not communicate well to the scientific community. Furthermore, some of the scientific requirements (and perhaps the most important) cannot be quantified or tested within the current understanding of the system. For example, estimates of whether or not certain data products fall within acceptable uncertainty limits may require computer power that exceeds that of any foreseeable system. Within this complexity, we must develop ways of communicating the technical material of the system design so that both the Science Team and the Data Management Team can successfully assemble the necessary parts of the system and make it operate as a single entity.

The second strategic concern is that the CERES system will operate at the limits of computer CPU, data throughput, network capacity, and system complexity. All preliminary estimates suggest that CERES data processing might exceed foreseeable growth in computer resources unless substantial care is taken to specify the processing system.

The third strategic concern is with operations. The CERES software system is complex and must operate asynchronously. In other words, the input data do not arrive on a synchronous schedule, yet processing may depend on arrival of several different data sets. For example, the CERES instrument data from the TRMM platform may arrive within 24 hours of data collection, the TRMM ephemeris may arrive 2 weeks later, and the VIRS data from TRMM may come in 1 month later. At the same time, the EOS-AM CERES data may arrive 6 hours after data collection, while the MODIS data on the EOA morning platform arrive 3 days after collection. We can process the CERES data for each platform through the ERBE-like part of the system almost immediately after receipt of the instrument and ephemeris data. The cloud identification part of the system cannot proceed until the VIRS or MODIS data have arrived. Production of the monthly averages of combined cloud and radiation field data cannot be completed until the full month's processing through synoptic fields is finished. Clearly, a major strategic concern is with the logistics of the data processing.

A further complication comes from the fact that the CERES data processing must allow rapid validation of the data products. This requirement forces us to consider systematic design of the processing system, so that we have identified the individuals and data products that they will have to prepare and examine. The same requirement also forces us to make every provision for having tools available to examine unexpected artifacts in the data products. Thus, we will need both quality control products and tools that can select a subset of data in which an artifact appears and can then track the causes of the artifact back to their roots. In other words, we need to provide a clear description of the processing schedule, of the individuals needed to carry out the quality control operations, and the tools they need for trouble shooting in the expectation that there will be unexpected artifacts in the data.

0.7.2. Risk Mitigation Strategy

To meet the strategic concerns, we have adopted a number of specific actions. These include heavy emphasis on clear and early development of design requirements and constraints, early specification of external and internal interfaces, rapid prototyping of system operation, and integration of Science Team and Data Management Team activities from the beginning of the program.

To meet concerns over the complexity of the system development activity, we have adopted the following strategies:

- Early development and prototyping of design documentation with the integrated science and data management teams
- Use of precise and proven tools for describing software design, such as data flow diagrams, data dictionaries, and structured process descriptions
- Systematic trade-off studies of programming languages and environments early in the design effort
- Early development of design, inspection, coding, and testing standards and use of group software development as a means of enforcing these standards

To meet concerns over system storage, and CPU demand, we have adopted the following strategies:

- Top-down decomposition of the system to get early interface definition and early description of critical algorithms
- Early specification of external and internal data products to provide explicit size and throughput estimates

To meet the concerns over logistics of data processing, we have adopted the following actions:

- Early estimates of system operations concepts, so that systematic scheduling tools can be developed early
- Early prototyping of system operations and documentation
- Early planning of routine operations and specialized validation activities to identify individual positions needed for Q/C and to identify tools for validation and Q/C

0.7.3. CERES Processing System Development

The CERES data processing system must respond to improved understanding of the algorithms in a way that accommodates the need for change, yet does not break down under the stress of substantial revisions to that understanding. As we have seen, our intent has been to manage this development process through a set of four software releases:

- Version 0, an experimental confederation of available algorithms intended to aid in testing some of the preliminary ideas for CERES processing against available software and to develop a baseline for estimating system processing loads
- Release 1, the initial prototype system that will be developed from the technical basis provided by this set of ATBD's
- Release 2, the first operational system that will be ready to process the first CERES data following the launch of TRMM and continuing through the launch of EOS-AM1
- Release 3, the first postlaunch operational system that will include the new ADM's based on CERES data rather than on Nimbus 7 data

Version 0 algorithms have been used in many of the sensitivity studies that are described in other ATBD Subsystem volumes. Their code also forms the basis for the system performance estimates we include later in this section of the CERES System ATBD. For estimating the processing load for the ERBE-like portion of the system, we have used a porting of the ERBE code from CDC computers to UNIX workstations. This code forms one of the major bases of the Version 0 software.

Release 1 will contain the first set of CERES algorithms designed to operate as a system. Thus, we expect it to allow us to check out the interfaces between the major subsystems and to verify some of our expectations regarding system loading. This release should be sufficiently complete to allow us to test the algorithms on a month of existing data for October 1986. These data are global in extent and comes from simultaneous observations by ERBE, AVHRR, and HIRS from NOAA-9. Similar observations are available on a more limited basis, covering the period from December 15, 1986 to January 15, 1987. During this period, data from NOAA-9 and NOAA-10 can be used, particularly for testing multi-satellite algorithms.

Release 2 will be based on the experience we develop in designing and implementing release 1, as well as on new technical developments. This system will be the one ready at the launch of the Tropical Rainfall Measuring Mission in August 1997. To be ready for processing with this release, we expect to begin to migrate the source code to EOSDIS computers at the Langley Research Center's Distributed Active Archive Center (DAAC) about a year before the TRMM launch. There, the code will undergo integration and system testing.

Release 3 will be developed based on experience with the way the release 2 algorithms interact with the actual data from both the CERES instruments and the cloud imagers. The most important new feature of the release 3 algorithms that we foresee now is the set of new ADM's based on observations with the CERES instruments operated in the rotating azimuth plane scan mode and simultaneous cloud property retrievals. We also expect the release 3 algorithms to increase the number of vertical levels in the atmosphere radiative flux calculations. When the new ADM's are available, we will reprocess the older CERES data and the ERBE data sets to ensure that we obtain a consistent, long-term climate data set for the community's benefit.

The initial plans for this development were distributed to the EOS Project in the CERES Data Management Plan in June 1990. This plan was part of the required documentation for the CERES investigation. During the early part of 1992, the CERES Data Management and Science Teams conducted an investigation of the possibility of using Ada or FORTRAN as programming languages for CERES software development. As a result of this study, it seemed appropriate to use a multilingual approach, allowing Ada, FORTRAN, or C, as appropriate. In addition, CERES has adopted Software Through

Pictures, a Computer Aided Software Engineering (CASE) Tool for much of the definition and design work. We expect to be able to extend this tool's database to allow us to capture documentation and to assist in keeping the documentation consistent with the software design.

0.7.4. Organizations Involved In Processing

In the next few subsections, we want to describe our current understanding of how the CERES processing system will work operationally. We begin with the organizations involved in CERES and then consider how these organizations will interact. Then, we will develop a standard operational scenario from which we can estimate how much processing load CERES will have on the EOSDIS computers and networks.

We are now ready to consider how the individuals and organizations involved in CERES processing must interact. The CERES investigation itself contains several different organizations. For operational work, the distinct entities we want to keep in mind are

- CERES Science Team
- CERES Data Management Team
- CERES Science Computing Facility
- LaRC Distributed Active Archive Center (DAAC)
- EOSDIS

Figure 0-23 shows the various organizations we expect to interact during the operational phase of CERES data processing. We need to show how the algorithms and data products we have described interact with them.

The CERES Science Team is the basic user of the CERES processing system and of the software development process. The Science Team is responsible for reaching a consensus on the algorithms we must use, for defining the data products from the system, and for conducting the initial scientific research with the CERES data products.

The Science Team is organized into Working Groups (WG's), to which team members have attached themselves because of their technical expertise. These WG's are

- Instrument WG
- Cloud WG
- Inversion WG
- Surface and Atmospheric Radiation Budget (SARB) WG
- Time Interpolation and Spatial Averaging (TISA) WG

In addition, where needed, we will draw from the members of the CERES Science Team those members who have dealt with the ERBE processing to assist in operations and quality control of the ERBE-like data products. We call this group

- ERBE WG

The ERBE WG will be responsible for the technical correctness of the conversion of the ERBE processing system from the old CDC Network Operating System hardware to UNIX machines.

The *CERES Data Management Team (DMT)* is responsible for ensuring that the Science Team algorithms are computable within the limitations of the CERES budget and the computer facilities available for CERES processing and data storage. During the CERES system development, the DMT will work with the Science Team to help translate the Science Team algorithms into computer code that is correct and adheres to the CERES documentation and software development standards. During the CERES system operations, the DMT will have operational responsibility for producing the data products and seeing that they are properly archived in the EOSDIS.

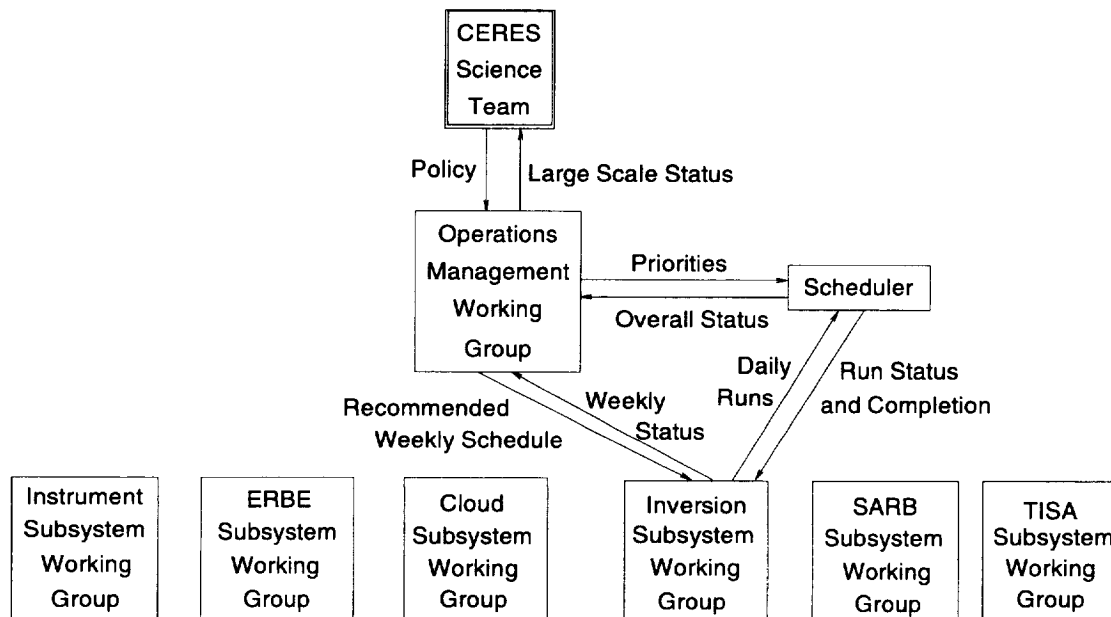


Figure 0-23. Operations entities for organizing the large scale CERES processing. All of the subsystem working groups interact with the Operations Management WG in the same way. We show only one set of interactions for clarity.

The Science Team and the Data Management Team are the major organizations specifying and using the CERES processing system. There are three other entities with which we must deal:

- CERES Science Computing Facility
- LaRC Distributed Active Archive Center
- EOSDIS

From the perspective of the operational aspect of CERES data processing, we are concerned with these three entities because they contain the computer source code, shell scripts, and the CERES data.

The *CERES Science Computing Facility (SCF)* is the networked computer system and data storage facilities at LaRC on which the CERES processing algorithms will be developed. During the initial stages of system development, we expect the computers we use to be UNIX workstations, such as Sun SparcStations. We will have a central documentation server, which will contain the current standard version of the CERES algorithm descriptions and code, as well as the operational scenarios. As we move forward with the processing system development, we expect to use the workstations and the server to test both algorithms and operational scenarios.

The *LaRC Distributed Active Archive Center (DAAC)* will eventually contain the EOSDIS connection at NASA's Langley Research Center. This facility will contain three functional entities:

- Information Management Services (IMS)
- Data Archive and Distribution Services (DADS)
- Product Generation Services (PGS)

Although these entities will be designed over the next several years through the interaction of the EOSDIS Core System (ECS) contractor and the EOS Project and community, we already have a moderately complete picture of the jobs each part of the DAAC will perform.

The *IMS* will serve as the primary entry point to CERES data for both the scientific community and the CERES Science Team. The IMS will allow users to obtain information about EOS data, including that from CERES. The IMS will also inventory the CERES data products and will send out notification

of the completion of their processing to the appropriate members of the CERES Science and Data Management Teams. During operations, we expect the IMS to contain the operational scheduling program that will translate the CERES processing schedule into instructions to the DADS and PGS.

The *DADS* will contain the CERES data products after they enter the system over the EOS network and after the data have been processed into the archival and intermediate data products. The *DADS* will probably be responsible for shipping data products to the scientific users and to the CERES Science Computing Facility.

The *PGS* will actually do the processing of the CERES data. The Product Generation System will take the requested input data from the *DADS*, run it through the software supplied by the CERES Science and Data Management Teams, and return the data products and quality control information to the *DADS*. During the initial phases of CERES operations, before the ECS contractor has produced a fully operational version of *EOSDIS*, we expect to produce CERES data on the Version 0 DAAC's *PGS*.

The *EOS Data and Information System (EOSDIS)* is the larger context within which both CERES and the LaRC DAAC operate. *EOSDIS* is responsible for providing data to LaRC and for distributing it to the users over the networks. *EOSDIS* will also extract some of the LaRC metadata and operational statistics for assisting the scientific community at large in finding data, and for tuning the operation of the networks and the other DAAC's to optimize performance.

0.7.5. How We Expect the Organizations To Interact During Operations

The entities we described in the previous section, such as the CERES Science and Data Management Teams or *EOSDIS*, are more or less permanent structures for dealing with the content of CERES or EOS. However, we will need other entities for routine operation of the CERES processing. It is easy to see why this is the case.

Consider, for example, what happens to the input data from CERES on the TRMM mission. The instrument subsystem's WG must prepare a set of instructions to the IMS identifying which parameter files must be used for calibration, for housekeeping count conversion, for expected orbital parameters, etc. After the data have been inventoried and converted from (CERES.TRMM) data packets into (IRB) standard scans, the (IRB) product must be inventoried.

When all of that day's (IRB) packets are available, the processing system should convert the instrument counts to filtered radiances, Earth locate the data, and rasterize the Earth scans, producing a single (BDS) product for archival and processing by the ERBE inversion subsystem, as well as 24 (IES) single hour data products. Both the (BDS) and (IES) products must be inventoried, and notification sent to the appropriate members of the instrument subsystem WG for verification and Q/C.

Data Management Team members of this working group will verify that the data were produced and inventoried, as well as perform a preliminary scan of the Q/C product. Science Team members of this WG will carefully examine the Q/C product looking for technical anomalies. Finally, both DMT and ST members of this WG will have to electronically 'initial' their concurrence in the Q/C description of the data products, thereby notifying the IMS of what is in good condition for distribution to the science community at large and what is not.

After the BDS product is available, the ERBE inversion process will produce the ES8 data product and enter these data into the ERBE data base. At the same time, the CERES processing on the IES data product can begin if the TRMM CID data have been received.

This example shows the complex nature of the day-to-day operations of the CERES processing system. The parameter files required by each subsystem are unique, and require substantial technical understanding in order to verify correctness. Likewise, the Q/C products are different from one

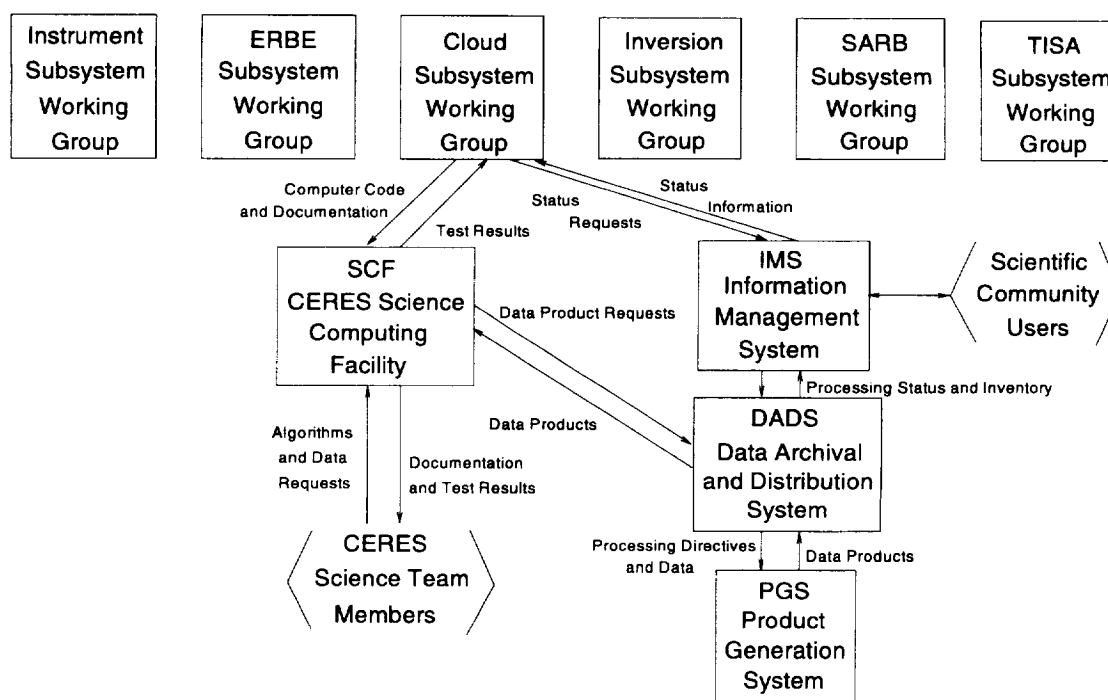


Figure 0-24. Subsystem working group interactions with EOSDIS. All of the subsystem working groups interact with the Langley DAAC in the same way. We show only one set of these interactions for clarity.

subsystem to another. It seems essential to establish Working Groups specifically associated with the daily operation of the CERES processing.

At the same time, we must have coordination of processing between the subsystems in order to obtain a satisfactory overall flow of data from the satellites to the scientific community. We expect a CERES Operational Management (OM) Working Group to perform this coordination in weekly sessions. The OMWG should have members of the CERES Data Management Team and the CERES Science Team. It will be chaired by the CERES Data Management Team leader. In a sense, this organization is familiar to the ERBE processing organization. The ERBE Data Management Team has long had regular Wednesday afternoon sessions to set weekly priorities and to establish ways of working around technical problems in the ERBE processing.

The role of the CERES Science Team is to provide long term priorities for data processing. As with ERBE, we expect the CERES Science Team to identify which months are highest priority for processing. Priority setting is one of the major functions of the CERES Science Team meetings, which will probably occur between two and three times per year when we are in the operational phase of CERES. The OMWG will then take these priorities and produce a suggested operational priority list for the subsystem WG's. Each of these WG's, in turn will establish its list of daily operational priorities.

The subsystem WG's are the lowest level of operational entity for CERES. These WG's are responsible for setting up the "command lists" for the PGS scheduling and for having the IMS return the notification that a particular stage of processing is complete. Figure 0-24 shows the connections between the subsystem WG's and EOSDIS. Table 0-6 summarizes the lead (L) and supporting (S) WG responsibilities for each of the CERES data products.

Table 0-6. Working Group Responsibilities for CERES Data Products

Product	Instr. WG	ERBE WG	Cloud WG	Inv. WG	SARB WG	TISA WG	EOSDIS
CERES Instrument Packets	L						
CERES Ephemeris and Attitude Data	L						
BDS	L	S					
ES8		L					
EDDB		L					
ES9		L					
ES4		L					
ES4G		L					
TRMM CID			L				S
MODIS CID			L				S
IES	L		S				
LWP			L		S		S
CRH-VIRS			L		S		
CRH-MODIS			L		S		
SURFMAP-DEM			S		S	S	L
SURFMAP-VEG			S		L	S	S
SURFMAP-SNOW			S		L	S	S
MDM			S	L			
SSF			L	S	S		
CRS					L		
FSW					S	L	
GEO						L	S
SYN					L	S	
AVG						L	
ZAVG						L	
SFC					S	L	
SRBAVG				S	L		
MWH			S		L		S
APD			S		L		S
GAP 3-D			S		L		S
GAP Surf			L				S
OPD			S		L		S
ASTR		S	S		L	S	

0.7.6. Procedural Considerations

The standard and internal data products that we described in the last subsection are logical files that will have inventory entries in the course of a month's processing. Because of the fact that we are dealing with up to three satellites, one of which carries only one CERES instrument, and two of which carry two CERES instruments, we can have a very large number of CERES data products in the course of a month. Table 0-7 provides a more quantitative basis for understanding how many of each product we may expect to have to work with in the course of a month.

Table 0-7. Number of Files for a CERES Production Run
for a Single Month of 30 Days

Product	After TRMM	After EOS-AM1	After EOS-PM1
INSTR	32	96	160
EPHANC	32	64	96
BDS	32	96	160
ES8	32	64	96
EDDB	1	1	1
ES9	32	32	32
ES4	1	1	1
ES4G	1	1	1
TRMM CID	768	768	768
MODIS CID	0	768	1536
IES	768	2304	3840
LWP	32	64	96
CRH	3	6	6
SURFMAP	34	34	34
MDM	1	1	1
SSF	768	2304	3840
CRS	768	2304	3840
FSW	768	2304	3840
GEO	257	257	257
SYN	241	241	241
AVG	1	1	1
ZAVG	1	1	1
SFC	768	2304	3840
SRBAVG	1	1	1
MWH	32	64	96
APD	32	32	32
GAP	32	32	32
OPD	32	32	32
ASTR	32	32	32
Total	5502	11 903	22 913

Our statement of the number of products in this table assumes that we have a 30-day month. To do a proper time interpolation at the beginning and end of the month, we need one day from the previous month and one day from the following month for most of the data products. Thus, in many cases, the number of products in this table is based on the fact that a thirty day monthly average will take thirty two days of CERES and cloud imager data. There are also products in this table that are required in volumes that are independent of the number of satellites. This is the case with such input products as GAP, APD, and OPD. We show only a single monthly average for still other products, such as ES4, ES4G, AVG, and ZAVG. Roughly speaking, we have about 5000 of these files to track during the period immediately following TRMM, about twice as many after the launch of EOS-AM1, and about five times as many after the launch of EOS-PM1. Owing to the current state of the CERES processing system design, of course, these numbers are subject to substantial revision.

0.7.6.1. CERES parameter files and quality control reports. None of the descriptions in the data flow diagrams show the parameter files that each process requires. Neither do they show the quality control reports that the processing system must produce. We need to include each of these complications in the design of the processing system.

In other words, each time we initiate a process, there are other files that we need to make sure have the proper numbers. Tracking these parameter files is an important job of the CERES operations teams. As an example, we have at least the following parameter files for CERES:

1. CERES instrument calibration coefficients
2. Earth geoid parameters
3. ERBE Angular Distribution Models
4. ERBE Directional Models
5. ERBE Scene ID Maximum Likelihood Estimator Parameters
6. ERBE Snow Map
7. CERES instrument optical properties
8. CERES scene ID category properties
9. CERES Angular Distribution Models
10. CERES Directional Models
11. CERES aerosol property models
12. Radiative transfer input parameters
13. CERES radiance library

Although we expect to automate the inclusion of these files, we do need to maintain version control over them. Their data can have as much influence over the final results as do calibration coefficients.

Likewise, each time we complete a process, there will be quality control reports regarding the operation of the system and of the characteristics of the data in the products. Usually, the numerical data in the reports are statistical summaries of the data products. Thus, we expect the reports to contain the following example quality control information:

1. Number of good instrument pixels
2. Number of bad pixels in each kind of pixel error condition
3. Fraction of pixels in each cloud category, as a function of latitude zone and climate region
4. Average TOA flux for each cloud category in a month

Table 0-8 shows the parameter files and quality control reports that each of the CERES process needs to deal with. We can see that there are a variety of input parameters and output Q/C reports, depending upon which process we need to invoke to run a month's worth of data through the system.

0.7.6.2. Individual process runs and product generation executables. It should be clear by now that a single process run may take many input products and create many output products. For example, if we run process 1 (in the upper left-hand corner of the main DFD), we take in one INSTR product and generate one BDS product and 24 IES products. If we add to this list the items from table 0-8, we can see that a single run of process 1 also requires the Instrument Command History, the Calibration Coefficients, the Earth Geoid, and the Housekeeping Coefficients. The output will generate 25 Q/C reports.

We assume that the process of running this part of the CERES processing is highly automated, so that it operates without much human intervention. We expect to have a single shell script that

1. Checks that the required input files are available
2. Starts the computers running the executable program that processes this kind of data
3. Provides the ID's of the output files
4. Sends out the Q/C readiness notification messages when the reports and output products are ready

Table 0-8. Parameter Files and Q/C Reports for CERES Processes

Process	Parameter Files	Q/C Reports
1	Instr. Cmmnd. Hist. Cal. Coefficients Earth Geoid Housekeeping Coeffs.	BDS IES
2	ERBE ADM's ERBE Spectral Corr. Coeffs.	ES8 EDDB Ingest
3	ERBE Directional Models	ES9 ES4 ES4G
4	CERES Cloud Categorizations Satellite Orbit Elements CERES Spectral Corr. Coeffs. CERES ADM's Li-Leighton Regression Coeffs. Ramanathan Regression Coeffs.	CRH SSF
5	Radiative Transfer Parameters	CRS
6		FSW
7	Satellite Merge List CERES Directional Models Radiative Transfer Parameters	SYN
8	Synoptic Times in Month	AVG ZAVG
9	Regions Observed in Hour	SFC
10	CERES Directional Models	SRBAVG
11	Dates Covered in CRHDB	CRH
12	Choice of Data Sources	ASTR

We call the shell script that performs these four functions a *Product Generation Executable*, or *PGE*. Table 0-9 shows the PGE's for the CERES processing, together with the input files, the parameter files, the output files, and the Q/C reports.

For the time being, we assume that each process shown in table 0-9 is the smallest element that could be included in the execution function (item 2 in the list in the last paragraph). It may be that at some other point in time, we could combine the processes in this table into a composite PGE. However, we do not expect to break down the processing into smaller steps, with the possible exception of processes 7 and 10. For each of these time periods, we have taken the number of jobs (in an old fashioned sense) that we will have to run through the system to accomplish the work for that month. We can see the number of jobs expanding from about 3000 per month after TRMM, to about 6000 per month after EOS-AM1, to about 9000 per month after EOS-PM1. We have taken into account the fact that some of these processes are only run once per month, e.g. the ERBE Daily Data Base run that produces the ERBE-like monthly averages, and the job that produces the CERES monthly averages, AVG and ZAVG. In most other cases, we have about one run for each satellite hour of data. The major difference here lies in whether or not we have included the data from the scanner using the rotating azimuth plane scan mode.

Table 0-9. Elements of CERES Product Generation Executables

Process	Input Products	Parameter Files	Output Products & Q/C Reports
1	1 - INSTR	Instr. Cmmds. Cal. Coeffs. Earth Geoid HK Coeffs.	1 - BDS 24 - IES
2	1 - BDS	ERBE ADM's ERBE Spectral Corr. Coeffs.	1 - ES9
3	1 - EDDB	ERBE Directional Models	1 - ES9 1 - ES4 1 - ES4G
4	2 - IES 1 - CID 1 - LWP 1 - MDM 1 - SURFMAP 1 - ASTR 1 - CRH	CERES Cloud Categories Sat. Orb. Elements CERES Spectral Corrs. Li-Leighton Repr. Coeff. Ramanathan Repr. Coeff.	2 - SSF
5	1 - SSF	Radiative Transfer Coeff.	1 - CRS
6	1 - CRS	Satellite Merge List	1 - FSW
7	720 to 2160 FSW 720 - GEO	CERES Directional Models Cal. Coeffs. Radiative Transfer Coeff.	240 - SYN
8	240 - SYN	CERES Directional Models	1 - AVG 1 - ZAVG
9	1 - SSF		1 - SFC
10	720 to 2160 SFC	CERES Directional Models	1 - SRBAVG
12	1 - MWH 1 - APD 1 - GAP 1 - OPD	Choice of Source	1 - ASTR

Table 0-10(a) shows the number of times each of the subsystem must run in a given month following the TRMM launch. The table shows other statistics of production that must happen as well. For example, subsystem 1 will run 30 times (assuming that there are 30 days in the month). To perform these runs, the operational planning service will have to prepare thirty PGE's, one for each run. To produce these PGE's, we will have to have thirty sessions set up, where we set up and check the files that must be read into the system in order to run the system. Such work involves checking that each PGE has the proper set of calibration coefficient files and that the output from this system will be routed to the proper places. This table also shows the number of Q/C reports that the system will generate, assuming that each product also generates a Q/C report that is placed in the EOSDIS archive. The scheduling and planning services for EOSDIS is also expected to generate a notice to the individuals monitoring Q/C that these reports have been generated. Since subsystem 1 generates one BDS product and 24 IES products, we have 720 IES Q/C reports and 30 BDS Q/C reports for a 30-day month of

Table 0-10. CERES Product Generation Executables for Standard Processing of a Month of CERES Data

(a) Following TRMM launch

Subsystem	Number of PGE's	Scripting Sessions	Q/C Sessions & Q/C Reports
1	30	30	750
2	30	30	60
3	1	1	3
4	720	720	1440
5	720	720	720
6	720	720	720
7	1	1	240
8	1	1	2
9	720	720	720
10	1	1	1
11	4	4	4
12	30	30	720
Total	2978	2978	5380

processing. The same kind of expansion continues through the operational scenario that governs this month's production.

Table 0-10(b) shows how the number of sessions and Q/C reports increases when we add the EOS-AM1 satellite to TRMM. There are now two CERES scanners, so the number of CERES instrument subsystem runs we need to make is trebled—one per instrument as might be expected. However, only cross-track scans are processed through the ERBE-like portion of inversion. Thus, the number of runs and Q/C products only doubles. Assuming that we run the ERBE-like monthly averaging only once per month, neither the number of runs nor the number of Q/C reports changes. Of course, it is possible that we will decide to alter this sequence when we gain more experience. However, what is important to us in this preliminary view of operations is that the number of runs and Q/C reports for monthly averaging does not depend upon the number of satellites or instruments. The cloud property subsystem, 4, runs twice for each hour in the month, once for the TRMM VIRS data, and once for the EOS-AM1 MODIS data. When it runs with the TRMM data, this subsystem outputs one SSF and one update to the CRH Database. Thus, this run produces 720 Q/C reports. When the subsystem runs with the EOS-AM1 data, it takes in two IES products (one for the scanner in cross-track mode, and one for the scanner in rotating azimuth plane scan mode). In this case, the subsystem also generates two SSF products and one update to the CRH database. During a month, this processing adds 1440 products and Q/C reports. Thus, the total number of Q/C reports subsystem 4 generates in a month of processing will be 2160. Similar operational considerations underlie the figures in the rest of this processing scenario. We only process cross-track scan data beyond SSF (although ADM construction is not included in this estimate of processing load). Here again, we can see processes that only operate once in a month (subsystems 8 and 10), as well as subsystems that operate on a fixed time basis (such as subsystem 3 or 12).

In Table 0-10(c) we can see the effect of adding the afternoon EOS-PM1 to the processing schedule. Again, we can see that subsystem 1 operates according to the number of instrument days during the month, whereas subsystems 3, 7, 8, and 10 effectively operate once per month. We have assumed that there is one VIRS version of CRH (and CRHDB) and one for MODIS. Thus, the number of updates to the clear-sky history are not changed from what we had when we added the EOS-AM1 to the TRMM

Table 0-10. Continued
(b) Following EOS-AM1 launch

Subsystem	Number of PGE's	Scripting Sessions	Q/C Sessions & Q/C Reports
1	90	90	2250
2	60	60	120
3	1	1	3
4	1440	1440	2160
5	1440	1440	1440
6	1440	1440	1440
7	1	1	240
8	1	1	2
9	1440	1440	1440
10	1	1	1
11	8	8	8
12	30	30	30
Total	5952	5952	9134

Table 0-10. Concluded
(c) Following EOS-PM1 launch

Subsystem	Number of PGE's	Scripting Sessions	Q/C Sessions & Q/C Reports
1	150	150	4050
2	90	90	180
3	1	1	3
4	2160	2160	5760
5	2160	2160	2160
6	2160	2160	2160
7	1	1	240
8	1	1	2
9	2160	2160	2160
10	1	1	1
11	8	8	8
12	30	30	30
Total	8922	8922	16 754

mission. For subsystem 4, we can see that the number of Q/C reports is proportional to the number of scanners, while the total number of runs is proportional to the number of satellites—we will still “double up” on the CERES data run through this subsystem for satellites with pairs of CERES instruments. On the other hand, the number of runs with subsystems 5, 6, and 9 is directly proportional to the number of satellites.

When we speak of scheduling the routine CERES processing, we are trying to organize the order of initiation of these processes. Clearly, some of them must be done before others. We cannot invert filtered radiances to TOA fluxes until there are filtered radiances; we cannot compute a synoptic product

before there are instantaneous fluxes; we cannot compute an ERBE monthly average before we have a full ERBE data base.

0.7.7. System Performance Estimation

An important aspect of planning for CERES processing is obtaining adequate planning estimates for computational loading. There are a number of important parameters that we need to obtain as part of this estimation, including rate of floating point operations, I/O channel throughput during processing, random access stores required during processing, and network bandwidth. It may also be appropriate to consider such possibilities as the design of code for parallelization. In this section of the document, we concentrate on the CPU processing load, although the other factors we mention may be even more important in the final analysis. The estimates we provide are based on material that does not incorporate many of the changes in data structures that we have been required to make during the past months of writing the ATBD's. We will be updating these estimates during the coming months as we proceed with the design of the system.

0.7.7.1. Estimation procedure. Estimation of CPU processing loads is a difficult problem. A simple estimate that is based on the idea that the total cost of processing a given data product scales as the number of parameters is seriously misleading. In much of the EOS processing, a major part of the time and CPU cycles required will be taken up with I/O tasks and page swapping of virtual memory. Indeed, it is quite possible that we could slip in a substantial increase in the number of parameters in a data product and not see the total computational burden increase to a noticeable degree.

It is also important to note that the CERES processing load does not scale linearly with the number of instruments or with the number of satellites. More care is required in the estimation process, and needs to be based on a moderately detailed understanding of the expected operational scenarios. Furthermore, we have not developed preliminary scenarios for the initial checkout and validation period, for the ADM calculations, for reprocessing after new ADM's are available, nor for operational calibration periods (although we expect that this last type of operation will not be as stressful of processing as the former types).

We base our processing load estimates either on runs of the ERBE-like portion of the system or upon running algorithms that are similar to those we expect to use. In the case of the ERBE-like processing, we have had the benefit of code ported from Control Data Corporation (CDC) Cyber computers to UNIX workstations. This porting involved code conversions from NOS FORTRAN to FORTRAN 77 on Sun Sparcstations. In the case of the non-ERBE code, we needed to use several different algorithms that had been coded for preliminary testing:

- For the cloud ID and inversion processing, we used code from Pat Minnis' work with AVHRR data at 2 km spatial resolution using two spectral bands
- For the surface and atmosphere radiation budget calculations, we used the Fu-Liou 31-level code with cloud scattering in the longwave, while in the shortwave we used the Chou 33-level code with the Fu-Liou formulation of a δ -4-stream approximation

We ran each of these codes on Sun SPARC 2 computers using Sun OS 4.1.2 and Sun FORTRAN 77, version 1.4. When we ran the tests, there were no other processes on the machine. Where the processes differ from those we describe in the ATBD subsystems, we have tried to extrapolate the hours of wall-clock time on this kind of workstation to arrive at a common basis for processing loads.

0.7.7.2. Cloud processing estimation procedure. Because of the importance of cloud property estimation, we have expanded the effort in estimating the processing load by using three separate procedures.

The code basis for these estimates comes from three algorithms currently running on workstations at Langley Research Center. These are

1. ERBE inversion subsystem
2. ISCCP+ code from Pat Minnis
3. Coakley's spatial coherence code

For each of these algorithms, we estimate the processing load by assuming that the load increases linearly with the number of pixels. First, we estimate the work per pixel for the given algorithm. Then, we multiply by a factor to account for the change in complexity as we go to the CERES algorithms. After that, we take the work for each pixel and multiply by the number of pixels we will be dealing with. At this point, we have an estimate of the number of floating point operations (FLOP's) we will need. By dividing this number by the processing rate for a Sun SPARC 2, we arrive at the expected wall-clock time it will take to process an hour of data. Later, we will add the hours together and include an appropriate factor for keeping ahead of the input data stream and another for reprocessing. With these calculations, we obtain an estimate of the CPU processing rate.

For the ERBE inversion subsystem, we are processing three channels of data at about 40 km resolution. There are about 60 scanner positions that sample the Earth in a 4-second scan. There are also about 900 scan lines in an hour. Thus, a single channel of ERBE data has 54000 footprints in one hour. For a single day of observations with three channels, we have about 3.9×10^6 single channel footprints of ERBE data. The ERBE inversion algorithms require about 1/6 hour to process an entire day. One-sixth hour is 600 seconds, and in this time we estimate that there should have been 2.40×10^9 FLOP's. It follows that we need about 617 FLOP's per ERBE single-channel footprint using the ERBE algorithms. The CERES algorithms are considerably more complex than is the ERBE inversion subsystem's. We assume a complexity factor of eight to go from ERBE to CERES. This factor means that we require about 4938 FLOP's per pixel.

How many pixels do we have to deal with? For VIRS, the data come in scan lines of 261 pixels each. In 1 hour, there are 11808 scan lines along the orbital track. Thus, with VIRS, there are about three million (3.08×10^6) pixel positions for each spectral channel. From MODIS, we use eight 1-km channels, two 0.5-km channels, and one 0.25-km channel. It will be easiest for us to track what happens with a single 1-km channel and then multiply by appropriate factors. A single MODIS scan line of 1-km pixels is 2048 pixels across. In 1 hour, there are 23616 scan lines. Thus, there are almost 50 million (4.84×10^7) MODIS 1-km pixels from a single channel in an hour.

How many FLOP's will we need for processing an hour of VIRS data if the CERES algorithms are like the ERBE inversion subsystem? We have five channels of VIRS, each having three million pixels (total of 15.4×10^6 pixels). At 4938 FLOP's per pixel, we will need 7.61×10^{10} FLOP's for the VIRS data. At 4 MFLOPS, it will take about 5.3 hours to process this data on a SPARC 2.

How much more extensive will the MODIS processing be? In this case, we have 32 times as much data as a single channel (eight 1-km channels, two 0.5-km channels with four times as much data, and one 0.25-km channel with 16 times as much data). Since there are about 48 million pixels of 1-km data in a single channel, in 1 hour, we have 1.54×10^9 pixels to deal with. After we multiply by the work per pixel and divide by the processing rate, we expect to spend about 530 (530.8) hours of SPARC 2 CPU time to process 1 hour of MODIS pixels.

The ISCCP+ code from Pat Minnis uses two channels of AVHRR GAC data and requires 1.5 minutes of SPARC 2 time per minute of AVHRR data. With AVHRR GAC data, we have a swath 409 pixels wide. In an hour, there will be about 6300 scan lines of data. Thus, a single channel should have about two and one-half million pixels in an hour (2.58×10^6). Since the algorithm worked on two channels, there were about 5×10^6 pixels in an hour of data. This hour of data took 90 minutes to process,

which means that each pixel required 4190 FLOP's. If we use a complexity factor of 2 to convert from AVHRR to CERES, we need about 8380 FLOP's per pixel.

The number of pixels to process for VIRS was calculated above as 15.4×10^6 . If we multiply by the number of operations per pixel (8380), we find that VIRS requires about 1.29×10^{11} FLOP's for one hour with the five VIRS channels. For MODIS, the number is about two orders of magnitude higher: 1.29×10^{13} FLOP's. At 4 MFLOPS, this estimate requires about 9 hours of SPARC 2 processing for VIRS and about 900 hours for MODIS.

Coakley's spatial coherence code requires the same processing time as does the ISCCP+ code. Thus, our estimate here is the same as the one we just derived in the previous paragraph. Table 0-11 shows a summary of the processing load normalized to hours of Sun SPARC 2 processing to produce the standard 1-hour run of subsystem 4.

We have also done some preliminary estimation of the processing load due to I/O with a fourth source of data: Baum's combined HIRS/AVHRR analysis code. For 1-km AVHRR data, where the AVHRR data volume swamps all other data sources by a factor of 200, Baum was able to strip out just the portion of the code that read in the data and unpacked it. A "read-only" version took only 2% of the total time. A "Read and Unpack" version took 25% of the time. Since unpacking from 10 bit data to 16 bit or 32 bit integers is dominated by CPU processing, we have a process controlled by CPU speed. However, this experiment does suggest that some processes can be I/O controlled in their CPU usage. In this case, we may have a process whose CPU usage varies little with the amount of data read in, but is related to the number of items opened or unpacked.

0.7.7.3. SARB processing estimation procedure. The computational burden due to subsystem 5 is summarized in section 5.6 of the ATBD volume 4. In this case, the algorithms are being run on a Sun SPARC 10, which we take to operate at 8 MFLOPS. It is also clear that in that section, the timing is done on a CERES footprint basis. On a comparative basis, the cost of the radiative transfer computations per CERES footprint is much larger than what we have seen so far on the cloud property identification processes. Based on the numbers in the ATBD for subsystem 5, we find that the Fu-Liou code requires about 26.4×10^6 FLOP's per longwave CERES footprint, while that code requires 32×10^6 FLOP's per shortwave footprint. We can now estimate the number of CERES footprints in each of the single hour production runs we are making. For TRMM, we have an arc of about 140° , which gives us footprints in a single 3.3 second scan, since the scanner is rotating at a rate of 63.5°s^{-1} . The EOS platforms, which are higher, have a smaller arc to which the Earth contributes. In this case, we have 203 footprints in a single 3.3 second scan. The scan rate is the same for both EOS and TRMM, thus we have 1091 scans in a single hour. On this basis, we have 240020 footprints in a single hour of TRMM observations and 221473 footprints in a single hour of EOS observations.

Table 0-11. Hours of Sun SPARC 2 Processing Time for Single Run of Subsystem 4

VIRS pixels processed per hour: 1.54×10^7 MODIS pixels processed per hour: 1.54×10^9			
Estimate Basis	FLOP per Imager Pixel	Hours for VIRS	Hours for MODIS
ERBE Inversion	4938	5.3	530.8
ISCCP+	8383	9.0	901.0
Spatial Coherence	8383	9.0	901.0
Most Likely	8400	9.0	901.0

Table 0-12. Hours of Sun SPARC 2 Processing Time for Single Run of Subsystem 5

TRMM footprints processed per hour: 240020 EOS footprints processed per hour: 221473			
Estimate Basis	MFLOP per CERES Footprint	Hours for TRMM	Hours for EOS
TRMM - Longwave	26.4	440	
TRMM - Shortwave	32.0	533	
TRMM - Average Day and Night		707	
EOS - Longwave	26.4		406
EOS - Shortwave			492
EOS - Average Day and Night			652

Table 0-13. Hours of Sun SPARC 2 Processing Time for Various Subsystems

Subsystem	Basis of Estimate	Frequency	Hours per Run
1	Measured from converted ERBE code and scaled to CERES characteristics	Daily	5.5
2	Measured and scaled from ERBE	Daily	1.0
3	Measured and scaled from ERBE S-9 and S-4	Monthly	12.5
4	Scaled from research code	Hourly	VIRS: 8.9 MODIS: 901.0
5	Scaled from research code	Hourly	VIRS: 707.0 MODIS: 652.0
6	Scaled from ERBE Daily Database	Hourly	1.3
7	Scaled from ERBE time and space averaging and research codes	Monthly	180.0
8	Scaled from ERBE S-4 generation	Monthly	60.0
9	Nearly identical to 6	Hourly	1.3
10	Scaled from ERBE Time Averaging	Monthly	65.0
12	Guess	Daily	10.0

Table 0-12 estimates the hours a SPARC 2 would take to process subsystem 5, using the processing load for each CERES footprint, together with the number of footprints that each of the two platforms will provide. In each case, we only process the cross-track data through the internal field calculation. Thus, the timing for this subsystem will be proportional to the number of satellites and the number of CERES pixels from a single satellite.

0.7.7.4. Computational loads for routine CERES processing. Table 0-13 shows the hours of SPARC 2 processing time that appear to be reasonable estimates for the CERES processing load. We have listed each of the subsystems in the DFD and provided the basis for our estimate. We do not have estimates currently for the update of the CRH database to create the CRH product, although we expect that this process will add a small amount to the overall computational burden. The column labelled "Frequency" shows the time interval of data covered in a single run of the subsystem. For the monthly averaging subsystems 7, 8, and 10, we assume a single monthly run to produce the averages. In the case

of subsystem 7, we may choose a different processing scenario for operations when we gain experience with release 1 and release 2 software.

Table 0-14 shows estimated number of hours of Sun SPARC 2 we would require for standard processing of the system we have described. We have made a number of assumptions in this table. In particular, we assume there are 31 days in a typical month, which gives 744 hours when we need to know how many hours to use in a month. The amount of processing varies from subsystem to subsystem, but is not a simple multiplicative factor times the number of CERES instruments or the number of satellites. Table 0-15 shows the fundamental assumptions we made in deriving the number of hours of SPARC 2 processing time we require.

Table 0-16 reduces these estimates of processing power to equivalent GigaFLOPS (billion floating point operations per second), assuming that we can scale from the Sun SPARC 2 performance at a rate of 4 MFLOPS per SPARC 2. The reprocessing load is estimated at a factor of three. Definition of processing loads is still very preliminary. It is important to note that this estimate of processing load does not include either the processing required to produce ADM's from Rotating Azimuth Plane scan data in the SSF data product, nor does this estimate include production of special data products needed to validate the data products.

Table 0-14. Hours of Sun SPARC 2 Processing Time to Run 1 Month of Data

Subsystem	TRMM	TRMM & EOS-AM1	TRMM & EOS-AM1 & EOS-PM1
1	171	511	852
2	31	62	93
3	13	13	13
4	6 622	676 966	1 347 310
5	526 008	1 011 096	1 496 184
6	967	1 934	2 902
7	180	180	180
8	60	60	60
9	967	1 934	2 901
10	65	65	65
11	TBD	TBD	TBD
12	310	310	310
Total	535 393	1 693 131	2 850 870
Process 11 not included in Total			

Table 0-15. Assumptions on Processing Time Estimates to Run 1 Month of Data

An average month is assumed to have 30.4 days and 730 hours. Any CERES instruments can operate in both cross-track and rotating azimuth plane scan mode; an instrument may shift from one mode to another at any time.	
Subsystem	Assumption
1	Processing proportional to number of CERES instruments.
2	Processing proportional to number of CERES instruments operating in cross-track mode, which is equal to the number of satellites.
3	Processing time dominated by I/O access control, so that processing time depends only on number of times this subsystem is run, which makes this processing estimate independent of number of instruments or satellites.
4	Processing time dominated by number of times imager data is processed; most efficient operation feeds as many CERES instrument products as possible together with imager data.
5, 6	Processing time proportional to number of satellites; we only use cross-track data for these procedures.
7	Processing time dominated by I/O access control, so that this process depends primarily upon number of runs, not on amount of data.
8	Processing time depends on number of regions accessed, not upon number of satellites; processing time also likely dominated by I/O access control.
9	Processing time proportional to number of satellites; we only use cross-track data for these procedures.
10	Processing time depends on number of regions accessed, not upon number of satellites; processing time also likely dominated by I/O access control.
11	Processing time for updating CRH not easily estimated based on existing experience; expected to be small compared with other processing loads.
12	Processing dependent only on number of days used, independent of number of instruments or satellites.

Table 0-16. CPU Processing Power for Normal Processing to Run 1 Month of Data

Estimated Quantity	TRMM	TRMM & EOS-AM1	TRMM & EOS-AM1 & EOS-PM1
Monthly total SPARC 2 hours	535 000	1 690 000	2 850 000
Daily total SPARC 2 hours assuming 20 work days per month	26 750	84 500	142 500
Daily total SPARC 2 hours allowing for normal reprocessing	80 250	253 500	427 500
Number of SPARC 2 CPU's to support processing	3 344	10 563	17 813
CPU Capacity [GFLOPS] assuming 4 MFLOPS per SPARC 2	14	42	71
Process 11 not included in Total			

0.8. References

- Barkstrom, Bruce R. 1984: The Earth Radiation Budget Experiment (ERBE). *Bull. Am. Meteorol. Soc.*, vol. 65, no. 11, pp. 1170–1185.
- Barkstrom, Bruce R.; and Smith, G. Louis 1986: The Earth Radiation Budget Experiment: Science and Implementation. *Rev. Geophys.*, vol. 24, no. 2, pp. 379–390.
- Barkstrom, Bruce R.; Harrison, Edwin F.; Lee, Robert B., III 1990: Earth Radiation Budget Experiment—Preliminary Seasonal Results. *EOS*, vol. 71, pp. 297 and 304.
- Barkstrom, B. R. 1992: The Physical Basis of Climate. *Phys. Soc.*
- Barkstrom, B. R.; Wielicki, B. A.; and CERES Science Team 1988: A Proposal to Investigate Clouds and the Earth's Radiant Energy System: Instruments for the NASA Polar Platform (CERES-IN).
- Barkstrom, B. R. 1989: Preliminary CERES Data Processing System Design: Functional Specification.
- Barkstrom, B. R.; and EOSDIS Advisory Panel 1990: A Preliminary EOS Investigator Software Development Roadmap.
- Baum, B. A.; Wielicki, B. A.; Minnis, P.; and Parker, L. 1992: Cloud Property Retrieval Using Merged HIRS and AVHRR Data. *J. Appl. Meteorol.*, vol. 31, no. 4, pp. 351–369.
- Brooks, D. R.; Harrison, E. F.; Minnis, P.; Suttles, J. T.; and Kandel, R. S. 1986: Development of Algorithms for Understanding the Temporal and Spatial Variability of the Earth's Radiation Balance. *Rev. Geophys.*, vol. 24, pp. 422–438.
- Budyko, Mikhail Ivanovich 1974: *Climate and Life*. Academic Press.
- Budyko, Mikhail Ivanovich 1982: *The Earth's Climate, Past and Future*. Academic Press.
- Cess, R. D.; Potter, G. L.; Ghan, S. J.; Blanchet, J. P.; and Boer, G. J. 1989: Interpretation of Cloud-Climate Feedback as Produced by 14 Atmospheric General Circulation Models. *Science*, vol. 245, pp. 513–516.
- Cess, R. D.; Potter, G. L.; Blanchet, J. P.; Boer, G. J.; Del Genio, A. D.; Déqué, M.; Dymnikov, V.; Galin, V.; Gates, W. L.; Ghan, S. J.; Kiehl, J. T.; Lacis, A. A.; Le Treut, H.; Li, Z.-X.; Liang, X.-Z.; McAvaney, B. J.; Meleshko, V. P.; Mitchell, J. F. B.; Morcrette, J.-J.; Randall, D. A.; Rikus, L.; Roeckner, E.; Royer, J. F.; Schlese, U.; Sheinin, D. A.; Slingo, A.; Sokolov, A. P.; Taylor, K. E.; Washington, W. M.; Wetherald, R. T.; Yagai, I.; and Zhang, M.-H. 1990: Intercomparison and Interpretation of Climate Feedback Processes in 19 Atmospheric General Circulation Models. *J. Geophys. Res.*, vol. 95, no. D10, pp. 16601–16615.
- Cess, Robert D.; Jiang, Feng; Dutton, Ellsworth, G.; and Deluisi, John J. 1991: Determining Surface Solar Absorption From Broadband Satellite Measurements for Clear Skies—Comparison With Surface Measurements. *J. Climat.*, vol. 4, pp. 236–247.
- CERES Data Management Team 1990: Clouds and the Earth's Radiant Energy System (CERES) Data Management Plan.
- Chahine, M. T. 1992: The Hydrological Cycle and Its Influence on Climate. *Nature*, vol. 359, no. 6394, pp. 373–379.
- Charlock, T. P.; Yang, S.-K.; Whitlock, C. H.; and Rose, F. G. 1992: Surface Longwave Radiation—Retrieval With Satellite Data, Calculations With NMCModel, and Radiometric Observations. WCRP-75, *Report of a GEWEX Workshop*, European Centre for Medium-Range Weather Forecasts, Reading, UK, October 28–November 1, 1991, World Meteorological Organization TD No. 492, pp. 2.5–2.24.
- Darnell, Wayne L.; Staylor, W. Frank; Gupta, Shashi K.; Ritchey, Nancy A.; and Wilber, Anne C. 1992: Seasonal Variation of Surface Radiation Budget Derived From International Satellite Cloud Climatology Project C1 Data. *J. Geophys. Res.*, vol. 97, no. D14, pp. 15741–15760.
- Davies, R.; Ridgway, W. L.; and Kim, K.-E. 1984: Spectral Absorption of Solar Radiation in Cloudy Atmosphere—A 20 cm^{-1} Model. *J. Atmos. Sci.*, vol. 41, pp. 2126–2137.
- Geiger, R. 1965: *The Climate Near the Ground*. Harvard Univ. Press, p. 611.
- GEWEX 1994: Utility and Feasibility of a Cloud Profiling Radar. WCRP-84, *Report of the GEWEX Topical Workshop*, Pasadena, CA, June 29–July 1, 1993, World Meteorological Organization TD No. 593.
- Green, R. N.; House, F. B.; Stackhouse, P. W.; Wu, X.; Ackerman, S. A.; Smith, W. L.; and Johnson, M. J. 1990: Intercomparison of scanner and Nonscanner Measurements for the Earth Radiation Budget Experiment. *J. Geophys. Res.*, vol. 95, pp. 11785–11798.

- Gupta, S. K. 1989: A Parameterization for Longwave Surface Radiation From Sunsynchronous Satellite Data. *J. Climat.*, vol. 2, pp. 305–320.
- Gupta, S. K.; Darnell, W. L.; and Wilber, A. C. 1992: A Parameterization for Longwave Surface Radiation From Satellite Data—Recent Improvements. *J. Appl. Meteorol.*, vol. 31, no. 12, pp. 1361–1367.
- Harrison, E. F.; Minnis, P.; Barkstrom, B. R.; Ramanathan, V.; and Cess, R. D.; and Gibson, G. G. 1990: Seasonal Variation of Cloud Radiative Forcing Derived From the Earth Radiation Budget Experiment. *J. Geophys. Res.*, vol. 95, no. D11, pp. 18687–18703.
- Hartmann, D. L.; Ramanathan, V.; Berroir, A.; and Hunt, G. E. 1986: Earth Radiation Budget Data and Climate Research. *Rev. Geophys.*, vol. 24, pp. 439–468.
- House, F. B.; Gruber, A.; Hunt, G. E.; and Mecherikunnel, A. T. 1986: History of Satellite Missions and Measurements of the Earth Radiation Budget (1957–1984). *Rev. Geophys.*, vol. 24, pp. 357–377.
- Hunt, G. E.; Kandel, R.; and Mecherikunnel, A. T. 1986: A History of Presatellite Investigations of the Earth’s Radiation Budget. *Rev. Geophys.*, vol. 24, pp. 351–356.
- Inamdar, A. K.; and Ramanathan, V. 1994: Physics of Greenhouse Effect and Convection in Warm Oceans. *J. Climat.*, vol. 7, no. 5, pp. 715–731.
- Jacobowitz, H.; Soule, H. V.; Kyle, H. L.; and House, F. B. 1984a: The Earth Radiation Budget (ERB) Experiment—An Overview. *J. Geophys. Res.*, vol. 89, pp. 5021–5038.
- Jacobowitz, H.; Stowe, L. L.; Tighe, R. J.; Arking, A.; Campbell, G.; Hickey, J. R.; House, F.; Ingersoll, A.; Maschhoff, R.; and Smith, G. L. 1984b: The Earth Radiation Budget Derived From the Nimbus-7 ERB Experiment. *J. Geophys. Res.*, vol. 89, pp. 4997–5010.
- Li, Z.-L.; and Becker, F. 1993: Feasibility of Land Surface Temperature and Emissivity Determination From AVHRR Data. *Remote Sens. Environ.*, vol. 43, pp. 67–85.
- Li, Zhanqing; and Leighton, H. G. 1993: Global Climatologies of Solar Radiation Budgets at the Surface and in the Atmosphere From 5 Years of ERBE Data. *J. Geophys. Res.*, vol. 98, no. D3, pp. 4919–4930.
- London, Julius 1957: *Study of the Atmospheric Heat Balance*. New York Univ.
- Lorenz, E. N. 1955: Available Potential Energy and the Maintenance of the General Circulation. *Tellus*, vol. 7, pp. 157–167.
- Lorenz, Edward N. 1967: *The Nature and Theory of the General Circulation of the Atmosphere*. World Meteorological Organization Publication 218, Geneva, Switzerland, pp. 161.
- Minnis, P.; Heck, P. W.; and Harrison, E. F. 1990: The 27–28 October 1986 FIRE IFO Cirrus Case Study—Cloud Parameter Fields Derived From Satellite Data. *Mon. Weather Rev.*, vol. 118, no. 11, pp. 2426–2446.
- Minnis, P.; Heck, P. W.; Young, D. F.; Fairall, C. W.; and Snider, J. B. 1992: Stratocumulus Cloud Properties Derived From Simultaneous Satellite and Island-Based Instrumentation During FIRE. *J. Appl. Meteorol.*, vol. 31, no. 4, pp. 317–339.
- Minnis, P.; Young, D. F.; and Harrison, E. F. 1991: Examination of the Relationship Between Outgoing Infrared Window and Total Longwave Fluxes Using Satellite Data. *J. Climat.*, vol. 4, no. 11, pp. 1114–1133.
- Munn, R. E. 1966: *Descriptive Micrometeorology*, Academic Press.
- Ohmura, A.; and Gilgen, H. 1993: Re-Evaluation of the Global Energy Balance. *Geophys. Monogr. 75, IUGG*, vol. 15, pp. 93–110.
- Ohmura, A.; and Gilgen, H. 1991: Global Energy Balance Archive GEBA. World Climate Program Water Project A7, Report 2—The GEBA Database: Interactive Applications, Retrieving Data. *Zücher Geographische Schriften Nr. 44*, Geographisches Institut ETH, Zürich, p. 66.
- Oort, A. H.; and Vonder Haar, T. H. 1976: On the Observed Annual Cycle in the Ocean-Atmosphere Heat Balance Over the Northern Hemisphere. *J. Phys. Oceanograph.*, vol. 6, pp. 781–800.
- Palmén, Erik Herbert; and Newton, Chester W. 1969: *Atmospheric Circulation Systems: Their Structure and Physical Interpretation*. Academic Press.
- Peixoto, José P.; and Oort, Abraham H. 1992: *Physics of Climate*. Am. Inst. Phys.
- Pinker, R. T.; and Laszlo, I. 1992: Modeling Surface Solar Irradiance for Satellite Applications on a Global Scale. *J. Appl. Meteorol.*, vol. 31, pp. 194–211.

- Ramanathan, V.; Cess, R. D.; Harrison, E. F.; Minnis, P.; Barkstrom, B. R.; Ahmand, E.; and Hartmann, D. 1989a: Cloud-Radiative Forcing and Climate: Results From the Earth Radiation Budget Experiment, *Science*, vol. 243, pp. 57–63.
- Ramanathan, V.; Barkstrom, Bruce R.; and Harrison, Edwin F. 1989b: Climate and the Earth's Radiation Budget. *Phys. Today*, vol. 42, pp. 22–32.
- Raschke, E.; Vonder Haar, T. H.; Bandeen, W. R.; and Pasternak, M. 1973: The Annual Radiation Balance of the Earth-Atmosphere System During 1969–70 From Nimbus 3 Measurements. *J. Atmos. Sci.*, vol. 30, pp. 341–364.
- Rossow, W. B.; Garder, L. C.; Lu, P-J, Lu; and Walker, A. 1991: International Satellite Cloud Climatology Project (ISCCP) Documentation of Cloud Data. WMO/TD, vol. 266, World Climate Research Programme, World Meteorol. Org.
- Sellers, P. J.; and Hall, F. G. 1992: FIFE in 1992—Results, Scientific Gains, and Future Research Directions. *J. Geophys. Res.*, vol. 97, no. D17, pp. 19091–19109.
- Sellers, William D. 1965: *Physical Climatology*. Univ. of Chicago Press.
- Slingo, A.; and Webb, M. J. 1992: Simulation of Clear-Sky Outgoing Longwave Radiation Over the Oceans Using Operational Analyses. *Q. J. R. Meteorol. Soc.*, vol. 118, pp. 1117–1144.
- Stephens, G. L.; Slingo, A.; Webb, M. J.; Minnett, P. J.; Daum, P. H.; Kleinman, L.; Wittmeyer, I.; and Randall, D. A. 1994: Observations of the Earth's Radiation Budget in Relation to Atmospheric Hydrology, Part IV—Atmospheric Column Radiative Cooling Over the Worlds Oceans. *J. Geophys. Res.*, vol. 99, pp. 18585–18604.
- Stuhlmann, R.; and Smith G. L. 1988a: A Study of Cloud-Generated Radiative Heating and Its Generation of Available Potential Energy. I—Theoretical Background. *J. Atmos. Sci.*, vol. 45, pp. 3911–3927.
- Stuhlmann, R.; and Smith, G. L. 1988b: A Study of Cloud-Generated Radiative Heating and Its Generation of Available Potential Energy. II—Results for a Climatological Zonal Mean January. *J. Atmos. Sci.*, vol. 45, pp. 3928–3943.
- Suttles, J. T.; Green, R. N.; Minnis, P.; Smith, G. L.; Staylor, W. F.; Wielicki, B. A.; Walker, I. J.; Young, D. F.; Taylor, V. R.; and Stowe, L. L. 1988: *Angular Radiation Models for Earth-Atmosphere System. Volume I—Shortwave Radiation*. NASA RP-1184.
- Suttles, J. T.; Green, R. N.; Smith, G. L.; Wielicki, B. A.; Walker, I. J.; Taylor, V. R.; and Stowe, L. L. 1989: *Angular Radiation Models for Earth-Atmosphere System. Volume II—Longwave Radiation*. NASA RP-1184.
- Suttles, J. T.; Wielicki, B. A.; and Vemury, S. 1992: Top-of-Atmosphere Radiative Fluxes—Validation of ERBE Scanner Inversion Algorithm Using Nimbus-7 ERB Data. *J. Appl. Meteorol.*, vol 31, pp. 784–796.
- Vonder Haar, T. H.; and Suomi, V. E. 1971: Measurements of the Earth's Radiation Budget From Satellites During a Five-Year Period. I—Extended Time and Space Means. *J. Atmos. Sci.*, vol. 28, pp. 305–314.
- Vonder Haar, T. H.; and Oort, A. H. 1973: New Estimates of Annual Poleward Energy Transport by Northern Hemisphere Oceans. *J. Phys. Oceanogr.*, vol. 3, pp. 169–172.
- Whitlock, C. H.; Charlock, T. P.; Staylor, W. F.; Pinker, R. T.; Laszlo, I.; Ohmura, A.; Gilgen, H.; Konzelman, T.; Dipasquale, R. C.; and Moats, C. D. 1995: First Global WCRP Shortwave Surface Radiation Budget Dataset. *Bull. Am. Meteorol. Soc.*, vol. 76, no. 6, pp. 905–922.
- Wielicki, B. A.; Barkstrom, B. R.; and CERES Science Team 1990: A Proposal for an Interdisciplinary Science Investigation of Clouds and the Earth's Radiant Energy System: (CERES-IDS).
- Wielicki, B. A. 1990: CERES Data Analysis Algorithm Plan.
- Wielicki, Bruce A.; and Green, Richard N. 1989: Cloud Identification for ERBE Radiative Flux Retrieval. *J. Appl. Meteorol.*, vol. 28, pp. 1133–1146.
- Wielicki, Bruce A.; and Parker, Lindsay 1992: On the Determination of Cloud Cover From Satellite Sensors—The Effect of Sensor Spatial Resolution. *J. Geophys. Res.*, vol. 97, no. D12, pp. 12799–12823.
- WMO 1991: Radiation and Climate. WCRP-64, *Second Workshop on Implementation of the Baseline Surface Radiation Network*, Davos, Switzerland, August 6–9, 1991, World Meteorological Organization TD No. 453.

REPORT DOCUMENTATION PAGE			Form Approved OMB No. 0704-0188	
Public reporting burden for this collection of information is estimated to average 1 hour per response, including the time for reviewing instructions, searching existing data sources, gathering and maintaining the data needed, and completing and reviewing the collection of information. Send comments regarding this burden estimate or any other aspect of this collection of information, including suggestions for reducing this burden, to Washington Headquarters Services, Directorate for Information Operations and Reports, 1215 Jefferson Davis Highway, Suite 1204, Arlington, VA 22202-4302, and to the Office of Management and Budget, Paperwork Reduction Project (0704-0188), Washington, DC 20503.				
1. AGENCY USE ONLY (Leave blank)	2. REPORT DATE December 1995	3. REPORT TYPE AND DATES COVERED Reference Publication		
4. TITLE AND SUBTITLE Clouds and the Earth's Radiant Energy System (CERES) Algorithm Theoretical Basis Document. <i>Volume I—Overviews (Subsystem 0)</i>		5. FUNDING NUMBERS WU 148-65-41-01		
6. AUTHOR(S) CERES Science Team				
7. PERFORMING ORGANIZATION NAME(S) AND ADDRESS(ES) NASA Langley Research Center Hampton, VA 23681-0001		8. PERFORMING ORGANIZATION REPORT NUMBER L-17520		
9. SPONSORING/MONITORING AGENCY NAME(S) AND ADDRESS(ES) National Aeronautics and Space Administration Washington, DC 20546-0001		10. SPONSORING/MONITORING AGENCY REPORT NUMBER NASA RP-1376, Volume I		
11. SUPPLEMENTARY NOTES				
12a. DISTRIBUTION/AVAILABILITY STATEMENT Unclassified-Unlimited Subject Category 47 Availability: NASA CASI (301) 621-0390		12b. DISTRIBUTION CODE		
13. ABSTRACT (Maximum 200 words) The theoretical bases for the Release 1 algorithms that will be used to process satellite data for investigation of the Clouds and the Earth's Radiant Energy System (CERES) are described. The architecture for software implementation of the methodologies is outlined. Volume I provides both summarized and detailed overviews of the CERES Release 1 data analysis system. CERES will produce global top-of-the-atmosphere shortwave and longwave radiative fluxes at the top of the atmosphere, at the surface, and within the atmosphere by using the combination of a large variety of measurements and models. The CERES processing system includes radiance observations from CERES scanning radiometers, cloud properties derived from coincident satellite imaging radiometers, temperature and humidity fields from meteorological analysis models, and high-temporal-resolution geostationary satellite radiances to account for unobserved times. CERES will provide a continuation of the ERBE record and the lowest error climatology of consistent cloud properties and radiation fields. CERES will also substantially improve our knowledge of the Earth's surface radiation budget.				
14. SUBJECT TERMS Earth Observing System; Clouds and the Earth's Radiant Energy System; Earth radiation budget; Clouds satellite measurements; Surface radiation; Atmospheric radiative divergence			15. NUMBER OF PAGES 114	16. PRICE CODE A06
17. SECURITY CLASSIFICATION OF REPORT Unclassified	18. SECURITY CLASSIFICATION OF THIS PAGE Unclassified	19. SECURITY CLASSIFICATION OF ABSTRACT Unclassified	20. LIMITATION OF ABSTRACT	



